NATIONAL AERONAUTICS AND SPACE ADMINISTRATION

Technical Report 32-1355

A Control System Study for an In-Core Thermionic Reactor

Lynn E. Weaver
Henrik G. Gronroos
James G. Guppy
Jerry P. Davis

JET PROPULSION LABORATORY
CALIFORNIA INSTITUTE OF TECHNOLOGY
PASADENA, CALIFORNIA

January 15, 1969

NATIONAL AERONAUTICS AND SPACE ADMINISTRATION

Technical Report 32-1355

A Control System Study for an In-Core Thermionic Reactor

Lynn E. Weaver
Henrik G. Gronroos
James G. Guppy
Jerry P. Davis

JET PROPULSION LABORATORY
CALIFORNIA INSTITUTE OF TECHNOLOGY
PASADENA, CALIFORNIA

January 15, 1969

TECHNICAL REPORT 32-1355

Prepared Under Contract No. NAS 7-100
National Aeronautics and Space Administration

Preface

The work described in this report represents one phase of studies on in-core thermionic reactor space powerplant dynamics and control performed by the Propulsion Division of the Jet Propulsion Laboratory. Dr. Lynn E. Weaver, head of the Nuclear Engineering Department at the University of Arizona, was retained as a consultant and developed the techniques of state-variable feedback design employed in this study. Mr. James G. Guppy, a student at the University of Arizona, was a summer employee at JPL.

Acknowledgments

The authors are indebted to Lieutenant Charles L. Moore for his assistance during his stay at JPL in the summer of 1967. Dr. Jerome L. Shapiro's continued supporting investigations and advice are gratefully acknowledged.

The authors also wish to thank Mr. Roy L. Mankovitz of the Spacecraft Control Section for providing computer programs, and Dr. M. Duncan McCormack of Programmatics Inc., for computer programming. The assistance of Mr. Carl Love in the use and programming of analog computers is much appreciated.

Contents

I. Introduction 1

II. General Considerations 2

A. Reference Design 2

B. Method of Control 5

C. Performance Under Constant-Voltage Control 7

III. System Equations 8

A. Description of Model 9

B. Equations 11

IV. Control System Design 20

A. State-Variable Feedback Control 20

B. Selection of Controller and System Specifications 25

C. Final Design 25

V. Results of Controller Performance Investigations 28

A. System Responses 29

B. Command Signal Changes 30

C. Disturbances 30

D. Sensitivity to Parameter Changes 31

VI. Applications to the Nonlinear System 36

A. Correlation With Results Obtained for the Linear Model 36

B. Effect of Restricting the Control Signal to Limit Reactivity Rate 40

VII. Summary and Conclusions 42

Appendix A. Equations and Diagram for Analog Computer Simulation of the Fourth-Order Linear Model of a Thermionic Reactor Space Powerplant 43

Appendix B. Equations and Diagrams for Analog Computer Simulation of the Complete Nonlinear Model of a Thermionic Reactor Space Powerplant 45

Nomenclature 55

References 56

Contents (contd)

Tables

1. Dimensions, materials, and operating conditions for thermionic reactor powerplant reference design 4
2. Parameter values for thermionic diode performance evaluation 7

Figures

1. Reactor with thermionic diodes stacked in series 1
2. Thermionic reactor fuel element 2
3. Schematic of thermionic reactor powerplant 3
4. Simplified diagram for analysis of thermionic reactor space powerplant 3
5. Illustration of dead-band and dead-time determination for thermionic reactor controller 6
6. Output current density vs net output voltage at various emitter temperatures 8
7. Net efficiency vs net output voltage at various emitter temperatures 8
8. Current density vs voltage characteristics at two cesium-reservoir temperatures 9
9. Current–voltage characteristics used in analytical studies . . . 10
10. Emitter heat flow for current–voltage characteristics used in analytical studies 10
11. Thermionic reactor space powerplant model 11
12. Temperature distributions for thermionic reactor space powerplant models 15
13. Responses of nonlinear and linear models of open-loop thermionic reactor space powerplant to a 2¢ step and a −2¢ step reactivity perturbation 16
14. Responses of nonlinear and linear models of open-loop thermionic reactor space powerplant to a step change of −0.02 Ω cm² in electric load 17
15. Comparison of Bode plots for linear fourth-order open-loop and nonlinear open-loop system models 18
16. Block diagram of state-variable feedback control 21
17. Block diagram of closed-loop system 22
18. Single-input, single-output system 23

Contents (contd)

Figures (contd)

19. System with open-loop pole at α 23

20. Block diagram for applying Popov stability criterion 24

21. Regions of known stability in the $[\sigma, f(\sigma)]$-plane 24

22. Frequency plot of the Kalman equation 26

23. Root locus plot for controlled system as a function of controller gain constant 27

24. Modified frequency function for controlled system 27

25. Response of controlled linear system to a step command in voltage 29

26. Response of controlled linear system to a step change in electric load 30

27. Response of controlled linear system to a step command in voltage when voltage feedback coefficient is halved 31

28. Response of controlled linear system to a step command in voltage when reactivity feedback coefficient is halved 32

29. Response of controlled linear system to a step command in voltage when reactivity rate feedback coefficent is halved . . . 33

30. Response of controlled linear system to a step disturbance in core reactivity of 20¢ 34

31. Response of controlled linear system to a step command in voltage when coefficient of heat-transfer term in interelectrode gap is varied by $\pm$ 10% 35

32. State-variable feedback design of thermionic reactor controller. 36

33. Responses of linear and nonlinear controlled systems to a step command in voltage 37

34. Responses of linear and nonlinear controlled systems to a step disturbance of $-0.02\ \Omega\ cm^2$ in electric load 38

35. Response of nonlinear controlled system to reactivity noise . . . 39

36. Response of nonlinear controlled system to a step disturbance of $-0.02\ \Omega\ cm^2$ in electric load when the control signal is constrained to limit reactivity rate to 10¢/s 40

37. Responses of linear and nonlinear controlled systems to a step command in voltage when the control signal is constrained to limit reactivity rate to 10¢/s 41

Contents (contd)

Figures (contd)

A-1. Analog-simulation diagram for fourth-order linear model of thermionic reactor space powerplant with controller 44

B-1. Equipment setup for computer simulation of thermionic reactor space powerplant — nonlinear model 45

B-2. Analog-simulation diagram for nonlinear model of thermionic reactor space powerplant: thermionics; net current 46

B-3. Analog-simulation diagram for nonlinear model of thermionic reactor space powerplant: thermionics; collector current 47

B-4. Analog-simulation diagram for nonlinear model of thermionic reactor space powerplant model: thermionics; electric load 48

B-5. Analog-simulation diagram for nonlinear model of thermionic reactor space powerplant: energy transport in interelectrode gap. 49

B-6. Analog-simulation diagram for nonlinear model of thermionic space powerplant: neutron kinetics 50

B-7. Analog-simulation diagram for nonlinear model of thermionic reactor space powerplant: reactor heat transfer 51

B-8. Analog-simulation diagram for nonlinear model of thermionic reactor space powerplant: coolant heat transfer 52

B-9. Analog-simulation diagram for nonlinear model of thermionic reactor space powerplant: coolant-loop heat transfer 53

Abstract

Conceptual reactor controllers for in-core thermionic reactor space powerplants have been investigated by analysis and by analog simulation. The control system was specified to maintain constant output voltage at the reactor terminals, while minimizing the effect of electric load changes and internal and external disturbances.

Using state-variable feedback design techniques and linearized system equations, constant feedback coefficients were determined so as to give the desired system response. The sensitivity to parameter variations and noise was evaluated. The controller design obtained by analysis of the linear model was applied to the corresponding nonlinear model simulated on analog computers. The correlation between the results predicted with the linear model and those obtained by the simulation was found to be good.

The investigations were exploratory; however, it appears that an in-core thermionic reactor can be controlled by relatively simple means. Loss of controller feedback elements does not cause stability problems if the control signal is constrained. All results are obtained for constant-temperature current–voltage characteristics for the thermionic diodes that do not cross each other in the range of operating conditions.

A Control System Study for an In-Core Thermionic Reactor

I. Introduction

The work described in this report is an initial study of a control system for in-core thermionic reactors for space powerplant application. The control requirements for thermionic reactors differ from those for conventional reactor powerplants because of the direct coupling between the reactor and the thermionic diode matrix. As a result of this coupling, electric load disturbances have a pronounced effect on the dynamics of the reactor. The important tie between the diode array in the core and the reactor dynamics is the thermal coupling associated with the electron cooling in the diode.

To adjust for load changes and disturbances, and failure of individual diodes in the matrix, a feedback control system is needed. The formulation of a control law and the design of the controller depend on the control philosophy adopted. For the present study, the controller was designed to maintain a constant voltage output from the diode matrix, while minimizing the effect of load changes and internal and external disturbances on the constant voltage level. Choosing voltage as the controlled variable is compatible with the conjectured requirements of the systems to which this energy source will supply power. Viewed from a plant efficiency standpoint, this seems to be a reasonable choice.

In the development of a control law and the selection of a controller, a design technique developed at the University of Arizona, termed state-variable feedback design, is used (Ref. 1, 2). This method is applied to a reduced linearized version of a nonlinear thermionic reactor model (Ref. 3). From analysis of the linearized model, a control law is determined and applied to the nonlinear system. Results of simulation studies of the linear and nonlinear controlled thermionic reactor system show the effects of load disturbances, parameter variations, and noise on the system dynamics. It is

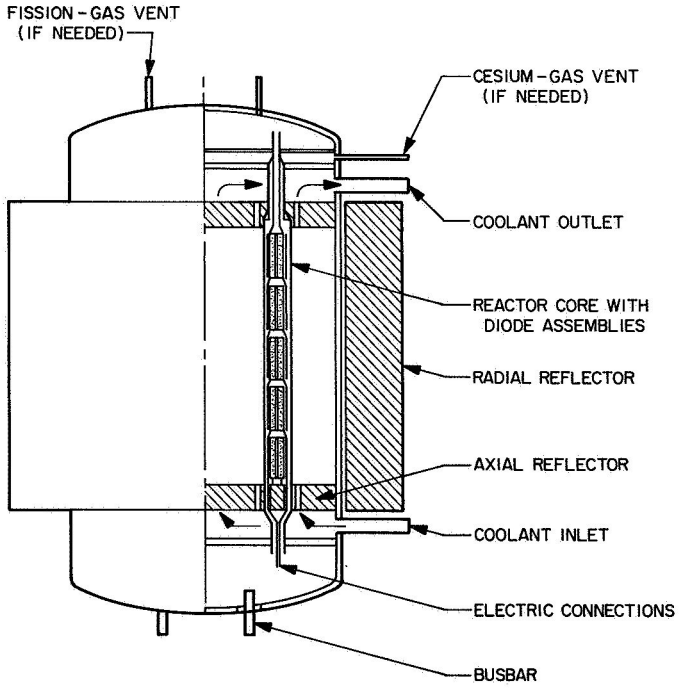

Fig. 1. Reactor with thermionic diodes stacked in series

evident from these studies that, for the thermionic reactor model considered, there is a good correlation between predicted results from the linear model and those observed in the nonlinear system. The main attention of the report is directed toward the operating phase of the system.

A brief description of the chosen reference design is given in Section II and the method of control is discussed. In Section III, the nonlinear and linearized system equations are given. Section IV describes in some detail the state-variable feedback design method, the choice of controller, and choice of system dynamics. Section V gives analytical results and system response trajectories for the linear model. In Section VI, the results of the linear theory are applied to a nonlinear model. The results of the study are summarized in Section VII.

No detailed discussion of thermionic reactor control seems to have appeared in the open literature. However, classified documents relating to specific reactor concepts, describing control system studies done by General Electric, Gulf General Atomic, and Republic Aviation, have been published recently.

II. General Considerations

A. Reference Design

Several in-core thermionic reactor designs for space powerplant application have been suggested, but such a reactor is still to be built. Various parts of the system have been investigated and tested intensively, and of these, the thermionic diodes have shown promising advances towards reliable use in a reactor core. At the present stage of development, however, it is difficult to

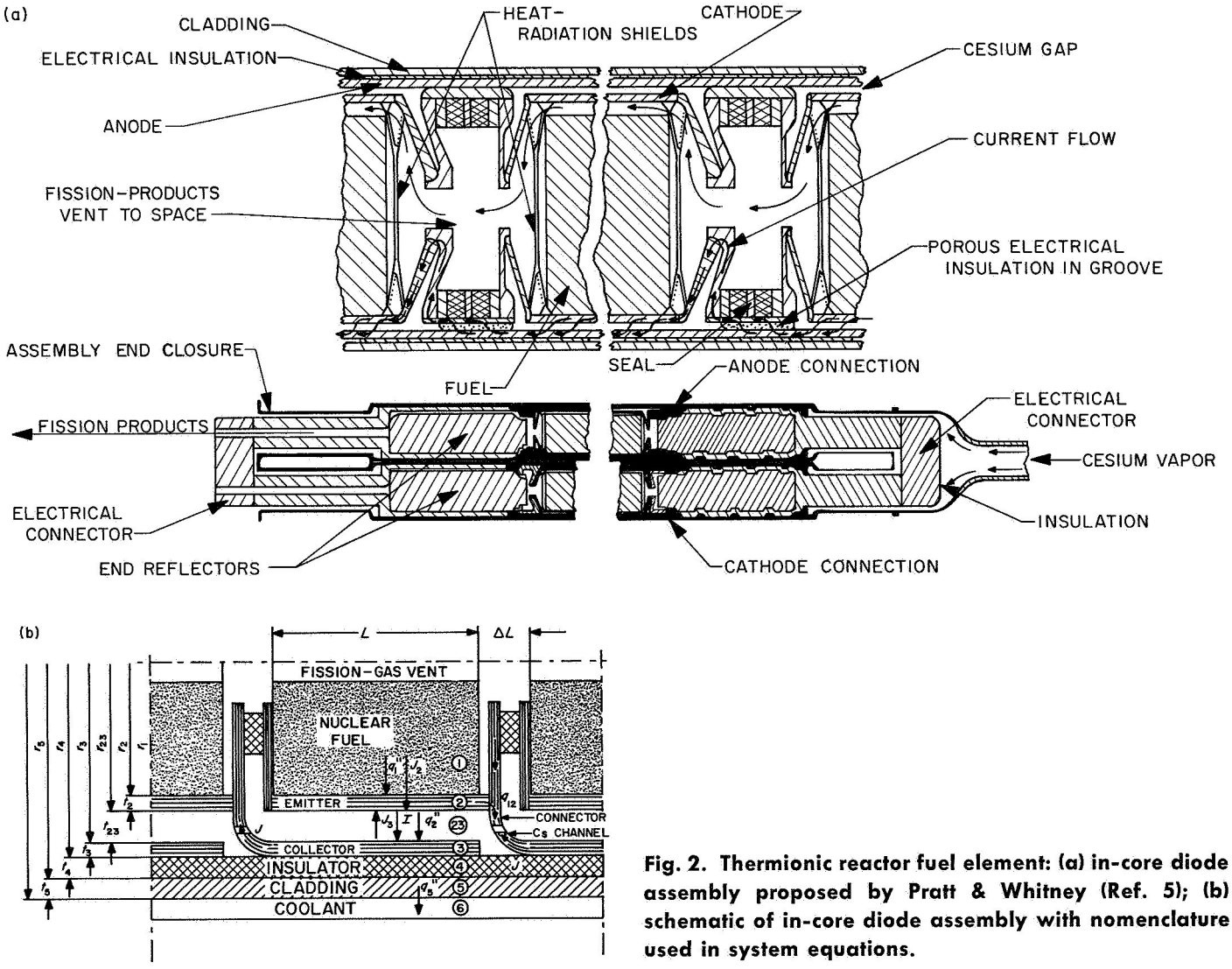

Fig. 2. Thermionic reactor fuel element: (a) in-core diode assembly proposed by Pratt & Whitney (Ref. 5); (b) schematic of in-core diode assembly with nomenclature used in system equations.

select any one design as superior for a given application. A general discussion of the relative merits of various in-core thermionic reactor concepts is given in Ref. 4.

For the initial study of thermionic reactor control described in this report, a low-power, liquid-metal-cooled system was selected. Figure 1 is a representation of the reactor concept, in which the diodes are in series-stacked modules—the so-called flashlight concept (Ref. 5). A cross-sectional view and a schematic of the in-core diode assembly are shown in Fig. 2. Figure 3 is a schematic representation of the thermionic reactor powerplant reference design. A simplified block diagram of the various elements of the system considered in the analysis is shown in Fig. 4. The main dimensions, materials, and nominal operating conditions for the powerplant reference design

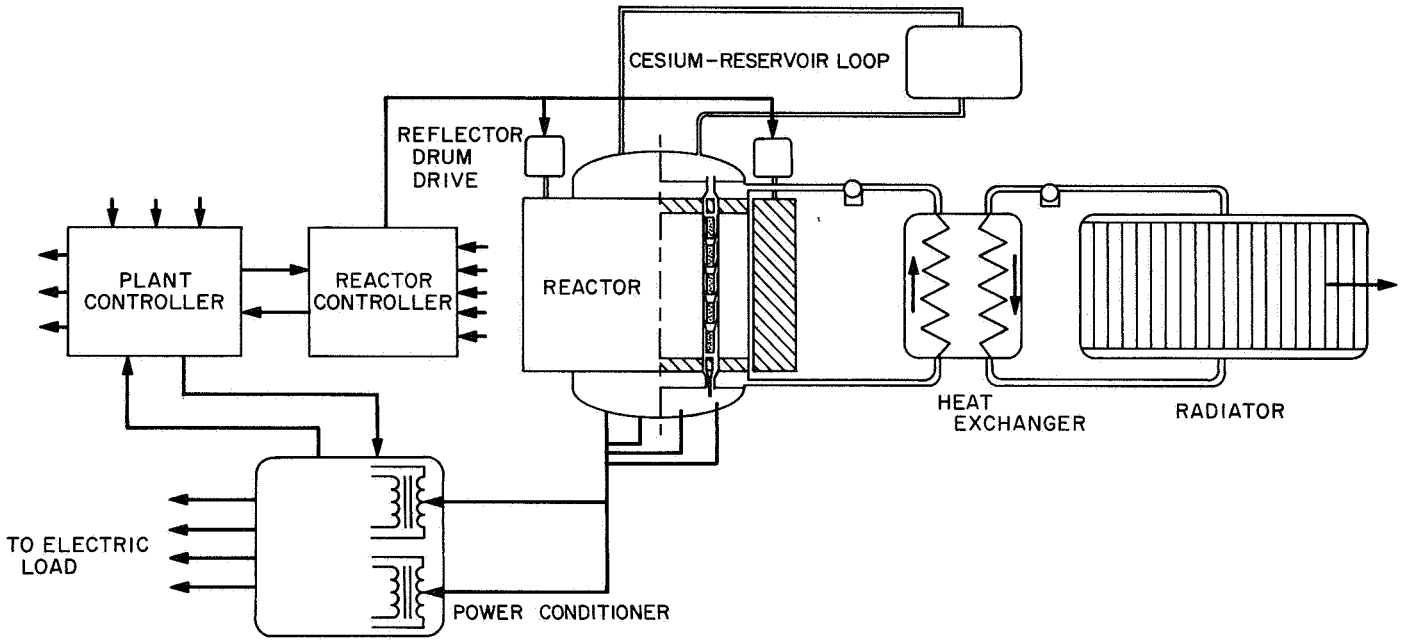

Fig. 3. Schematic of thermionic reactor powerplant

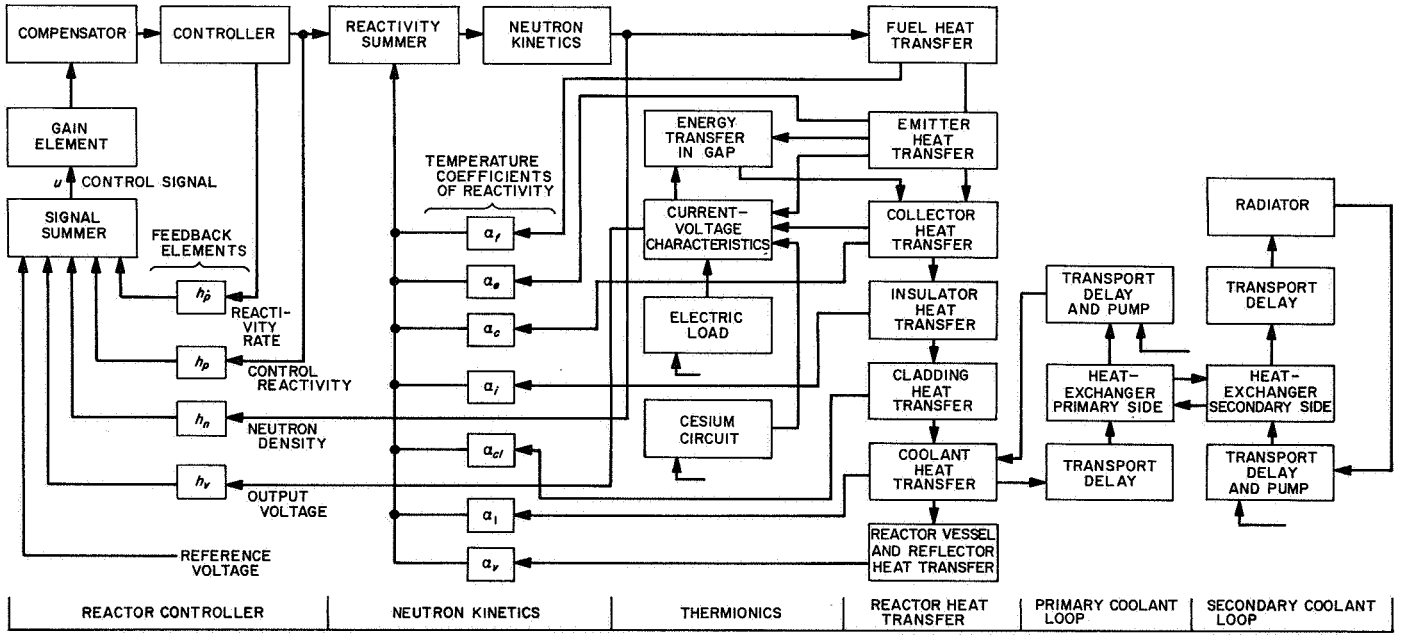

Fig. 4. Simplified diagram for analysis of thermionic reactor space powerplant

Table 1. Dimensions, materials, and operating conditions for thermionic reactor powerplant reference design

Thermionic diode heat transfer

Item	Symbol, unit	Fuel, UC (1)[a]	Emitter, W (2)[a]	Gap (23)[a]	Collector, Nb (3)[a]	Insulator, AL_2O_3 (4)[a]	Cladding, Nb (5)[a]	Coolant, Li-7 (6)[a]
Average temperature	T, °K	2150	2050		1300	1266	1232	1225
Volume	V, cm^3							
Density	ρ, g/cm^3	9.90	18.00		8.30	3.20	8.35	0.44
Heat capacity	c_p, W s/g °K	0.268	0.188		0.31	1.19	0.31	4.14
Thermal conductivity	k, W/cm °K	0.23	1.59	0.0165	0.63	0.0347	0.63	6.00
Outer radius	r, cm	1.50	1.60	1.625	1.725	1.775	1.850	
Thickness	t, cm		0.10	0.025	0.10	0.05	0.075	
Length	L, L', cm	5.00	5.00	5.00	5.00	5.00	6.00	6.00
Temperature coefficients of reactivity	$\delta k/k$ °K	$+2.5 \cdot 10^{-7}$	$-5 \cdot 10^{-7}$		$-1 \cdot 10^{-6}$	0	$-1 \cdot 10^{-6}$	$-1 \cdot 10^{-6}$

Thermionics

Item	Symbol, unit	Value	Item	Symbol, unit	Value
Net current density	I, A/cm^2	10.0	Diode electric load	R_{LD}, $\Omega\ cm^2$	0.06
Effective emitter current	J_2, A/cm^2	11.0	Collector work function	ϕ_3, eV	2.10
Effective collector back emission	J_3, A/cm^2	1.0	Boltzmann constant/electron charge	k_B/e, eV/°K	$8.616 \cdot 10^{-5}$
Diode voltage	V, V	0.6	Stefan-Boltzmann constant	σ_{SB}, $W/cm^2\ °K^4$	$5.67 \cdot 10^{-12}$
Diodes in series	N_{DS}	5.0	Emitter and collector emissivity	ϵ_2, ϵ_3	0.3
Diode assemblies	N_{DP}	50.0			

Primary coolant loop

Item	Symbol, unit	Value	Item	Symbol, unit	Value
Reactor coolant inlet temperature	T_{6i}, °K	1200	Heat-exchanger inlet temperature	T_{Hi}, °K	1250
Reactor coolant outlet temperature	T_{6e}, °K	1250	Heat-exchanger outlet temperature	T_{He}, °K	1200
Coolant flow rate	w_6, g/s	75.3	Heat-exchanger median temperature	T_H, °K	1225
Coolant transport delay	τ_1, τ_2, s	0–10	Heat-exchanger primary side mass	M_H, kg	29.5
Coolant channel velocity	v_6, cm/s	117.0	Heat-exchanger heat capacity	c_{pH}, W s/g °K	0.837

Secondary coolant loop

Item	Symbol, unit	Value	Item	Symbol, unit	Value
Heat-exchanger secondary temperature	T_s, °K	1185	Radiator temperature	T_r, °K	1185
Heat-exchanger secondary inlet temperature	T_{si}, °K	1135	Radiator inlet temperature	T_{ri}, °K	1235
Heat-exchanger secondary outlet temperature	T_{se}, °K	1235	Radiator outlet temperature	T_{re}, °K	1135
Heat-exchanger secondary side mass	M_s, kg	29.5	Radiator pipe length	L_r, cm	200.0
Heat-exchanger heat capacity	c_{p_s}, W s/g °K	0.837	Radiator armor cross section	A_s, cm^2	1.26
Total coolant flow rate	w_{Li}, g/s	1564.0	Armor density	ρ_r, g/cm^3	8.35
Coolant transport delay	τ_3, τ_4, s	0–20	Radiator emissivity	ϵ_r	0.8
Coolant flow rate in radiator pipe	w_r, g/s	31.3	Radiation area (one pipe)	A_r, cm^2	1420.0

[a]Numbers in parentheses are keyed to regions designated in Fig. 2b by circled numbers.

are listed in Table 1, along with the nomenclature used in developing the system equations. The chosen design values do not represent an optimized system, but do represent data close to those expected in a real system.

The reference design has been used for transient and stability studies of the open-loop uncontrolled plant (Ref. 3). Since these are discussed in Ref. 3, only superficial attention will be given to them in this report, and no detailed derivation of the system equations will be given. The extension of these studies to include the control system evaluations was relatively straightforward and could rely on known open-loop dynamic characteristics.

B. Method of Control

The control philosophy adopted for an in-core thermionic reactor powerplant naturally depends on the application. For a potential nuclear–electric ion-propulsion application, a constant-voltage electric power source is desirable. Information on hardware is available for the power-conditioning equipment. The ion-engine system (Refs. 6–9) requires that the low voltage and high current from the thermionic reactor (10–20 V, 5000–2500 A at the reactor terminals for a 50-kW system) be converted to higher voltage. The power-conditioning equipment consists of inverters, transformers, rectifiers, and filters. The internal logic provides the ion-engine startup-shutdown-restart program.

Of the total reactor electrical power output, 10% or less is delivered to "hotel-load" and experimental equipment, the rest being applied to the propulsion system. Up to half the mission time may be spent in a coast mode. The nuclear–electric propulsion application therefore points to the desirability of a variable power output from the reactor. The power conditioner that provides the power and impedance match between the reactor and the electric load gives a coupling that reflects impedance variations directly to the reactor terminals. The thermionic diode current–voltage characteristics, on the other hand, show that the diode voltage and efficiency for a given emitter temperature are sensitive to load changes. This holds particularly at low electrical power demand (high impedance). Since it is desirable, from a power-conditioning point of view, to operate at nearly constant reactor output voltage, it follows that active control must provide a matching between thermal input power and electrical output demand.

During the thrust modes of a mission, electric load perturbations may arise randomly from engine arcs, in which case the driving power-conditioning modules will be shut down. The engine is then immediately restarted ($\lesssim$ 1s time constant) automatically. Other random failures arise from component failures and subsequent switching in of standby modules, and from internal open- and short-circuiting of the thermionic diodes. If the electric load perturbation is relatively small and load-compensating action is taken by the power conditioner within a few seconds, there is no need for adjustment of the reactor power level during the transient. The heat capacity and thermal lag of the reactor system will give small temperature perturbations even for relatively large load variations. For this reason, a dead band and dead time for reactor control-element activation should be built into the controller. A stepping motor would provide discrete reactivity insertions with the stepping rate limited by thermal and safety constraints.

Figure 5 illustrates the above conjectures further. Shown in the figure is a typical set of current–voltage characteristics with the nominal operating point and the equilibrium thermal power lines indicated. Shown also is a constant-voltage control trajectory with specification range. For deviations within the cross-hatched area, no reactor control action is necessary. Within this area, the temperature perturbations are also tolerable and the corresponding reactivity feedback is negligible. But, as mentioned, even for larger electric load perturbations followed by load correction by the power conditioner, no reactor thermal power change is needed by reactivity control. The control dead time is essentially determined by the time it takes for the emitter to change temperature by a set amount, say 50°K. For the worst case, open circuit at the reactor terminals, this time is about 3 s at the nominal operating point for the reference system. Within this time, restart of an ion engine or switch-on of standby modules can be readily achieved. Past the dead time, reactivity control is implemented as required.

The details of the safety requirements are not known at this time. However, thermal-stress considerations imply a relatively slow rate of temperature change for the thermionic diodes. In addition, reactivity rates and reactivity limits will probably be different for insertions and retractions, respectively.

Application of the control features discussed here depends on the particular reactor system. For the purposes of this study, only general investigations are made of the effect of reactivity and reactivity-rate limiting. Startup and shutdown sequences, which also depend on the application, are not discussed. It is assumed that the

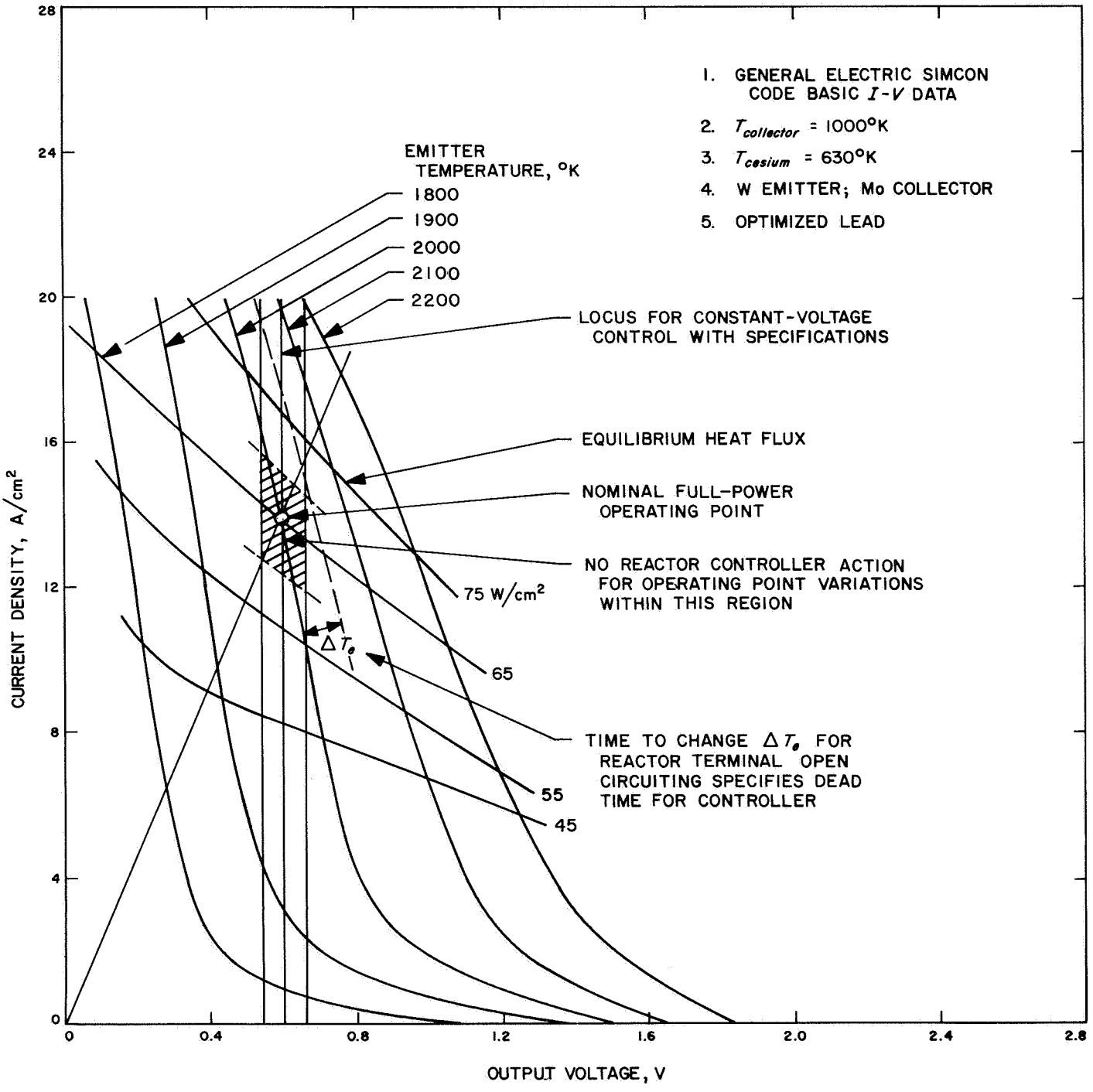

Fig. 5. Illustration of dead-band and dead-time determination for thermionic reactor controller

controller gives a continuous signal to a continuously active control-element driving motor. The controller design is derived from linear theory. A desired dynamic characteristic, which is selected to balance hardware constraints and response demands, is realized exactly.

C. Performance Under Constant-Voltage Control

To minimize fuel burnup during the coast mode of a space mission, it is desirable that the nuclear plant be capable of supplying reduced power at some reasonable fraction of its full-power design efficiency. There is some question about the performance of a thermionic reactor at power levels considerably reduced from its design point, particularly with respect to efficiency. With respect to a spacecraft power conditioner, it is advantageous to operate the thermionic reactor in a constant-voltage-output mode at all power levels.

To assess the efficiency penalty associated with constant-voltage control as opposed to optimum matching of diode characteristics at reduced power, an investigation was made independently of the control system studies to evaluate thermionic diode performance. Although the diode design was different from the one used in the control system studies, the designs are similar enough that general conclusions can be drawn from the data. Operating conditions were set as follows:

(1) Current–voltage characteristics were derived from SIMCON code data with extrapolations to temperatures below 1700°K.[1]

(2) The collector temperature was held constant at 1000°K.

(3) The emitter was of tungsten and the collector of molybdenum. The interelectrode gap was 0.010 in. and the cesium temperature was optimized at each operating point.

It was necessary to select a diode design to make it possible to calculate emitter–collector axial voltage drop, but all other parameters are essentially independent of design details. A survey of output power and efficiency at the operating temperature of 2000°K with lead optimized for each output point was the basis for selection of the nominal full-power operating point. These values and other key parameters are tabulated in Table 2.

The nominal operating point was selected as a compromise between peak efficiency and peak power density.

[1]Private communication of SIMCON code calculations, D. R. Wilkins, General Electric Co., Vallecitos, Calif.

Table 2. Parameter values for thermionic diode performance evaluation

Nominal operating point 14 A/cm², 0.667 V, 9.35 W/cm², 14.4% efficiency (unconditioned net power after emitter–collector and lead losses are subtracted)
Maximum efficiency point 15.3% at 10 A/cm² (P = 8.14 W/cm²)
Maximum power density point 9.76 W/cm² at 18 W/cm² (η = 12.9%)
Nominal operating-point losses Emitter–collector axial voltage drop = 0.070 V Optimized lead voltage drop = 0.081 V Optimized lead thermal conduction loss = 7.8 W/cm² Thermal radiation loss = 11.6 W/cm² Thermal cesium conduction loss = 2.5 W/cm² Thermal electron cooling loss = 43.0 W/cm²
Power desired during coast 10% of nominal full power.

(A criticality-limited core might be designed closer to peak power density and a burnup-limited core might be designed closer to peak efficiency.)

All losses were recomputed at various current–voltage values and emitter temperatures to construct the output current density vs net output voltage curves shown in Fig. 6. The locus of the 10% full-power requirement (0.935 W/cm²) is indicated. Figure 7 shows the efficiency curves replotted against net output voltage with the loci of maximum efficiency, 10% full-power, and constant-voltage output superimposed. To supply 10% of full power at a voltage equal to the full-power voltage, emitter temperature falls to about 1600°K and efficiency falls to 6.7%. If the constraint of constant voltage is removed and efficiency maximized, the result is 1500°K emitter temperature at 7.4% efficiency.

At 10% of full power, a relatively minor efficiency penalty is paid for constant-voltage control as contrasted to that obtained at the optimum voltage output of 0.45 V. The emitter temperature is already 400°K lower than the nominal operating temperature, so little incentive exists for further temperature reduction of 100°K or so. Also, the magnitude of the efficiency, 6.7%, is relatively high for reduced power operation. It appears that in general only minimal efficiency penalties are incurred by the use of constant-voltage control instead of optimal voltage control, down to as low as 10% of full-rated power.

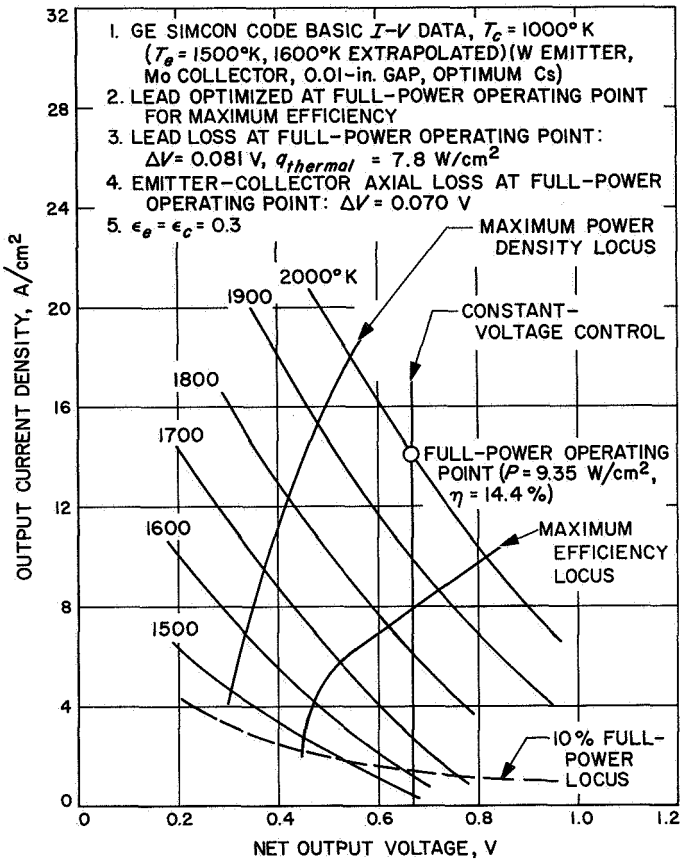

Fig. 6. Output current density vs net output voltage at various emitter temperatures

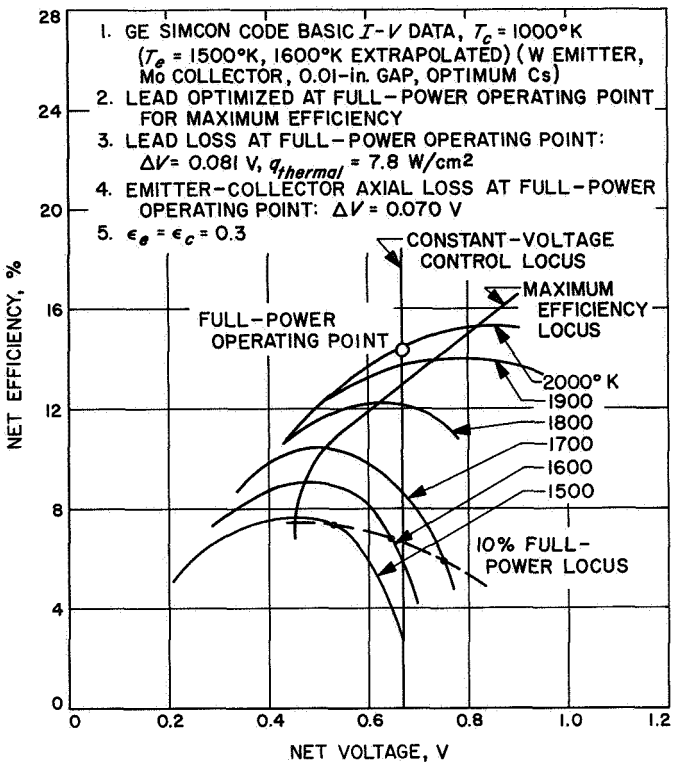

Fig. 7. Net efficiency vs net output voltage at various emitter temperatures

A selected full-power operating point at the peak power density results in a somewhat more favorable reduced-power operating point under constant-voltage control, but the improvement is not very significant: $\eta = 7.3\%$ vs $\eta = 6.7\%$. Besides, full-power flexibility to compensate for diode failures and performance degradation is desired.

Three qualifying statements are in order:

(1) A fixed collector temperature was assumed, implying radiator-area or coolant-flow variation, or both. Fixed coolant-flow rate leading to variable coolant, and hence collector, temperature should also be investigated as probably the simplest system operating mode.

(2) The 1500 and 1600°K emitter temperature curves were extrapolated and substantial uncertainties exist. The effect of these uncertainties on the results, however, are more in the direction of modifying the equilibrium operating temperature and less on the resulting efficiency.

(3) At low emitter temperatures, peculiar inversions and multivalued current–voltage curves exist at fixed cesium conditions for low current densities. Diode output stability in this region may pose some further problems.

III. System Equations

The dynamic characteristics of a liquid-metal-cooled in-core thermionic reactor space powerplant differ from those of other types of nuclear-reactor space powerplants. Because of lack of experimental correlations, there was uncertainty about the best way to develop the system equations within the analytical and computer-time constraints. For the purposes of this preliminary study, a lumped-parameter, spatially averaged model is used. The simplifications are substantial, but from past experience with models for other reactor types, it is believed that the model description suffices for an acceptable first evaluation.

A nonlinear set of equations is developed as the basis for the linear and reduced linear system equations. The linearization is performed by expansion into a Taylor series and retaining zero and first-order terms. The system

equations are then reduced to low order, so as to make more effective their application in the state-variable feedback design of the control system.

A. Description of Model

There is considerable understanding of the effect of linearization of the neutron kinetics equations with associated temperature feedback terms (Refs. 10–14). For the present application, these equations are further simplified by using the prompt-jump approximation, i.e., the prompt-neutron population follows instantaneously the reactivity variations. The effect of the simplifications is to limit the applicability of the linearized equations to well below $100¢$ for both positive and negative step reactivity insertions. Estimates indicate that thermal power transients up to $\pm 50\%$ from equilibrium are acceptable. This corresponds to about a $+40\%$ to -80% change in electric power output at constant emitter temperature or voltage. Over this range in diode performance, the linearization of the equations for the selected current–voltage characteristics and of the equations describing the energy transport in the interelectrode gap gives the same relative accuracy as that of the neutron kinetic equations.

It is assumed that the cesium-reservoir temperature variations are less than $\pm 10°K$ and may be neglected, and that the reservoir temperature is higher than optimum. This implies a penalty in thermal–electric conversion performance. Each current–voltage characteristic point is uniquely determined by a single emitter temperature value in the region of nominal operating conditions. If a current–voltage point is not uniquely determined, i.e., the characteristics cross over, a much more complicated situation arises, and possibilities of open-loop oscillatory behavior exist (Ref. 15). It is, therefore, desirable to operate at higher-than-optimum cesium-reservoir temperature to avoid such system behavior. Figure 8 illustrates the sensitivity of the current–voltage characteristics to cesium-

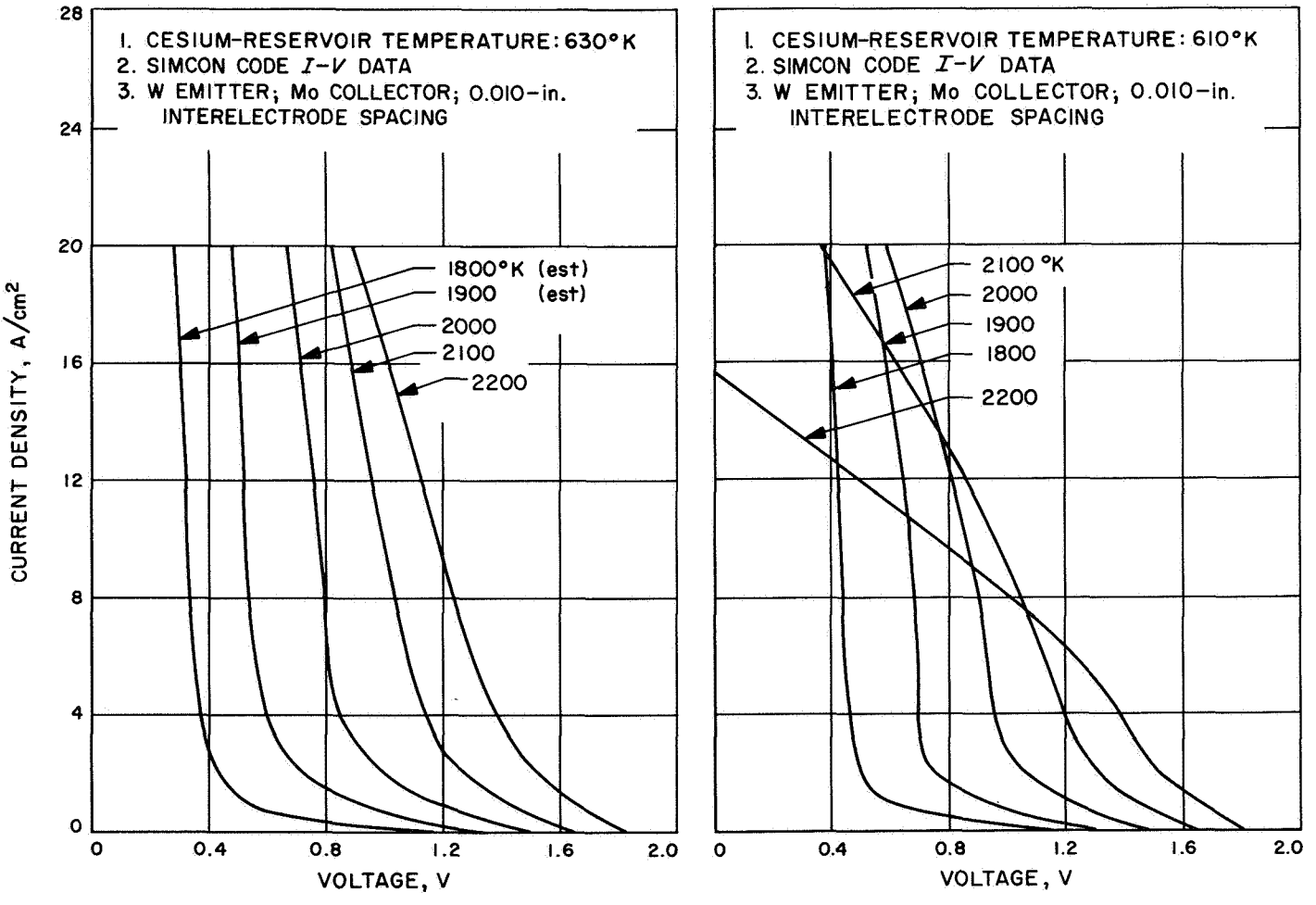

Fig. 8. Current density vs voltage characteristics at two cesium-reservoir temperatures

reservoir temperature changes (saturated vapor pressure) and Fig. 9 shows the characteristics used for the studies in this report. Figure 10 shows the resulting conversion performance for the characteristics in Fig. 9.

Other limitations arise from the assumption of constant parameters and lumping of the spatial regions. The frequency response above ~1 Hz is therefore of limited quantitative accuracy. However, the relevant frequency range for the open-loop uncontrolled plant is below the 1-Hz value.

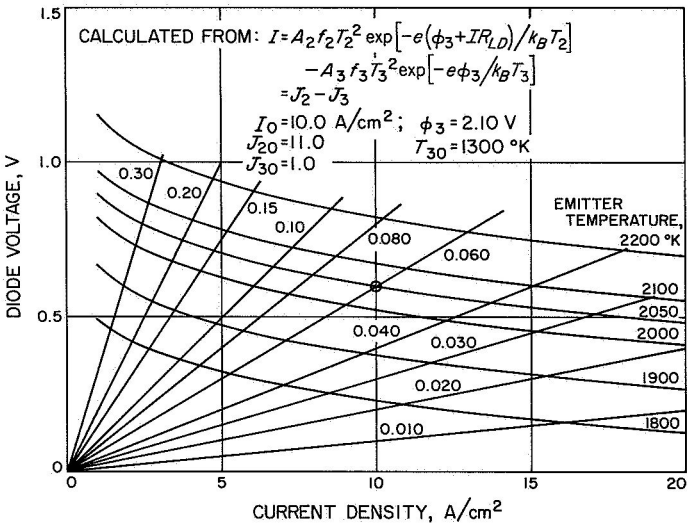

Fig. 9. Current–voltage characteristics used in analytical studies

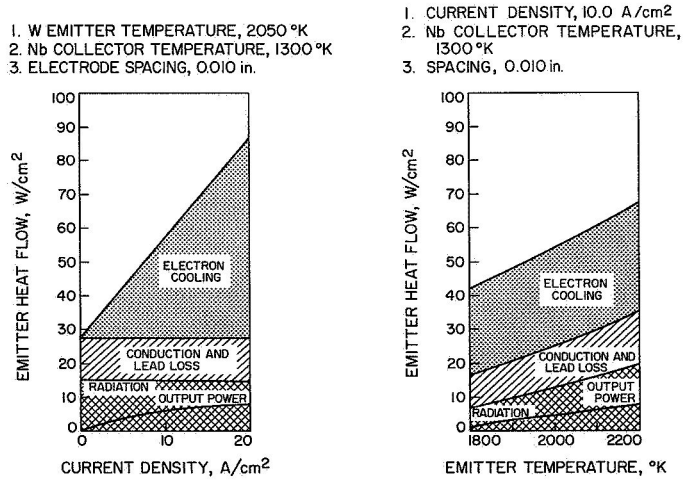

Fig. 10. Emitter heat flow for current–voltage characteristics used in analytical studies

The selection of a proper nonlinear model, which is subsequently linearized, for the thermionic conversion performance presents difficulties. If the range of variation in the operating point is relatively small, substantially different descriptions can be made to yield the experimentally observed behavior. However, for large variations in the operating parameters, the phenomena require complex analytical formulations with correspondingly large computer programs (Ref. 16). The chosen model in this study is essentially a curve fit of a Richardson-Dushman-type equation to experimental data. The energy-balance expression for the diode is written consistent with that equation. These formulations allow a convenient simulation on an analog computer, the principal tool used in the computer studies of the transients. However, as a result of the simplification, the emitter and collector temperature variations should be kept within ±150°K and the current density variation within ±7 A/cm².

It is assumed that all thermionic diodes behave in the same manner in the core and that the electric circuits have no time constants (purely resistive load). Joule heating in the electrodes and leads has been neglected. The thermal conduction losses have been set so as to give an efficiency of 10% at the selected operating point.

The neutron lifetime in the core is in the range of 10^{-7} to 10^{-6} s and the median neutron energy for fission is above 0.1 MeV. The reactor is very fast, which is assumed to lead to a positive doppler effect contribution to the reactivity feedback from temperature variations in the fuel. Negative values are assumed for the tungsten emitter and the niobium collector. The doppler coefficients were estimated from values and procedures given in Ref. 17. This doppler effect is the major prompt-reactivity feedback contributor for the nuclear fuel, emitter, and collector regions. The temperature coefficients of reactivity for other parts of the reactor core and vessel also give significant delayed contributions due to thermal expansion. The values assigned to these regions were estimated.

The thermal-balance equations are written on the assumption that parameters are constant. A radially parabolic temperature profile is used for the nuclear fuel region, and the temperature drop in the emitter, collector, and cladding is neglected. From open-loop transient and stability studies, this has been found to be permissible for the thermal lags and coolant-transport times applicable for the reference design.

B. Equations

The nonlinear and linear versions of the system equations are given in this section. Table 1 gives the initial conditions, parameters, and nomenclature, and Fig. 11 identifies the geometry.

1. Nonlinear equations

a. Neutron kinetics in prompt-jump approximation

$$n = \frac{\sum_{i=1}^{6} \lambda_i C_i}{1-\rho}, \qquad C_i = \Lambda c_i \tag{1}$$

$$\frac{dC_i}{dt} = a_i n - \lambda_i C_i, \qquad i = 1, \cdots, 6 \tag{2}$$

$$\rho = \rho_{control} + \sum_k \alpha_k (T_k - T_{k0}) \tag{3}$$

Equation (1) linearized becomes

$$\delta n = \rho n_0 + \sum_{i=1}^{6} \lambda_i C_i - n_0 \tag{4}$$

b. Nuclear fuel (region 1, Fig. 2b)

$$V_1 \rho_1 c_{p_1} \frac{dT_1}{dt} = V_1 \gamma_1 n - 8\pi L k_1 (T_1 - T_2) \tag{5}$$

c. Emitter (region 2, Fig. 2b)

$$V_2 \rho_2 c_{p_2} \frac{dT_2}{dt} = 8\pi L k_1 (T_1 - T_2) - 2\pi r_2 L q_2'' \tag{6}$$

d. Interelectrode gap (region 23, Fig. 2b)

$$q_{2t}'' = I(IR_{LD} + \phi_3) + \frac{2k_B}{e}(J_2 T_2 - J_3 T_3) + \frac{\sigma_{SB}}{\frac{1}{\epsilon_2} + \frac{1}{\epsilon_3} - 1}(T_2^4 - T_3^4) \tag{7}$$

$$q_{2l}'' = h_{23}(T_2 - T_3) \quad \text{(set to give 10\% efficiency at the selected operating point)} \tag{8}$$

$$q_2'' = q_{2t}'' + q_{2l}'' = 57.5\ \text{W/cm}^2 \text{ at time } t = 0 \tag{9}$$

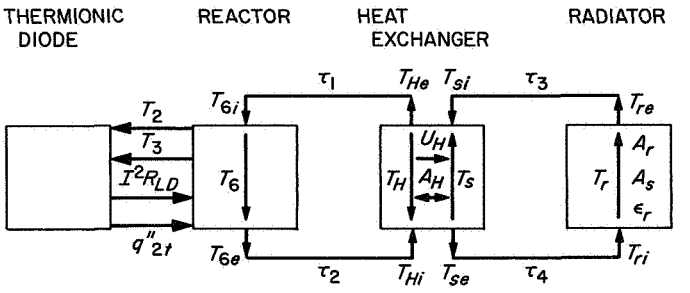

Fig. 11. Thermionic reactor space powerplant model

e. Current–voltage characteristics

$$I = Af_2 T_2^2 \exp\left[-e\frac{\phi_3 + IR_{LD}}{k_B T_2}\right] - Af_3 T_3^2 \exp\left[-e\frac{\phi_3}{k_B T_3}\right] = J_2 - J_3 \tag{10}$$

f. Collector (region 3, Fig. 2b)

$$V_3 \rho_3 c_{p_3} \frac{dT_3}{dt} = 2\pi r_2 L (q_{2t}'' + q_{2l}'' - I^2 R_{LD}) - 4\pi r_{34} L \frac{k_4}{t_4}(T_3 - T_4) \tag{11}$$

g. Insulator (region 4, Fig. 2b)

$$V_4 \rho_4 c_{p_4} \frac{dT_4}{dt} = 4\pi r_{34} L \frac{k_4}{t_4}(T_3 - T_4) - 4\pi r_{34} L \frac{k_4}{t_4}(T_4 - T_5) \tag{12}$$

h. Cladding (region 5, Fig. 2b)

$$V_5 \rho_5 c_{p_5} \frac{dT_5}{dt} = 4\pi r_{34} L \frac{k_4}{t_4}(T_4 - T_5) - h_{56} 2\pi r_5 L'(T_5 - T_6) \tag{13}$$

i. Coolant in reactor (region 6, Fig. 2b)

$$N_{DS} V_6 \rho_6 c_{p_6} \frac{dT_6}{dt} = N_{DS} h_{56} 2\pi r_5 L'(T_5 - T_6) - w_6 c_{p_6}(T_{6e} - T_{6i}) \tag{14}$$

$$T_6 = \frac{1}{2}(T_{6e} + T_{6i}) \tag{15}$$

j. Primary coolant loop

$$M_H c_{p_H} \frac{dT_H}{dt} = N_{DP} w_6 c_{p_6} (T_{Hi} - T_{He}) - U_H A_H (T_H - T_s) \tag{16}$$

$$T_H = \frac{1}{2}(T_{He} + T_{Hi}) \tag{17}$$

$$T_{Hi}(t) = T_{6e}(t - \tau_2) \tag{18}$$

$$T_{6i}(t) = T_{He}(t - \tau_1) \tag{19}$$

k. Secondary coolant loop

$$M_s c_{p_s} \frac{dT_s}{dt} = U_H A_H (T_H - T_s) - w_{Li} c_{p_{Li}} (T_{se} - T_{si}) \tag{20}$$

$$T_s = \frac{1}{2}(T_{se} + T_{si}) \tag{21}$$

$$T_{si}(t) = T_{re}(t - \tau_3) \tag{22}$$

$$T_{ri}(t) = T_{se}(t - \tau_4) \tag{23}$$

$$L_r A_s \rho_r c_{p_r} \frac{dT_r}{dt} = w_r c_{p_{Li}} (T_{ri} - T_{re}) - \epsilon_r \sigma_{SB} A_r T_r^4 \tag{24}$$

2. *Linear equations.* Linearization of the nonlinear equations in the set (1) through (24) and rewriting the whole set in terms of deviations from the postulated equilibrium gives the following system equations. Parameter values given in Table 1 have been substituted into the thermal-balance equations.

a. Neutron kinetics in prompt-jump approximation

$$\delta n = n_0 \left(\rho_{control} + \sum_k \alpha_k \theta_k \right) + \sum_{i=1}^{6} \lambda_i \delta C_i \tag{25}$$

$$\delta \dot{C}_i = a_i \, \delta n - \lambda_i \, \delta C_i, \quad i = 1, \cdots, 6 \tag{26}$$

b. Thermal-balance equations ($\Delta T_i = \theta_i$)

$$\dot{\theta}_1 = 3.082 \, \delta n - 0.3082 (\theta_1 - \theta_2) \tag{27}$$

$$\dot{\theta}_2 = 1.754 (\theta_1 - \theta_2) - 0.05032 (\theta_2 - \theta_3) - 0.3297 \theta_2 + 0.05868 \theta_3 + 1161 \, \delta R_{LD} \tag{28}$$

$$\dot{\theta}_3 = 0.3297 (\theta_2 - \theta_3) - 5.636 (\theta_3 - \theta_4) + 0.04552 \theta_2 + 0.2122 \theta_3 - 1198 \, \delta R_{LD} \tag{29}$$

$$\dot{\theta}_4 = 4.639 (\theta_3 - \theta_4) - 4.639 (\theta_4 - \theta_5) \tag{30}$$

$$\dot{\theta}_5 = 6.928 (\theta_4 - \theta_5) - 31.54 (\theta_5 - \theta_6) \tag{31}$$

$$\dot{\theta}_6 = 26.10 (\theta_5 - \theta_6) - 7.778 (\theta_6 - \theta_{6i}) \tag{32}$$

$$\dot{\theta}_{6i} = -10 \theta_{6i} - 10 \theta_{Hi} + 20 \theta_H, \quad \tau_1 = 0.1 \text{ s} \tag{33}$$

$$\dot{\theta}_{Hi} = -10 \theta_{6i} - 10 \theta_{Hi} + 20 \theta_6, \quad \tau_2 = 0.1 \text{ s} \tag{34}$$

$$\dot{\theta}_H = 1.0483 (\theta_{Hi} - \theta_H) - 0.6552 (\theta_H - \theta_s) \tag{35}$$

$$\dot{\theta}_s = 0.6552 (\theta_H - \theta_s) - 0.5242 (\theta_s - \theta_{si}) \tag{36}$$

$$\dot{\theta}_{si} = -10 \theta_{si} - 10 \theta_{ri} + 20 \theta_r, \quad \tau_3 = 0.1 \text{ s} \tag{37}$$

$$\dot{\theta}_{ri} = -10 \theta_{si} - 10 \theta_{ri} + 20 \theta_s, \quad \tau_4 = 0.1 \text{ s} \tag{38}$$

$$\dot{\theta}_r = 0.3971 (\theta_{ri} - \theta_r) - 0.0669 \theta_r \tag{39}$$

The linearized equations for the energy transport in the interelectrode gap (Eq. 8) and for the current–voltage characteristics (Eq. 10), become, respectively,

$$\delta q''_{2t} = 0.1081 \theta_2 - 0.0192 \theta_3 - 380.6 \, \delta R_{LD} \tag{40}$$

$$\delta I = 0.0196 \theta_2 - 0.0036 \theta_3 - 131.49 \, \delta R_{LD} \tag{41}$$

$$\delta V = 0.001175 \theta_2 - 0.000202 \theta_3 + 2.111 \, \delta R_{LD} \tag{42}$$

$$\delta I = -61.3 \, \delta V + 0.0928 \theta_2 - 0.01618 \theta_3 \tag{43}$$

Finally, writing out Eqs. (25) through (39) in matrix notation gives the 19 × 19 matrix shown in Eq. (44). Two perturbing inputs are considered: reactivity perturbations and electric load variations. The controller is to be designed so that $\rho_{control}$ effectively counteracts electric load variations to keep the output voltage constant.

Eq. (44). Matrix representation of linearized system equations for thermionic reactor powerplant reference design, $\dot{\mathbf{x}} = A\mathbf{x} + \mathbf{b}u$

$$
\begin{bmatrix}
\delta\dot{C}_1 \\ \delta\dot{C}_2 \\ \delta\dot{C}_3 \\ \delta\dot{C}_4 \\ \delta\dot{C}_5 \\ \delta\dot{C}_6 \\ \dot{\theta}_1 \\ \dot{\theta}_2 \\ \dot{\theta}_3 \\ \dot{\theta}_4 \\ \dot{\theta}_5 \\ \dot{\theta}_6 \\ \dot{\theta}_{6i} \\ \dot{\theta}_{Hi} \\ \dot{\theta}_H \\ \dot{\theta}_s \\ \dot{\theta}_{si} \\ \dot{\theta}_{ri} \\ \dot{\theta}_r
\end{bmatrix}
=
\begin{bmatrix}
-3.7787 & 0.0367 & 8.12 \cdot 10^{-3} & 3.03 \cdot 10^{-3} & 8.28 \cdot 10^{-4} & 3.22 \cdot 10^{-4} & 1.011 \cdot 10^{-5} & -2.022 \cdot 10^{-5} & -4.044 \cdot 10^{-5} & 0 & -4.044 \cdot 10^{-5} & -4.044 \cdot 10^{-5} & 0 & 0 & 0 & 0 & 0 & 0 & 0 \\
0.406 & -1.2211 & 0.03975 & 0.01482 & 4.05 \cdot 10^{-3} & 1.622 \cdot 10^{-3} & 4.95 \cdot 10^{-5} & -9.90 \cdot 10^{-5} & -1.98 \cdot 10^{-4} & 0 & -1.98 \cdot 10^{-4} & -1.98 \cdot 10^{-4} & 0 & 0 & 0 & 0 & 0 & 0 & 0 \\
1.586 & 0.572 & -0.184 & 0.0474 & 0.01295 & 5.19 \cdot 10^{-3} & 1.585 \cdot 10^{-4} & -3.17 \cdot 10^{-4} & -6.33 \cdot 10^{-4} & 0 & -6.33 \cdot 10^{-4} & -6.33 \cdot 10^{-4} & 0 & 0 & 0 & 0 & 0 & 0 & 0 \\
0.728 & 0.253 & 0.0584 & -0.0942 & 5.95 \cdot 10^{-3} & 2.38 \cdot 10^{-3} & 7.27 \cdot 10^{-5} & -1.454 \cdot 10^{-4} & -2.91 \cdot 10^{-4} & 0 & -2.91 \cdot 10^{-4} & -2.91 \cdot 10^{-4} & 0 & 0 & 0 & 0 & 0 & 0 & 0 \\
0.8245 & 0.2975 & 0.06615 & 0.02464 & -0.02496 & 2.70 \cdot 10^{-3} & 8.24 \cdot 10^{-5} & -1.648 \cdot 10^{-4} & -3.295 \cdot 10^{-4} & 0 & -3.295 \cdot 10^{-4} & -3.295 \cdot 10^{-4} & 0 & 0 & 0 & 0 & 0 & 0 & 0 \\
0.1474 & 0.0532 & 0.01183 & 4.41 \cdot 10^{-3} & 1.204 \cdot 10^{-3} & -1.222 \cdot 10^{-2} & 1.473 \cdot 10^{-5} & -2.946 \cdot 10^{-5} & -5.892 \cdot 10^{-5} & 0 & -5.892 \cdot 10^{-5} & -5.892 \cdot 10^{-5} & 0 & 0 & 0 & 0 & 0 & 0 & 0 \\
11.96 & 4.32 & 0.959 & 0.348 & 0.0977 & 0.0391 & -0.3070 & 0.3058 & -4.78 \cdot 10^{-3} & 0 & -4.78 \cdot 10^{-3} & -4.78 \cdot 10^{-3} & 0 & 0 & 0 & 0 & 0 & 0 & 0 \\
0 & 0 & 0 & 0 & 0 & 0 & 1.754 & -2.134 & 0.109 & 0 & 0 & 0 & 0 & 0 & 0 & 0 & 0 & 0 & 0 \\
0 & 0 & 0 & 0 & 0 & 0 & 0 & 0.3752 & -5.7535 & 5.636 & 0 & 0 & 0 & 0 & 0 & 0 & 0 & 0 & 0 \\
0 & 0 & 0 & 0 & 0 & 0 & 0 & 0 & 4.639 & -9.278 & 4.639 & 0 & 0 & 0 & 0 & 0 & 0 & 0 & 0 \\
0 & 0 & 0 & 0 & 0 & 0 & 0 & 0 & 0 & 6.928 & -38.468 & 31.54 & 0 & 0 & 0 & 0 & 0 & 0 & 0 \\
0 & 0 & 0 & 0 & 0 & 0 & 0 & 0 & 0 & 0 & 26.10 & -33.878 & 7.778 & 0 & 0 & 0 & 0 & 0 & 0 \\
0 & 0 & 0 & 0 & 0 & 0 & 0 & 0 & 0 & 0 & 0 & 0 & -10 & -10 & 20 & 0 & 0 & 0 & 0 \\
0 & 0 & 0 & 0 & 0 & 0 & 0 & 0 & 0 & 0 & 0 & 20 & -10 & -10 & 0 & 0 & 0 & 0 & 0 \\
0 & 0 & 0 & 0 & 0 & 0 & 0 & 0 & 0 & 0 & 0 & 0 & 0 & 1.0483 & -1.7035 & 0.6552 & 0 & 0 & 0 \\
0 & 0 & 0 & 0 & 0 & 0 & 0 & 0 & 0 & 0 & 0 & 0 & 0 & 0 & 0.6552 & -1.1794 & 0.5242 & 0 & 0 \\
0 & 0 & 0 & 0 & 0 & 0 & 0 & 0 & 0 & 0 & 0 & 0 & 0 & 0 & 0 & 0 & -10 & -10 & 20 \\
0 & 0 & 0 & 0 & 0 & 0 & 0 & 0 & 0 & 0 & 0 & 0 & 0 & 0 & 0 & 0 & 20 & -10 & -10 & 0 \\
0 & 0 & 0 & 0 & 0 & 0 & 0 & 0 & 0 & 0 & 0 & 0 & 0 & 0 & 0 & 0 & 0 & 0.3971 & -0.464
\end{bmatrix}
\begin{bmatrix}
\delta C_1 \\ \delta C_2 \\ \delta C_3 \\ \delta C_4 \\ \delta C_5 \\ \delta C_6 \\ \theta_1 \\ \theta_2 \\ \theta_3 \\ \theta_4 \\ \theta_5 \\ \theta_6 \\ \theta_{6i} \\ \theta_{Hi} \\ \theta_H \\ \theta_s \\ \theta_{si} \\ \theta_{ri} \\ \theta_r
\end{bmatrix}
+
\begin{bmatrix}
0.261 & 0 \\ 1.278 & 0 \\ 4.079 & 0 \\ 1.877 & 0 \\ 2.125 & 0 \\ 0.380 & 0 \\ 30.82 & 0 \\ 0 & 1161.2 \\ 0 & 1198.3 \\ 0 & 0 \\ 0 & 0 \\ 0 & 0 \\ 0 & 0 \\ 0 & 0 \\ 0 & 0 \\ 0 & 0 \\ 0 & 0 \\ 0 & 0 \\ 0 & 0
\end{bmatrix}
\begin{bmatrix}
\rho_c \\ \delta R_{LD}
\end{bmatrix}
$$

3. Reduced linear system equations. The developed linear 19th-order powerplant description (Eqs. 25 through 39), along with the auxiliary thermionic performance equations (40 through 43), is far too complicated for effective use in the initial design of the control system. As mentioned earlier, the state-variable feedback design method is used, but obviously not all state variables are of equal importance as feedback elements to the controller. In reducing the system further, use is made of the information obtained from transient and stability studies of the complete model. From these results it may be concluded that it is important to keep the fuel–emitter complex and the collector as separate entities, but that the entire heat-rejection system may be lumped. A somewhat improved model in which the fuel and emitter are kept as separate regions was also developed. The delay times for coolant transport may be neglected because of large thermal lags associated with the heat-rejection system components. The equations for the collector and heat-rejection system are, respectively,

$$V_3\rho_3 c_{p_3}\dot{\theta}_3 = 2\pi r_2 L\,[\delta q_2'' - \delta\,(I^2R_{LD})] - U_{eq}A_c\,(\theta_3 - \theta_r) \tag{45}$$

$$\sum_l V_l\rho_l c_{p_e}\dot{\bar{\theta}}_r = U_{eq}A_c\,(\theta_3 - \theta_r) - 0.0669\,\theta_r \tag{46}$$

From the temperature profile shown in Fig. 12, the thermal resistance becomes

$$\frac{1}{U_{eq}A_c} = \sum_l \frac{1}{h_l A_l} = \frac{1}{22.51}\ ^\circ\text{K/W} \tag{47}$$

where the index l refers to all regions past the collector.

For simplicity, $\dot{\bar{\theta}}_r$ may be set equal to $\dot{\theta}_r$ in Eq. (46). The neutron kinetics equations may be reduced to a single equation with $\bar{\lambda} = 0.1\ s^{-1}$. The temperature coefficients of reactivity for the cladding and coolant regions are assigned to θ_r in Eq. (46). Also, since voltage will be the controlled variable, it is convenient to select the voltage as one of the state variables by use of Eq. (42) and eliminate the emitter temperature variable. With the above modifications, the reduced set of system equations for the fourth-order powerplant is as follows:

a. Neutron kinetics equations

$$\delta\dot{n} = 0.1\,\delta C - 1.64\cdot 10^{-3}\,\theta_3 - 0.40\,\delta V - 0.00313\,\theta_r + 10\,\rho_{control} + 1.4\,\delta\dot{R}_{LD} \tag{48}$$

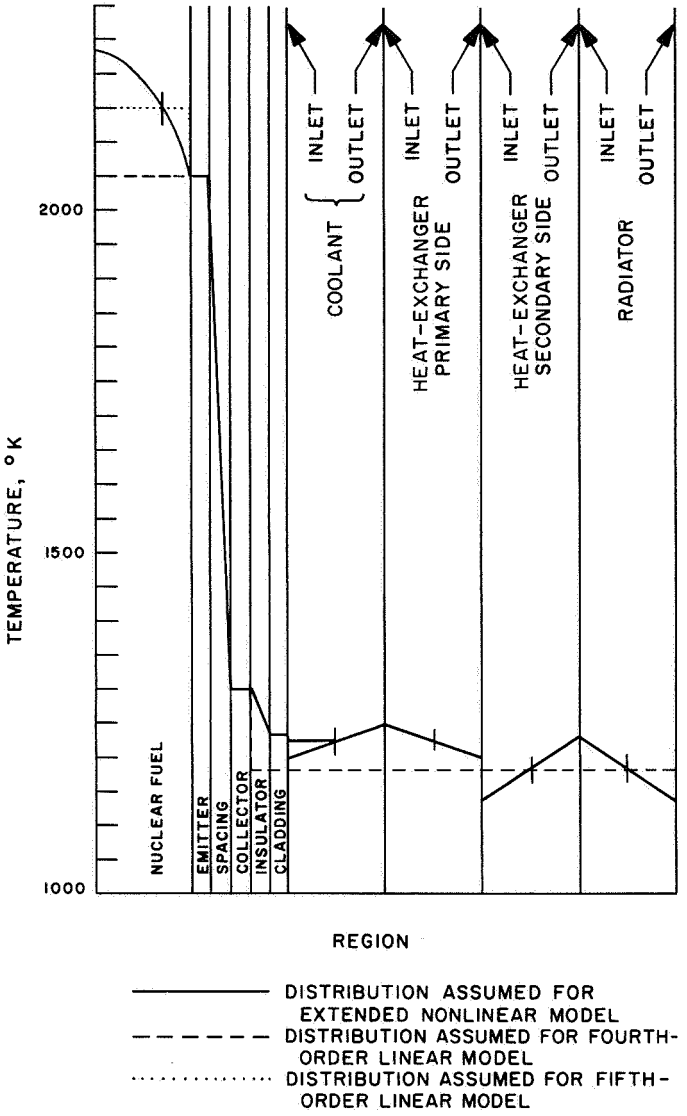

Fig. 12. Temperature distributions for thermionic reactor space powerplant models

$$\delta\dot{C} = \delta n - 0.1\,\delta C \tag{49}$$

b. Thermal-balance equations

$$\dot{\theta}_3 = 1.714\,\theta_3 + 319.3\,\delta V + 1.662\,\theta_r + 1872\,\delta R_{LD} \tag{50}$$

$$\delta\dot{V} = 3.08\cdot 10^{-4}\,\delta C + 3.53\cdot 10^{-4}\,\theta_3 - 0.123\,\delta V - 3.44\cdot 10^{-4}\,\theta_r + 6.248\,\delta R_{LD} + 2.111\,\delta\dot{R}_{LD} \tag{51}$$

$$\dot{\theta}_r = 0.0819\,\theta_3 - 0.1137\,\theta_r \tag{52}$$

For the fifth-order powerplant, in which the fuel and emitter regions are separated, the equations are as follows:

a. Neutron kinetics equations

$$\delta n = 3.91 \cdot 10^{-4}\,\theta_1 - 1.69 \cdot 10^{-3}\,\theta_3 - 0.665\,\delta V - 0.00313\,\theta_r + 0.1\,\delta L + 10\,\rho_{control} + 1.4\,\delta R_{LD} \quad (53)$$

$$\delta \dot{C} = \delta n - 0.1\,\delta C \quad (54)$$

b. Thermal-balance equations

$$\dot{\theta}_1 = 3.082\,\delta n - 0.3082\,\theta_1 + 0.053\,\theta_3 + 262.3\,\delta V - 553.8\,\delta R_{LD} \quad (55)$$

$$\dot{\theta}_3 = 1.714\,\theta_3 + 319.3\,\delta V + 1.662\,\theta_r + 1872\,\delta R_{LD} \quad (56)$$

$$\delta \dot{V} = 2.061 \cdot 10^{-3}\,\theta_1 + 4.31 \cdot 10^{-5}\,\theta_3 - 2.198\,\delta V - 3.347 \cdot 10^{-4}\,\theta_r + 6.248\,\delta R_{LD} + 2.111\,\delta \dot{R}_{LD} \quad (57)$$

$$\dot{\theta}_r = 0.0819\,\theta_3 - 0.1137\,\theta_r \quad (58)$$

$$\dot{\theta}_2 = 851.5\,\delta V + 0.172\,\theta_3 - 1795\,\delta R_{LD} \quad (59)$$

4. Transfer function for the uncontrolled system. The linear models represented by the set of reduced system equations (48) through (52) and the set (53) through (59) were simulated on an analog computer. The response trajectories to reactivity and electric load perturbations were compared with simulation results for the complete nonlinear model (Eqs. 1–24). Figure 13 shows the comparison for the fourth-order model for a 2ϕ positive and negative reactivity step. The reduced linear system response shows the same general behavior as that of the nonlinear system, with tolerable errors in the state-variable trajectories.

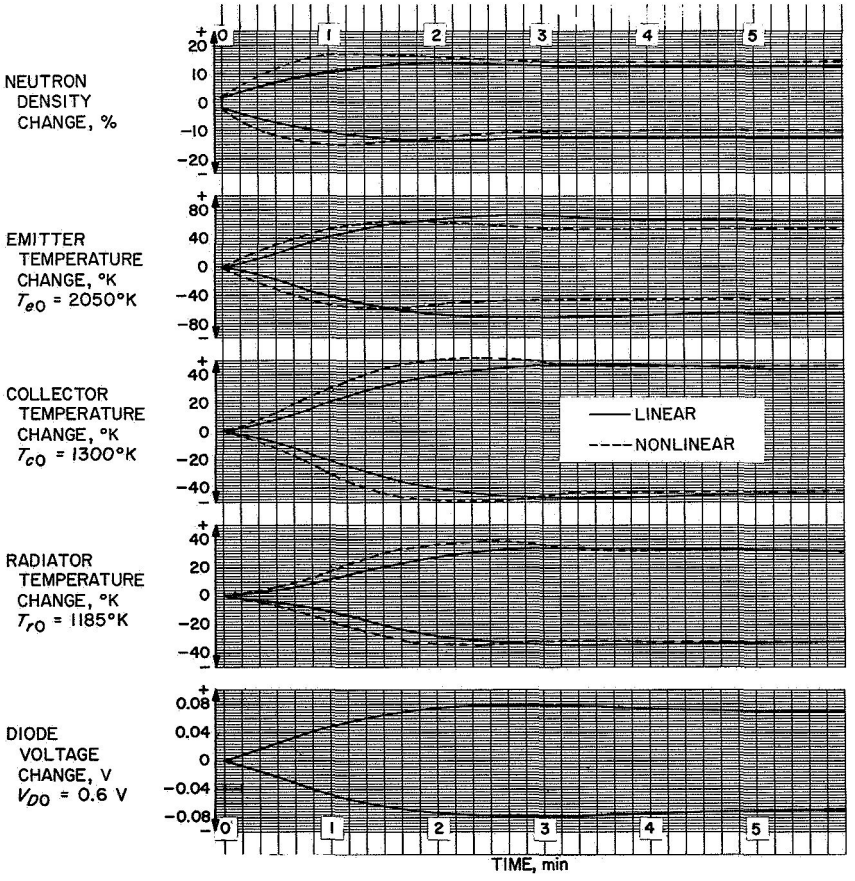

Fig. 13. Responses of nonlinear and linear models of open-loop thermionic reactor space powerplant to a 2ϕ step and a -2ϕ step reactivity perturbation

Figure 14 compares the linear model response with the nonlinear model for a $-0.02\ \Omega\ cm^2$ step change in electric load. The new equilibrium corresponds to approximately a 20% increase in electric current output. The general behavior of the linear and nonlinear system models is again the same, but at some time instants the deviations in the state variables are quite large. However, for large perturbations in the uncontrolled nonlinear system, one would expect a significant difference between its response and that of the low-order linear system. The Bode plots for the two system descriptions are shown in Fig. 15 for the transfer function $\rho_c(s)/\delta V(s)$. The Bode plot for the nonlinear system was measured with the analog simulation and a transfer-function analyzer. A small reactivity perturbation was used so as to stay within the range of applicability of the linear system equations (25) through (43).

It is noted from Fig. 15 that the frequency response of the low-order model closely matches that of the high-order model for amplitudes close to the 0 dB, or gain of 1, line. Since this is the frequency range that will dominate the response, the low-order model is a good approximation.

Supported by the preceding comparisons, one may expect to obtain from the reduced set of linear equations a control system with associated state-variable feedback coefficients that may be applied to the linear high-order model. Further, state-variable feedback control, which is

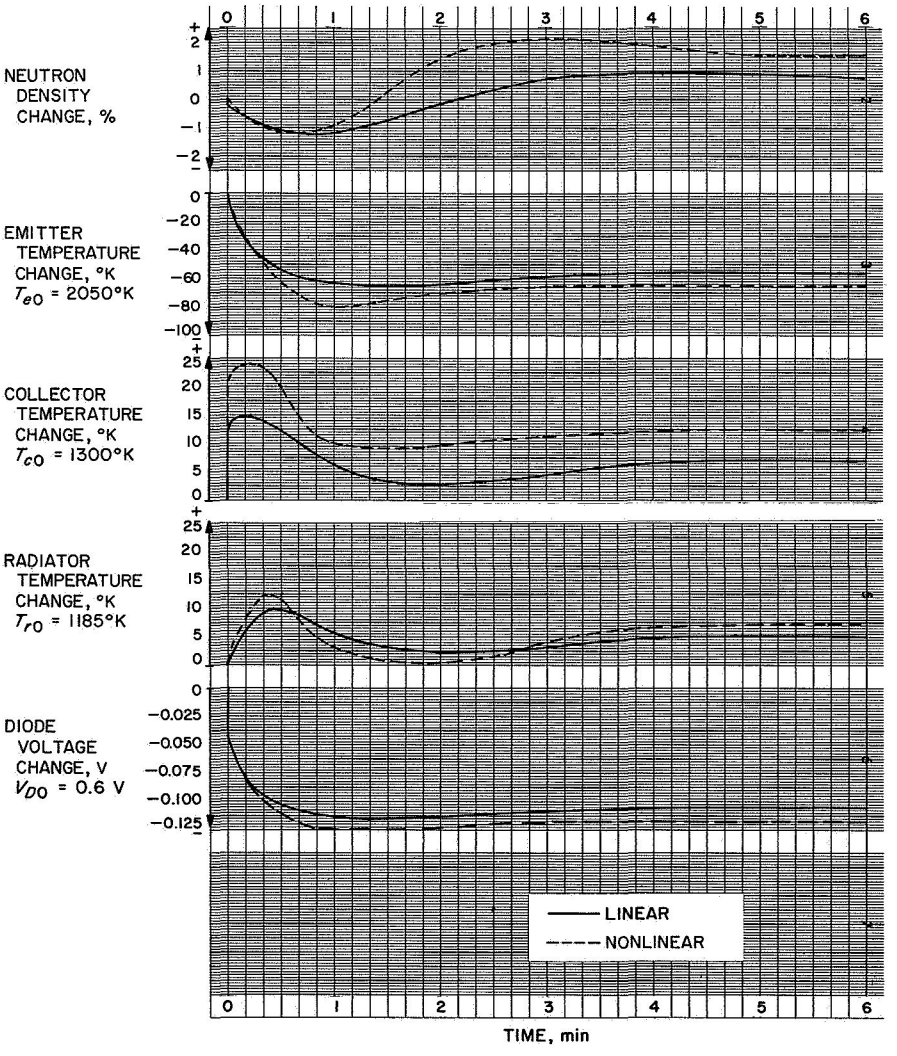

Fig. 14. Responses of nonlinear and linear models of open-loop thermionic reactor space powerplant to a step change of $-0.02\ \Omega\ cm^2$ in electric load

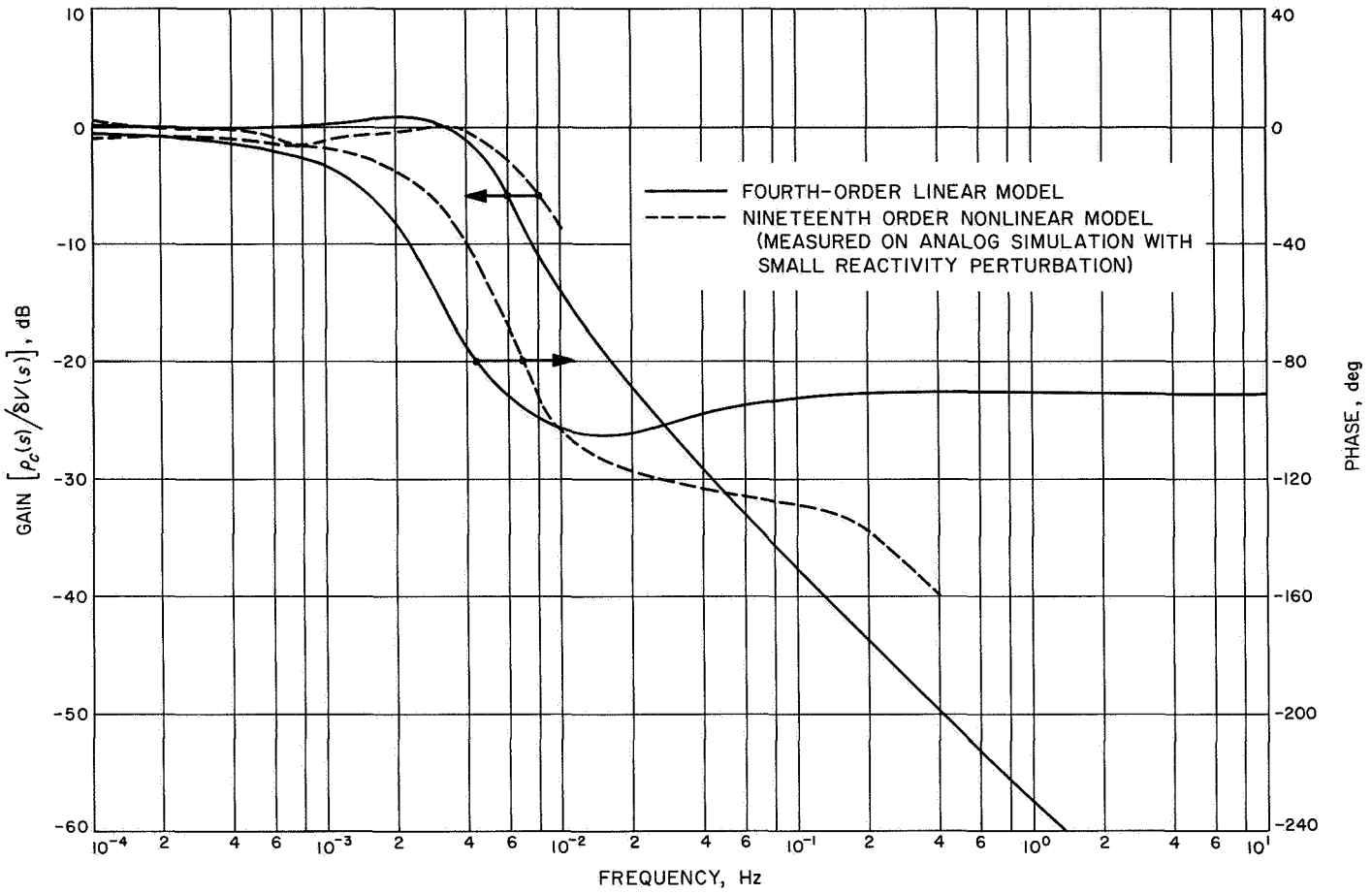

Fig. 15. Comparison of Bode plots for linear fourth-order open-loop and nonlinear open-loop system models

the method of control used in this study (as described in Section IV), tends to keep the signal level low throughout the system, and thus in the linear range of operation. As a result, the linear model can also be expected to be a valid approximation for the controlled nonlinear system.

A computer code has been written at the University of Arizona to calculate open- and closed-loop transfer functions as well as the feedback coefficients required to obtain the desired system dynamics (Ref. 18). The code can handle systems up to order twenty. This code, together with root locus and transfer-function computing and plotting programs developed at JPL[2], was used extensively.

In matrix notation, the linearized system equations for single input and single output are written as follows:

$$\dot{\mathbf{x}} = A\mathbf{x} + \mathbf{b}u \qquad \text{(system equations)} \qquad (60)$$

$$y = \mathbf{c}^T\mathbf{x} \qquad \text{(system output)} \qquad (61)$$

where $\mathbf{x}$ is the state vector, A the system matrix, $\mathbf{b}$ the control vector, u a scalar control of the system output, and $\mathbf{c}$ the output vector that relates the state variables to the system output. Applying the Laplace transform to Eq. (61) and assuming that all initial conditions are zero, one finds the system transfer function to be

$$\left[\frac{y(s)}{u(s)}\right] = G(s) = \mathbf{c}^T(sI - A)^{-1}\mathbf{b} \qquad (62)$$

where s is the transform variable. The above notation is used in the computed results that follow for the fifth-order linear system with reactivity perturbations. (The results for the fourth-order system are given in Section IV-C in connection with the discussion of the final controller design.)

[2]E. Kopf and R. Mankovitz, *Linear Control System Analysis Package for the IBM 7094*, JPL internal document, Engineering Memo 344-72, Aug. 1967.

a. Equations with voltage as state variable

$$A = \left[\begin{array}{c|c|c|c|c|l} 0 & 3.91 \cdot 10^{-4} & -1.69 \cdot 10^{-3} & -0.665 & 3.12 \cdot 10^{-3} & \text{Precursor density} \\ 0.3082 & -0.307 & 4.8 \cdot 10^{-3} & 260.2 & 9.62 \cdot 10^{-3} & \text{Fuel temperature} \\ 0 & 0 & -1.714 & 319.3 & 1.662 & \text{Collector temperature} \\ 0 & 2.061 \cdot 10^{-3} & 4.31 \cdot 10^{-5} & -2.198 & 3.357 \cdot 10^{-4} & \text{Voltage} \\ 0 & 0 & 8.19 \cdot 10^{-2} & 0 & -0.1137 & \text{Radiator temperature} \end{array}\right] \tag{63}$$

$$\mathbf{b}^T = \left[\begin{array}{c|c|c|c|c} 10 & 30.82 & 0 & 0 & 0 \end{array}\right] \tag{64}$$

$$G_i(s) = \frac{N_i(s)}{D(s)}$$

$$= \frac{N_i(s)}{(s + 1.617 \cdot 10^{-3} + j1.725 \cdot 10^{-3})(s + 1.617 - j1.725 \cdot 10^{-3})(s + 7.631 \cdot 10^{-2})(s + 1.811)(s + 2.442)} \tag{65}$$

Output variables and associated transfer-function zeros are tabulated as follows:

i	Output variable	Transfer-function zeros			
1	Precursor density , δC	$-2.617 \cdot 10^{-3}$	$-7.631 \cdot 10^{-2}$	-1.811	-2.442
2	Fuel temperature , θ_1	$-3.014 \cdot 10^{-2}$	-0.1	-1.776	-2.220
3	Collector temperature, θ_3	-0.1	-0.1137		
4	Voltage , δV	$-3.274 \cdot 10^{-2}$	-0.1	-1.795	
5	Radiator temperature , θ_r	-0.1			

b. Equations with emitter as state variable

$$A = \left[\begin{array}{c|c|c|c|c|l} 0 & 3.91 \cdot 10^{-4} & -7.81 \cdot 10^{-4} & -1.56 \cdot 10^{-3} & -3.12 \cdot 10^{-3} & \text{Precursor density} \\ 0.3081 & -0.307 & -.3058 & -4.81 \cdot 10^{-3} & -7.62 \cdot 10^{-3} & \text{Fuel temperature} \\ 0 & 1.754 & -2.134 & 0.109 & 0 & \text{Emitter temperature} \\ 0 & 0 & 0.3752 & -1.779 & 1.662 & \text{Collector temperature} \\ 0 & 0 & 0 & 8.19 \cdot 10^{-2} & -0.1137 & \text{Radiator temperature} \end{array}\right] \tag{66}$$

$$\mathbf{b}^T = \left[\begin{array}{c|c|c|c|c} 10 & 30.82 & 0 & 0 & 0 \end{array}\right] \tag{67}$$

$$G_i(s) = \frac{N_i(s)}{D(s)}$$

$$= \frac{N_i(s)}{(s + 1.82 \cdot 10^{-2} + j1.554 \cdot 10^{-2})(s + 1.182 \cdot 10^{-2} - j1.554 \cdot 10^{-2})(s + 4.901 \cdot 10^{-2})(s + 1.798)(s + 2.453)} \tag{68}$$

The output variables and associated transfer-function zeros are tabulated as follows:

i	Output variable	Transfer-function zeros			
1	Precursor density , δC	$-2.557 \cdot 10^{-2}$	$-5.591 \cdot 10^{-2}$	-1.801	-2.453
2	Fuel temperature , θ_1	$-3.478 \cdot 10^{-2}$	-0.1	-1.754	-2.238
3	Emitter temperature , θ_2	$-3.561 \cdot 10^{-2}$	-0.1	-1.857	
4	Collector temperature, θ_3	-0.1	-0.1137		
5	Radiator temperature , θ_r	-0.1			

IV. Control System Design

This section discusses a control system design for the thermionic reactor model presented in Section III. To begin, a discussion of the state-variable feedback design method and its relation to system specifications, sensitivity, and stability is presented. Next, consideration is given to the selection of a controller and overall system dynamics. The section concludes with a discussion of limiting the control u, in order to constrain the system states, and the final control system design.

A. State-Variable Feedback Control

In the state-variable feedback design method, the control philosophy and design specifications are developed by feeding back all the state or system variables through constant-gain, frequency-independent elements. The values of these elements or feedback coefficients depend upon the desired system dynamics, which are specified in terms of a desired system transfer function. Through state-variable feedback design, the desired system dynamics can be realized exactly. To apply this design method, the system equations must be put in the form

$$\dot{\mathbf{x}}(t) = A\mathbf{x}(t) + \mathbf{b}u(t) \tag{69}$$

$$y(t) = \mathbf{c}^T\mathbf{x}(t) \tag{70}$$

where

$$u(t) = \mathbf{h}^T\mathbf{x}(t) + r(t)$$

and $\mathbf{x}$ is an n-dimensional state vector, u is the control, A is an $n \times n$ system matrix, $\mathbf{b}$ is an n-dimensional control vector, $\mathbf{h}$ is an n-dimensional feedback vector, and r is the input variable.

The superscript T denotes the transpose of the column matrix and $\mathbf{c}$ is the output vector, relating the output y to the state variables x. Figure 16 is a block diagram of state-variable feedback control.

The system transfer function [y(s)/r(s)] is obtained by applying the Laplace transform to Eqs. (69) and (70) with the usual assumption in transfer-function determination that all initial conditions are zero. Transformation of Eqs. (69) and (70) gives

$$s\mathbf{x}(s) = A\mathbf{x}(s) + \mathbf{b}\mathbf{h}^T\mathbf{x}(s) + \mathbf{b}r(s) \tag{71}$$

$$y(s) = \mathbf{c}^T\mathbf{x}(s) \tag{72}$$

When the terms in $\mathbf{x}(s)$ are grouped, Eq. (71) becomes

$$(sI - A - \mathbf{b}\mathbf{h}^T)\mathbf{x}(s) = \mathbf{b}r(s) \tag{73}$$

where I is the identity matrix. Premultiplying both sides of Eq. (73) by the inverse $(sI - A - \mathbf{b}\mathbf{h}^T)^{-1}$ gives

$$\mathbf{x}(s) = (sI - A - \mathbf{b}\mathbf{h}^T)^{-1}\mathbf{b}r(s) \tag{74}$$

When this result is substituted into Eq. (72), $y(s)$ is given by

$$y(s) = \mathbf{c}^T(sI - A - \mathbf{b}\mathbf{h}^T)^{-1}\mathbf{b}r(s) \tag{75}$$

and the transfer function is

$$\frac{y(s)}{r(s)} = \mathbf{c}^T(sI - A - \mathbf{b}\mathbf{h}^T)^{-1}\mathbf{b} \tag{76}$$

The zeros of Eq. (76) are independent of the feedback coefficients and are the zeros of the open-loop system: controller plus fixed plant. However, the pole locations

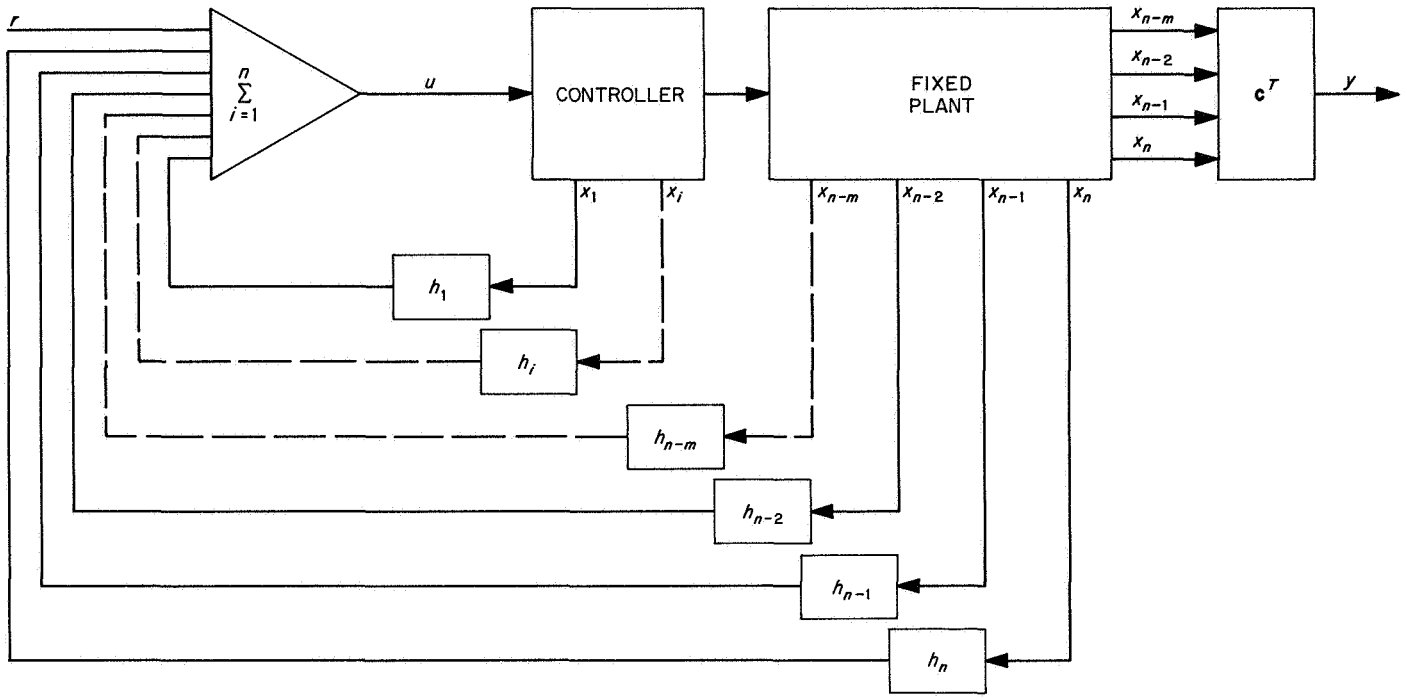

Fig. 16. Block diagram of state-variable feedback control

of Eq. (76) depend upon the values of the feedback coefficients h_i. The values of h_i, necessary to realize some desired overall system transfer function $[y(s)/r(s)]_d$, are determined by equating the coefficients of powers of s in the denominator of Eq. (76) to the coefficients of like powers of s in the denominator of $[y(s)/r(s)]_d$, and solving the resultant n linear simultaneous algebraic equations, n being the order of the open-loop system. It is usually found that some of the feedback coefficients thus calculated have little effect on system dynamics, and therefore can be neglected. The sensitivity of the overall system dynamics to the various feedback coefficients can be determined from simulation studies or by calculating sensitivity functions (Ref. 19). In some cases, the calculated values of h_i or the controller gain constant K_c may be relatively large and hard to realize physically. Since the controller gain constant and feedback coefficients appear as a product in the simultaneous linear algebraic equations, this problem can sometimes be overcome by a tradeoff between the feedback coefficients and the controller gain constant. That is, the controller gain constant can be reduced without affecting the desired system transfer function, except for its gain constant, provided the values of the feedback coefficients are each multiplied by the reduction in K_c and vice versa. Changing the gain constant of the desired system transfer function affects only the position error, which usually is no problem.

In many physical systems it is not possible to measure all the system or state variables. However, inaccessible state variables can be generated, provided they can be determined from a mathematical relationship. For example, consider one of the state equations, given below, and assume that the state variable x_i is not available to be fed back:

$$\dot{x}_i = ax_{i-1} - bx_i \tag{77}$$

The Laplace transform of Eq. (77), assuming that all initial conditions are zero, is

$$sx_i(s) = ax_{i-1}(s) - bx_i(s) \tag{78}$$

Solving for $x_i(s)$ gives

$$x_i(s) = \frac{ax_{i-1}}{s+b} \tag{79}$$

From Eq. (79) it is seen that x_i can be generated from the state variable x_{i-1} by simply passing x_{i-1} through a low-pass filter.

The state-variable feedback design technique is adaptable to digital computation and therefore can be applied to high-order systems (Ref. 18).

1. Sensitivity to parameter variations. Sensitivity as discussed in this report is measured in terms of sensitivity functions, peak sensitivity, and integral sensitivity. To define the sensitivity function, let λ be a system parameter with a nominal value λ_0. Further, let $y(t,\lambda)$ be the system response to a step input. Then for a change in λ, the step response can be expanded into a Taylor series as follows:

$$y(t,\lambda_0 + \Delta\lambda) =$$

$$y(t,\lambda_0) + \left.\frac{dy(t,\lambda)}{d\lambda}\right|_{\lambda_0} \Delta\lambda + \left.\frac{d^2y(t,\lambda)}{d\lambda^2}\right|_{\lambda_0} \frac{(\Delta\lambda)^2}{2!} + \cdots \quad (80)$$

The linear approximation to Eq. (80) is given by the term

$$\left.\frac{dy(t,\lambda)}{d\lambda}\right|_{\lambda_0}$$

which gives the approximate change in $y(t,\lambda)$ at time t, due to a change $\Delta\lambda$ in the parameter λ from its nominal value λ_0. An estimate of the change in $y(t,\lambda)$ for a percentage in λ is

$$u_\lambda(t) = \frac{dy(t,\lambda)}{\frac{d\lambda}{\lambda}} \quad (81)$$

where $u_\lambda(t)$ is the sensitivity function for the parameter λ.

The peak sensitivity of the system with respect to a parameter λ is defined as

$$u_\lambda^* = |\, u_\lambda(T)\,| \quad (82)$$

where T is the time at which $u_\lambda(t)$ is a maximum. The peak sensitivity is usually given for a 1% change in λ.

Integral sensitivity of the system with respect to a parameter λ is defined as

$$S_\lambda = \int_0^\infty u_\lambda^2(t)\, dt \quad (83)$$

when the integral exists. The integral of Eq. (83) does exist as long as λ does not affect the final value of $y(t)$. It is obvious from Eq. (83) that large values of λ are weighted more heavily than smaller values.

To discuss sensitivity in terms of the frequency domain, it is best to represent the system in terms of a forward-loop and a feedback-loop transfer function as shown in Fig. 17. Applying the Laplace transform to Eqs. (69) and (70) gives

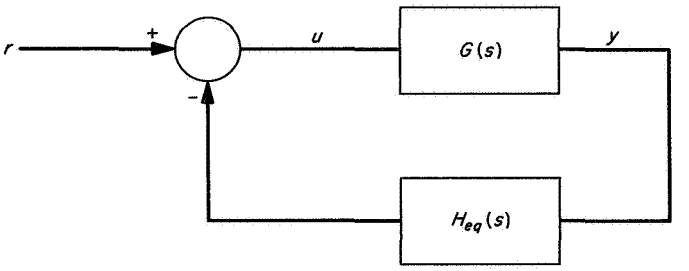

Fig. 17. Block diagram of closed-loop system

$$s\mathbf{x}(s) = A\mathbf{x}(s) + \mathbf{b}u(s) \quad (84)$$

$$y(s) = \mathbf{c}^T\mathbf{x}(s) \quad (85)$$

and

$$\mathbf{x}(s) = \Phi(s)\,\mathbf{b}u(s) \quad (86)$$

where

$$\Phi(s) = (sI - A)^{-1} \quad (87)$$

and is referred to as the resolvent matrix. From Eqs. (85) and (86)

$$y(s) = \mathbf{c}^T\,\Phi(s)\,\mathbf{b}u(s) \quad (88)$$

or

$$G(s) = \frac{y(s)}{u(s)} = \mathbf{c}^T\,\Phi(s)\mathbf{b} \quad (89)$$

where $G(s)$ is the forward-loop transfer function. The feedback-loop transfer function $H_{eq}(s)$ is

$$H_{eq}(s) = \frac{u(s)}{y(s)} = \frac{\mathbf{h}^T\mathbf{x}(s)}{\mathbf{c}^T\mathbf{x}(s)} \quad (90)$$

The closed-loop transfer function for the system shown in Fig. 17 is

$$\frac{y(s)}{r(s)} = \frac{G(s)}{1 + G(s)\,H_{eq}(s)} \quad (91)$$

Several examples will be used to illustrate the determination of sensitivity functions in the frequency domain. First, consider the system shown in Fig. 18, where it is desired to determine the system sensitivity to variations

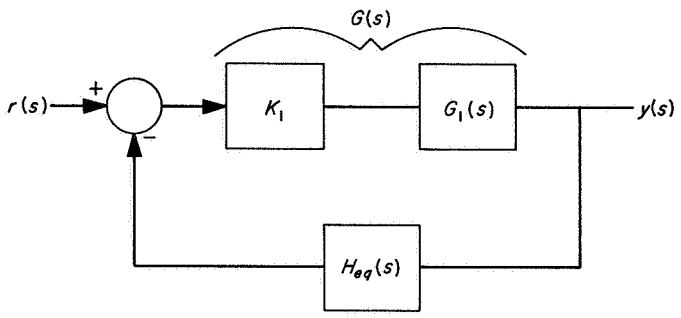

Fig. 18. Single-input, single-output system

in the gain constant K_1. The sensitivity of $[y(s)/r(s)]$ to gain K_1 is defined as

$$S_{K_1}^{y/r} = \frac{K_1}{\frac{y(s)}{r(s)}} \frac{\partial}{\partial K_1}\left[\frac{y(s)}{r(s)}\right] \tag{92}$$

For the single-input, single-output system shown in Fig. 18, the sensitivity function is easily calculated and is given by

$$S_{K_1}^{y/r} = K_1\left[\frac{1 + K_1G_1(s)H_{eq}(s)}{K_1G_1(s)}\right]\left\{\frac{G_1(s)}{[1 + K_1G_1(s)H_{eq}(s)]^2}\right\}$$
$$= [1 + G(s)H_{eq}(s)]^{-1} \tag{93}$$

The sensitivity of $[y(s)/r(s)]$ to the movement of an open-loop pole at $-\alpha$, shown as an interior block of the system in Fig. 19, is similarly defined and calculated.

If sensitivity is defined as

$$S_{\alpha}^{y/r} = \frac{\alpha}{\frac{y(s)}{r(s)}} \frac{\partial}{\partial \alpha}\left[\frac{y(s)}{r(s)}\right] \tag{94}$$

and another function $F(s)$ as

$$F(s) = 1 + K_1G_2(s)H_1(s)$$

and

$$G(s) = K_1\frac{G_2(s)G_3(s)}{(s + \alpha)}$$

$$H_{eq}(s) = H_2(s) + \frac{s + \alpha}{G_2(s)}H_1(s)$$

then

$$S_{\alpha}^{y/r} = \alpha\left[\frac{1 + G(s)H_{eq}(s)}{G(s)}\right]$$
$$\times \frac{\partial}{\partial \alpha}\left[\frac{K_1G_2(s)G_3(s)}{sF(s) + K_1G_2(s)G_3(s)H_2(s) + \alpha F(s)}\right]$$
$$= -\alpha\left\{\frac{\frac{F(s)}{s + \alpha}}{1 + G(s)H_{eq}(s)}\right\} \tag{95}$$

These examples illustrate the importance of making $1 + G(s)H_{eq}(s)$ as large as possible for all values of s. It can be shown that to minimize the effect of parameter variations and system disturbances, the following equation must be satisfied:

$$1 + G(s)H_{eq}(s) \geq 1 \tag{96}$$

Equation (96) is often called the Kalman equation, and is one of the design criteria used in the present investigation.

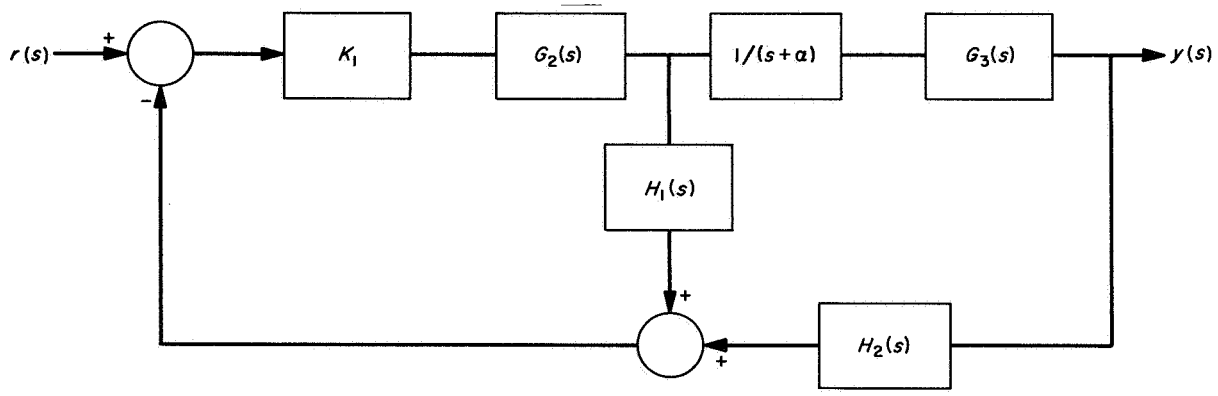

Fig. 19. System with open-loop pole at α

2. *System stability.* Since the exact realization of a desired system transfer function is possible by the state-variable design method, system stability is assured. Further, if the fixed plant is minimum phase, i.e., there are no zeros in the right half of the complex plane, then the system root locus as a function of the controller gain constant will lie completely in the left half of the complex plane for most physically realizable systems (Ref. 2). With proper selection of the desired system transfer function, the system dynamics can be made to be relatively insensitive to changes in the controller gain constant. This will be demonstrated in this design study.

Particular consideration is given to the effect of saturation upon system stability. For safety reasons, saturation-limiting may be purposely introduced to limit one or several of the system state variables. To investigate the effect of limiting the state variables on nonlinear stability, the Popov criterion will be used. To apply the Popov criterion to the thermionic reactor system discussed in this report, the system is put in the form shown in Fig. 20, where $G_1(s)$ is the transfer function of the linear part of the system and $f(\sigma)$ is the gain-dependent, time-invariant nonlinearity. If the input is assumed to be zero, the location of the nonlinearity in the loop is immaterial. Any system with a single nonlinearity can be put in the form of Fig. 20. The Popov criterion essentially states that the system in Fig. 20 is absolutely stable for any gain-dependent, time-invariant, single-valued nonlinearity lying in the sector $0 \leq f(\sigma)/\sigma \leq k$ of the $[\sigma,f(\sigma)]$-plane if the following inequality is satisfied (Ref. 2):

$$Re(1 + j\beta\omega)\, G_1(j\omega) + \frac{1}{k} > 0 \qquad (97)$$

where Re denotes the real part of the function, and β is a real number. Figure 21 shows the section of known stability in the $[\sigma,f(\sigma)]$-plane. If $G_1(s)$ contains a pole at the origin, the sector in the $[\sigma,f(\sigma)]$-plane does not include the σ-axis. Since the Popov criterion gives only sufficient conditions for stability, the results are conservative. That is, system stability for points falling outside the sector of known stability is undetermined. A graphical interpretation of Eq. (97) can be obtained by plotting the function

$$W(\omega) = Re\, G_1(j\omega) + \omega Im\, G_1(j\omega) \qquad (98)$$

where Im signifies the imaginary part of the function. Equation (98) is referred to as the modified frequency function. The procedure is to plot a polar plot of $W(\omega)$ and to find the point on the negative real axis nearest the origin at which a straight line drawn through the

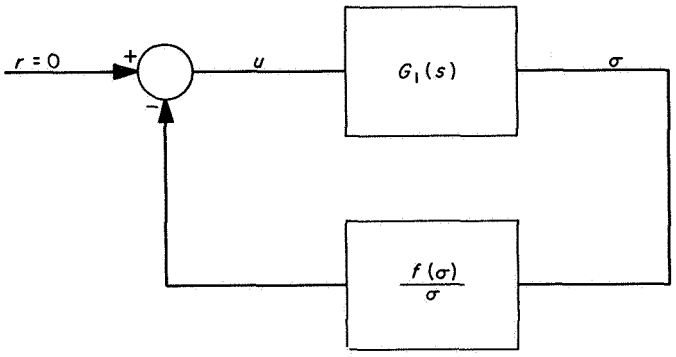

Fig. 20. Block diagram for applying Popov stability criterion

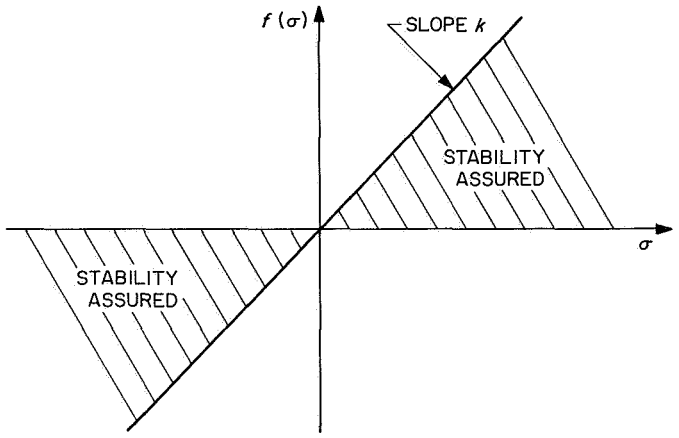

Fig. 21. Regions of known stability in the $[\sigma, f(\sigma)]$-plane

point does not intersect the modified frequency plot. The location of this point on the axis is $-1/k$, where the value of k is the slope of the straight line through the origin, which along with the real axis σ, sets the boundary of known stability in the $[\sigma,f(\sigma)]$-plane. As demonstrated in this study, state-variable feedback design normally results in a system in which the region of known stability in the $[\sigma,f(\sigma)]$-plane encompasses the entire first and third quadrants. This is particularly true if the nonlinearity appears in the first portions of the forward loop immediately following the control u. As mentioned previously, the transfer function of a system with state-variable feedback control is

$$\frac{y(s)}{r(s)} = \frac{G(s)}{1 + G(s)H_{eq}(s)} \qquad (91)$$

where $G(s)$ is the transfer function of the forward-loop system and $H_{eq}(s)$ is an overall feedback transfer function due to feeding back all the state variables. Therefore, in applying the Popov criterion to the system of Eq. (91),

where it will be assumed that the nonlinearity will appear in u, $G_i(j\omega)$ is given by

$$G_i(j\omega) = G(j\omega)\, H_{eq}(j\omega) \tag{99}$$

Since the pole zero excess of $G(j\omega)\, H_{eq}(j\omega)$ is always 1, and since the relative positions of the poles and zeros are normally such that $W(j\omega)$ never crosses into the second quadrant, system stability is assured for any single-valued nonlinearity falling in the first and third quadrants of the $[\sigma,f(\sigma)]$-plane. This is an important result in constraining u to limit the system states.

B. Selection of Controller and System Specifications

The controller dynamics are represented by a second-order linear differential equation, in which parameter values were chosen to be representative of those encountered in practice. In transfer-function notation, the controller transfer function was selected to be

$$\frac{x_5}{u} = \frac{2}{s^2 + 2s + 2} \tag{100}$$

where the control reactivity ρ_c has been denoted by x_5. Representing controller dynamics by a second-order transfer function is usually a good engineering approximation for most systems. The parameter values of Eq. (100) were selected to give a critically damped system response with a fast rise time, 5% overshoot, and short settling time. The more relaxed the overall system specifications, the longer can be the controller rise time and settling. It is desirable, however, to maintain the same percentage of overshoot.

In specifying the overall system dynamics, two points were taken into consideration: (1) the response of the system to normal input commands $r(t)$, and (2) system response to internal and load disturbances. Since it is possible to obtain any reasonable controller dynamics, and since it is desirable to make the closed-loop response the same as that of the controller, the overall system transfer function was chosen to be that of Eq. (100). By this choice of system dynamics, zeros of $H_{eq}(s)$ will fall on the specified complex poles and thus these poles will be insensitive to changes in the controller gain constant. It should be noted that the zeros of $H_{eq}(s)$ do not appear in the closed-loop transfer function. As will be seen later, for the case in point, the system is sixth-order with a pole zero excess of 3. Therefore, to realize overall second-order dynamics, with no zeros, three of the closed-loop poles were chosen to cancel the three system zeros. The remaining pole was placed at -100 so that its residue would have no effect on the dominant second-order complex poles. As a further note, it is pointed out that since there are $n - 1$ finite zeros in $H_{eq}(s)$, the location of the closed-loop poles will be fairly insensitive to changes in the controller gain constant and thus guarantee reasonable assurance of effectively canceling the open-loop zeros. In addition to making its effect on system dynamics negligible, the location of the pole at -100 was chosen to satisfy Eq. (96), thus minimizing the effect of disturbances. Equation (96) can be written in the form

$$\left|\frac{D_d(s)}{D_0(s)}\right| > 1 \tag{101}$$

where $D_0(s)$ is the denominator of the open-loop system transfer function, and $D_d(s)$ is the denominator of the desired system transfer function. Bode plot techniques provide a means for quickly determining the relative locations of the zeros of $D_d(s)$ (poles of the desired system transfer function) to satisfy Eq. (101).

In applying the linear state-variable feedback design method, it is assumed that the system can be adequately described by linear differential equations. Because of physical limitations of the system and purposely introduced limiters, the system for large signals will become nonlinear. The signal level in systems designed by state-variable feedback is normally lower than in systems designed by conventional methods. Therefore, description of the system by linear differential equations is usually not a bad approximation. In certain instances it is desirable to limit one or several of the system states so as not to violate some safety requirement. One such example is to limit reactivity or reactivity rate. In this state, the system variables will be limited by placing a constraint on the control u. Since in state-variable feedback control the pole zero excess of $G(s)H_{eq}(s)$ is 1, it is clear from the preceding discussion that placing a limit on u will cause no stability problems. This is not necessarily true if a limit is placed on one of the state variables. Therefore, to be on the conservative side, states are limited in this study by constraining the control u.

C. Final Design

1. Fourth-order model. The design techniques described earlier in this section were applied to the thermionic reactor model described by Eqs. (48) through (52), with the use of the digital computer program described

in Ref. 18. When these equations are combined with that for the controller, Eq. (100), the complete system equations are expressed as follows:

$$\dot{x}_1 = -0.00164x_2 - 0.4x_3 - 0.00313x_4 + 10x_5$$

$$\dot{x}_2 = -1.71x_2 + 319x_3 + 1.66x_4$$

$$\dot{x}_3 = 0.00031x_1 + 0.000353x_2 - 0.123x_3 - 0.000344x_4 + 0.031x_5 \quad (102)$$

$$\dot{x}_4 = 0.0819x_2 - 0.114x_4$$

$$\dot{x}_5 = x_6$$

$$\dot{x}_6 = -2x_5 - 2x_6 + 2u$$

With the use of the computer program, the open-loop system transfer function was determined to be

$$G(s) = \frac{(s + 0.0329)(s + 0.1)(s + 1.79)}{(s^2 + 2s + 2)(s + 0.0119 + j0.0164)(s + 0.0119 - j0.0164)(s + 0.0663)(s + 1.85)} \quad (103)$$

Since the overall desired system dynamics are given by Eq. (100), the desired system transfer function between command input and output voltage is

$$\frac{x_3(s)}{r(s)} = \frac{2(s + 0.0329)(s + 0.1)(s + 1.79)}{(s^2 + 2s + 2)(s + 0.0329)(s + 0.1)(s + 1.79)(s + 100)} \quad (104)$$

As mentioned in Section IV-B, three of the closed-loop poles were selected to cancel the zeros in Eq. (103); the remaining pole was placed at -100 to have negligible effect on the desired system input–output dynamics, and to satisfy Eq. (104). Figure 22 is a frequency plot of the Kalman Eq. (96) for this system. It is obvious from the figure that the equation is satisfied for all positive values of frequency. With the aid of the digital program, the feedback coefficients and controller gain constant were calculated to be as follows:

Precursor concentration	$h_1 = -2.92 \cdot 10^{-4}$
Collector temperature	$h_2 = -1.53 \cdot 10^{-5}$
Voltage	$h_3 = -0.939$
Radiator temperature	$h_4 = 8.03 \cdot 10^{-6}$
Control reactivity	$h_5 = -3.04 \cdot 10^{-2}$
Control reactivity rate	$h_6 = -1.54 \cdot 10^{-2}$
Gain constant	$K_c = 3.25 \cdot 10^{3}$

The computer program is designed to give zero steady-state position error between command input and voltage response; that is, the system response to a step input in the steady state is the step itself. In Laplace transform notation,

$$\lim_{s \to 0} \frac{y(s)}{r(s)} = 1 \quad (105)$$

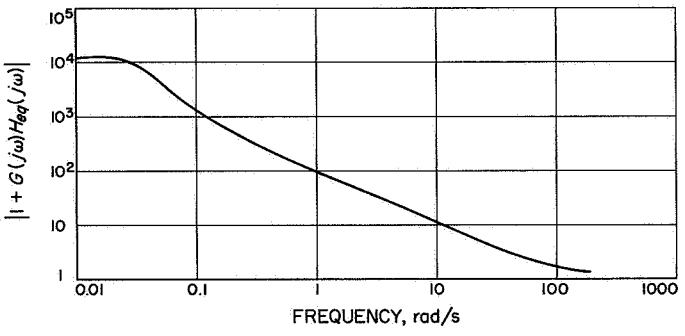

Fig. 22. Frequency plot of the Kalman equation

As stated earlier, if zero position error is not critical, as is usually the case, a tradeoff between K_c and the feedback coefficients can be accomplished without affecting the system dynamics. It is possible to increase or decrease K_c, provided all the feedback coefficients are changed in the opposite direction by an amount equal to the change in K_c. This is sometimes helpful in physically realizing the system design. In choosing the desired system dynamics, the overall system transfer function was chosen to be that of the controller. As discussed earlier, this will force two zeros of $H_{eq}(s)$ to appear at these pole locations, and thus the system dynamics become relatively insensitive to changes in the controller gain constant, particularly for larger values of gain. Figure 23 is a root locus plot of the final system design as a function of the controller gain constant K_c, and demonstrates the insensitivity of the dominant complex poles to changes in K_c.

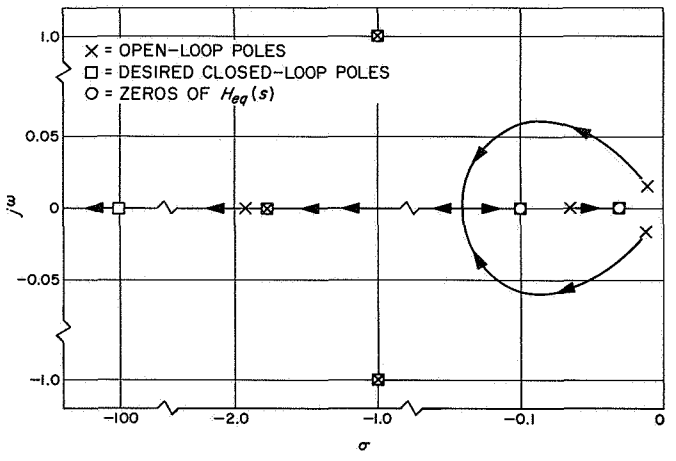

Fig. 23. Root locus plot for controlled system as a function of controller gain constant

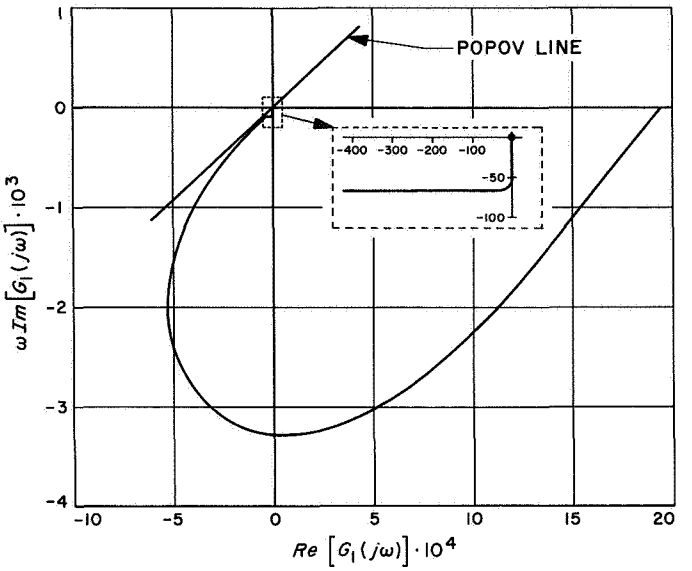

Fig. 24. Modified frequency function for controlled system

To limit the system states so as not to violate some constraint on reactivity and reactivity rate, a limiter was placed in the signal channel to limit the control u. The limit on u was adjusted to ensure that the reactivity rate did not exceed $10¢/s$. To investigate the effects of limiting the control on system stability, the Popov criterion described earlier was used. Figure 24 is a plot of the modified frequency function for this system. It is apparent from the figure that the Popov line can be placed arbitrarily close to the origin; therefore limiting u will cause no stability problem for the proposed design.

It can be shown that for a single-input disturbance, the transfer function from output response due to an external disturbance to that disturbance is given by

$$\frac{y(s)}{d(s)} = \frac{F(s)}{1 + G(s)\,H_{eq}(s)} \tag{106}$$

In Eq. (106), all the terms have been defined before except $F(s)$, which is the transfer function of the disturbance and depends on where the disturbance is applied. Equation (106) is often referred to as the output impedance and is given the symbol Z_0. It is clear from Eq. (106) that to minimize the effect of disturbance on the controlled variable, the denominator should be as large as possible for all frequencies. Therefore, if the Kalman Eq. (96) is satisfied, the effects of load disturbances are minimized. For the thermionic reactor, a disturbance in the form of a change in load resistance is not a simple single-input disturbance, since the load resistance term appears in several of the system equations. A change in load resistance behaves rather as a multiple-input disturbance. However, using the proposed design criterion for disturbance due to load resistance changes gave good results. The multiple-input problem is currently under investigation.

2. Fifth-order model. The effect of considering the fuel and emitter as separate spatial regions, instead of lumping them together, is to increase the system order by one. Calculations were performed for the obtained seventh-order control system, again with the purpose of obtaining overall system dynamics that are the same as for the controller described by Eq. (100). The open-loop system transfer functions are given in Section III (Eq. 65). As in the design of the sixth-order system described in Section IV-C1, three of the closed-loop poles were selected to cancel the zeros. However, there are now two remaining poles to be placed so that their effect is negligible on the desired dynamics. A choice satisfying this criterion, and the criterion for minimizing the effect of disturbances, is to place a pole pair at $s = 10 \pm j10$. The controlled system transfer function therefore becomes

$$\left[\frac{y(s)}{r(s)}\right]_d = \frac{2}{(s^2 + 2s + 2)\,(s^2 + 20s + 200)} \tag{107}$$

The corresponding feedback coefficients and controller gain constant were calculated to be as follows:

Precursor concentration	$h_1 = -3.08 \cdot 10^{-4}$
Fuel temperature	$h_2 = 2.43 \cdot 10^{-4}$

Collector temperature	$h_3 = -1.11 \cdot 10^{-5}$	Control reactivity rate	$h_7 = -2.81 \cdot 10^{-3}$
Voltage	$h_4 = -1.21$	Gain constant	$K_c = 3.13 \cdot 10^3$
Radiator temperature	$h_5 = -2.33 \cdot 10^{-5}$		
Control reactivity	$h_6 = -3.08 \cdot 10^{-2}$		

Analog-simulation studies have shown that there is no significant difference in the response trajectories between the sixth-order and seventh-order models.

V. Results of Controller Performance Investigations

The theory described in Section IV was applied to the reduced set of linear equations (48) through (52) given in Section III. To this set is added the equation describing the controller (Eq. 100). The state variables are labeled as follows:

Precursor concentration	$\delta C = x_1$
Collector temperature	$\theta_3 = x_2$
Voltage	$\delta V = x_3$
Radiator temperature	$\theta_r = x_4$
Control reactivity	$\rho_c = x_5$
Control reactivity rate	$\dot{\rho}_c = x_6$

Expressed in terms of this notation, the equations for the desired system response developed in Section IV take the form

$$\begin{bmatrix} \dot{x}_1 \\ \dot{x}_2 \\ \dot{x}_3 \\ \dot{x}_4 \\ \dot{x}_5 \\ \dot{x}_6 \end{bmatrix} = \left[\begin{array}{c|c|c|c|c|c} 0 & -1.64 \cdot 10^{-3} & -0.4 & -3.13 \cdot 10^{-3} & 10 & 0 \\ 0 & -1.71 & 319 & 1.66 & 0 & 0 \\ 3.1 \cdot 10^{-4} & 3.53 \cdot 10^{-4} & -0.123 & -3.44 \cdot 10^{-4} & 3.1 \cdot 10^{-2} & 0 \\ 0 & 0.0819 & 0 & -0.114 & 0 & 0 \\ 0 & 0 & 0 & 0 & 0 & 1 \\ 0 & 0 & 0 & 0 & -2 & -2 \end{array}\right] \begin{bmatrix} x_1 \\ x_2 \\ x_3 \\ x_4 \\ x_5 \\ x_6 \end{bmatrix} + \left[\begin{array}{c|c|c} 0 & 1.4 & 0 \\ 0 & 1872 & 0 \\ 0 & 6.25 & 2.11 \\ 0 & 0 & 0 \\ 0 & 0 & 0 \\ 2K_c & 0 & 0 \end{array}\right] \begin{bmatrix} u \\ \delta R_{LD} \\ \dot{\delta R}_{LD} \end{bmatrix} \tag{108}$$

$$u = [\,-2.92 \cdot 10^{-4} \mid -1.53 \cdot 10^{-5} \mid -0.939 \mid 8.04 \cdot 10^{-6} \mid -3.04 \cdot 10^{-2} \mid -1.54 \cdot 10^{-2}\,]\,\mathbf{x} + r \tag{109}$$

$$K_c = 3.25 \cdot 10^3$$

$$y = [\,0 \mid 0 \mid 1 \mid 0 \mid 0 \mid 0\,]\,\mathbf{x} \tag{110}$$

In these equations, u is the control variable, δR_{LD} represents the electric load disturbances, r is the command signal, and y is the output. As discussed in Section IV, electric load perturbations are treated as disturbances, and one of the design objectives is to minimize the effect of such disturbances.

A. System Responses

The system model described by Eqs. (108) through (110) was simulated on an analog computer and responses resulting from various perturbations were obtained. The analog-simulation diagram is given in Appendix A. The perturbations fall into three main categories: command signal changes, disturbances, and sensitivity to parameter changes.

The control system was not designed specifically to include constraints on the reactivity insertion rates and magnitudes. The selection of desired response to command signal changes was based on expected performance of the control drum actuator hardware. But, a very simple actuator is capable of inserting reactivity at rates far in excess of what will probably be tolerated when safety constraints are considered. Thus, if no reactivity limitations are incorporated, and because of the general dynamic nature of the system, one would expect to obtain response trajectories showing large reactivity insertions and retractions even for small perturbations. This is indeed the case, as shown in the following discussion of the response trajectories. It is useful first to consider unconstrained designs, since they are a guide in determining how the system should be constrained. The consequences

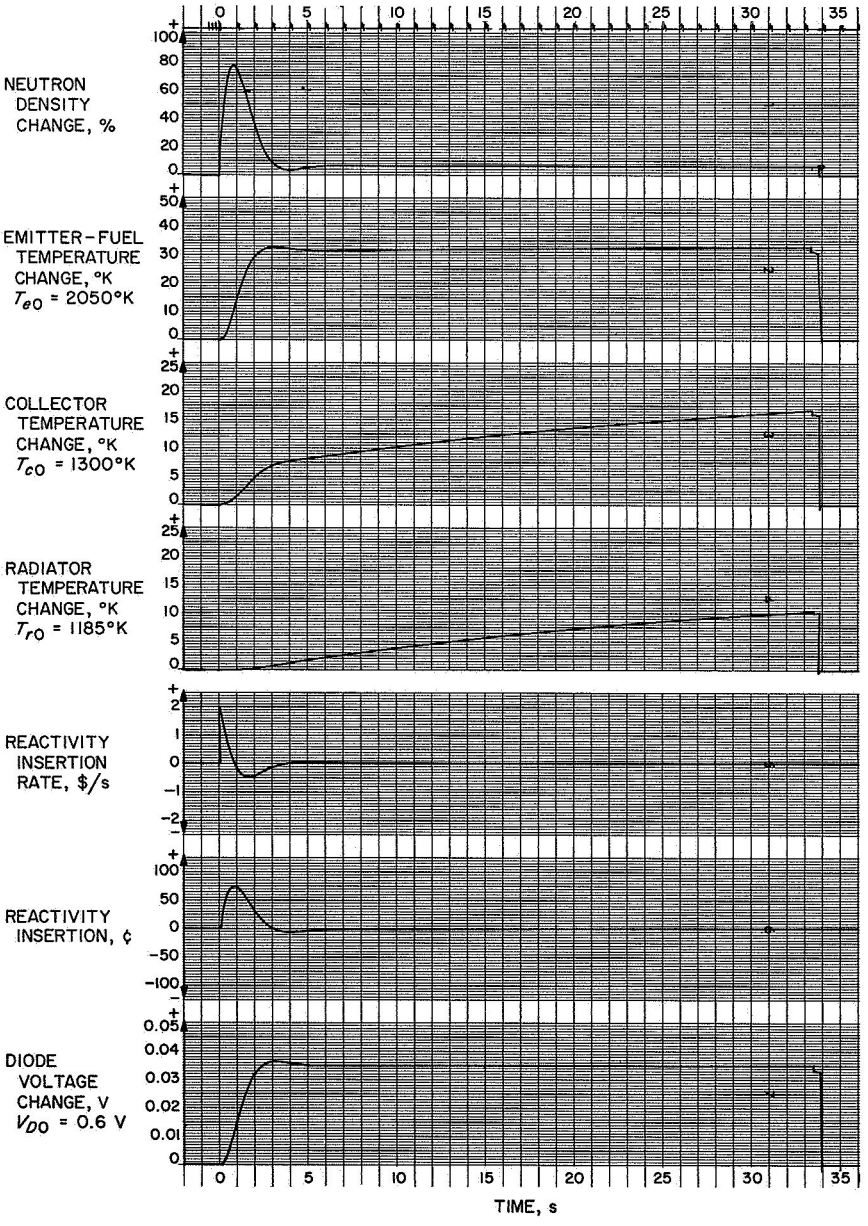

Fig. 25. Response of controlled linear system to a step command in voltage

of introducing nonlinear limiting elements in the controller are discussed in Section IV; their effect on the system response is described in Section VI.

B. Command Signal Changes

The response of the fourth-order linear model to a 0.035-V step change in the command voltage is shown in Fig. 25. The desired voltage response is reproduced exactly; however, as expected, the reactivity insertions and retractions are large. The thermal power pulse reaches 80%, but the equilibrium power change is only 6%. The temperature transients for the collector and heat-rejection system reach equilibrium with a time constant dictated by the large radiator thermal lag. These transients do not seem to require inclusion of any thermal-design constraint considerations. Since the system is linear, the response to other step changes in command voltage will be proportional to the response shown in Fig. 25.

C. Disturbances

The effect of an electric load change of $-0.02\ \Omega\ cm^2$ is shown in Fig. 26. Again, the reactivity variations are large and at the limit of the applicability of a linearized neutron kinetics description. One also observes a small steady-state error in the equilibrium voltage level. This error can be reduced, if necessary, by applying additional

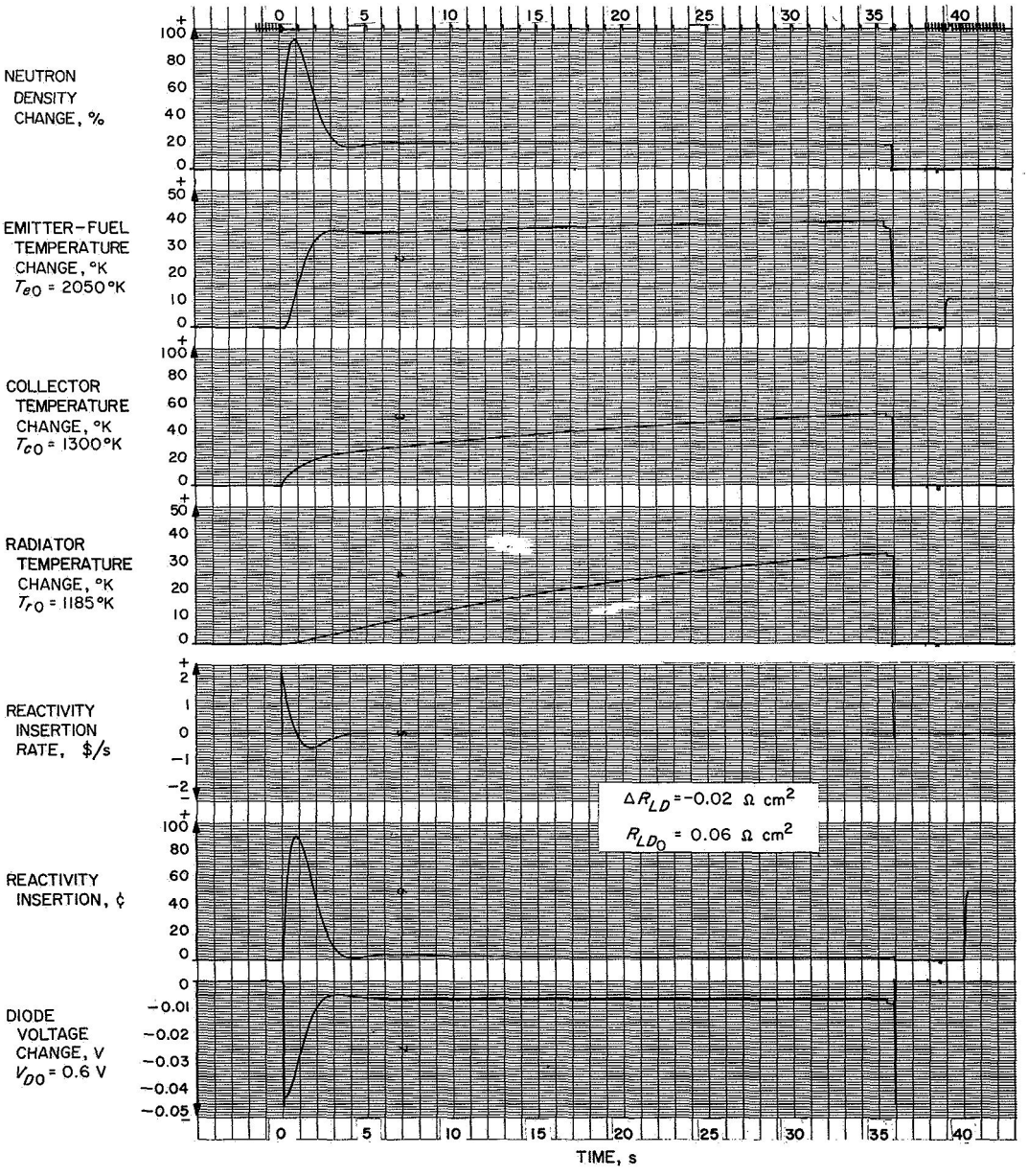

Fig. 26. Response of controlled linear system to a step change in electric load

dynamics to the system. The load perturbation corresponds to an increase of 50% in the electric power demand, but the error in the final voltage level is only about 1%. At 10% of full power, the load impedance is increased tenfold, but even then the voltage error is only about 6%.

D. Sensitivity to Parameter Changes

The internal parameter values for a reactor core are usually not known accurately. The errors in the temperature coefficients of reactivity may be as high as a factor of 5, while the error in the data for material properties may reach 50% for some quantities. These data are also subject to change during the lifetime of the system. It is therefore desirable that the system be insensitive to changes in parameter values and feedback coefficients to arrive at a simple design for the controller.

Figures 27 through 31 show the effect of various parameter changes. From a practical point of view, the

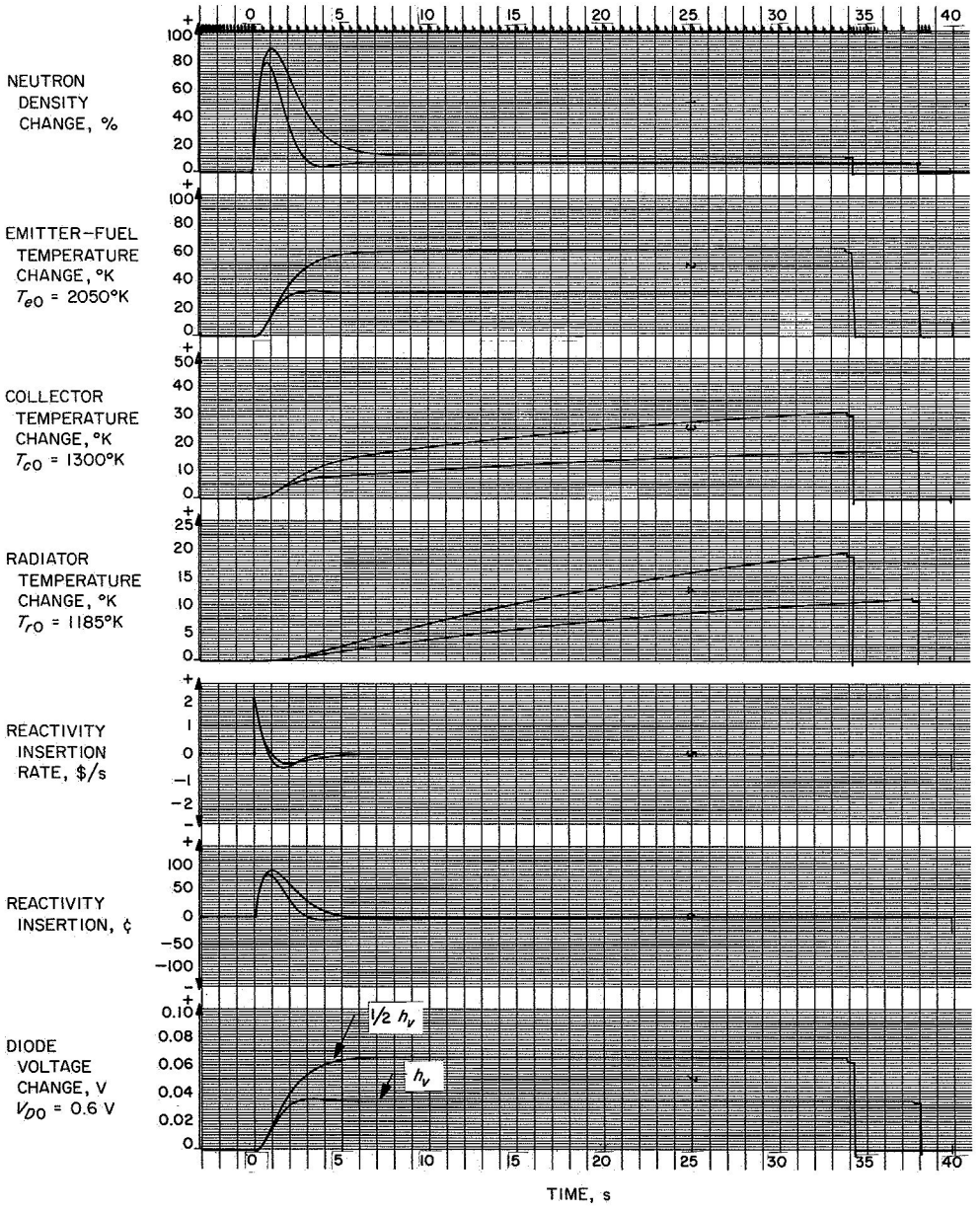

Fig. 27. Response of controlled linear system to a step command in voltage when voltage feedback coefficient is halved

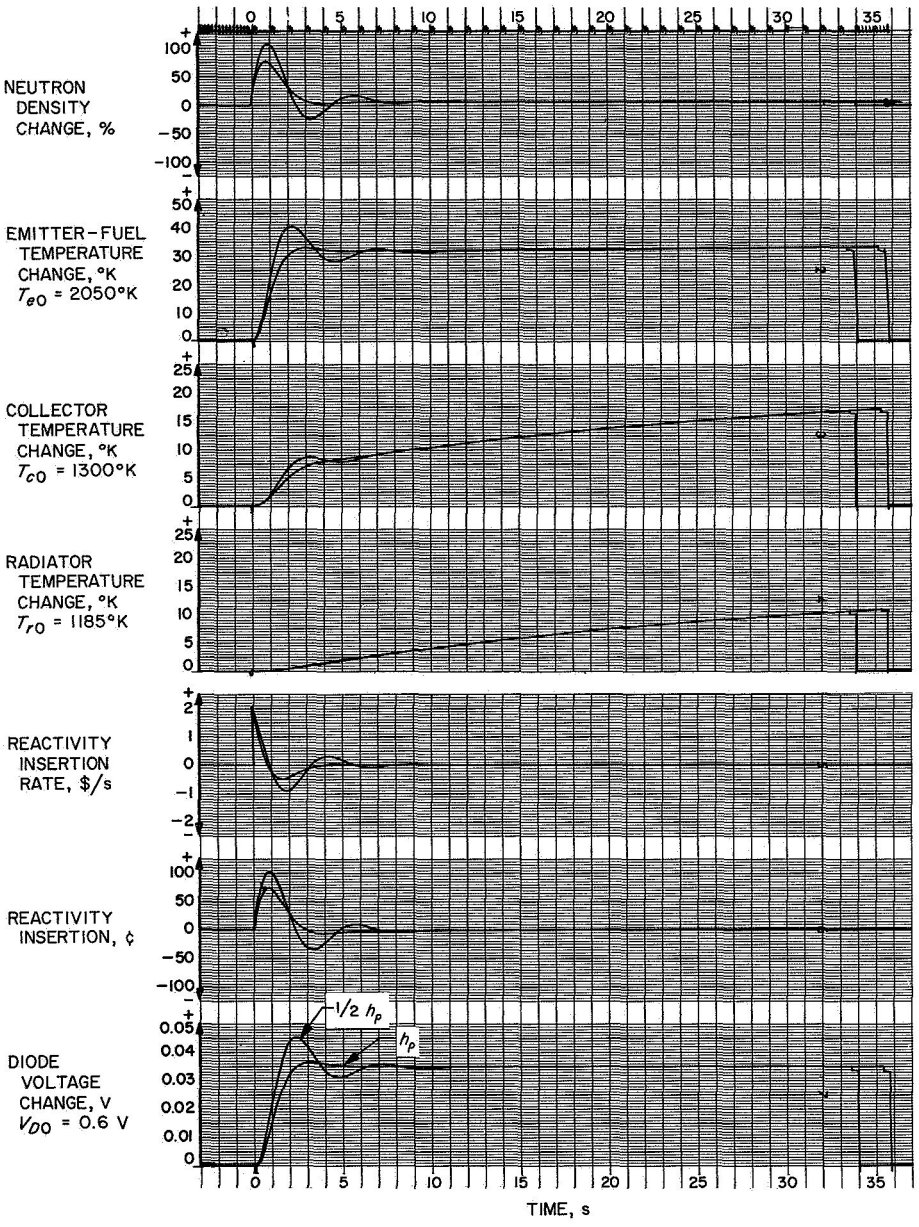

Fig. 28. Response of controlled linear system to a step command in voltage when reactivity feedback coefficient is halved

system is not very sensitive to the variations. The system remains stable if any one of the feedback elements, except the reactivity feedback, is omitted. If the reactivity feedback is set to zero the system is unstable, but if a reactivity limiter is inserted in the controller, this stabilizes the system. The beneficial effect of limiters has been demonstrated in many other control system designs; but, of course, the opposite may also be true. If the reactivity rate is limited (as contrasted to limiting the reactivity), instability still results for large enough perturbations. However, it was shown in Section IV that limiting the control signal, and therefore also the reactivity signal, causes no stability or control problems. It follows that the controlled powerplant can always be made stable against feedback-element casualties. If the feedbacks associated with the fuel, collector, and heat-rejection system temperatures are neglected, there is no discernible effect on the response trajectories. This is beneficial, since the fuel, emitter, and collector temperatures cannot be measured directly. Figure 32 is a block diagram representation of the controlled system with only the significant feedback elements included.

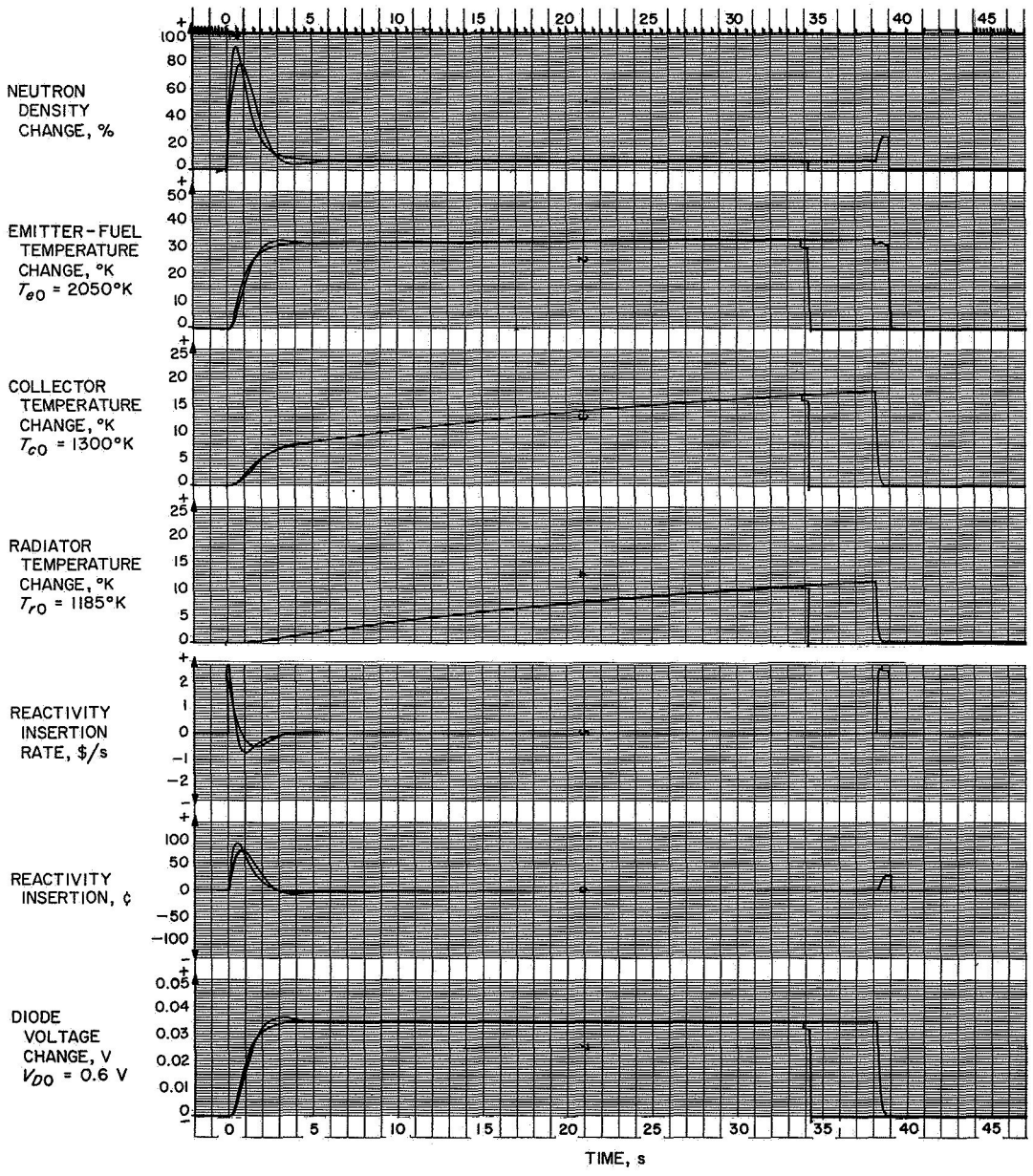

Fig. 29. Response of controlled linear system to a step command in voltage when reactivity-rate feedback coefficient is halved

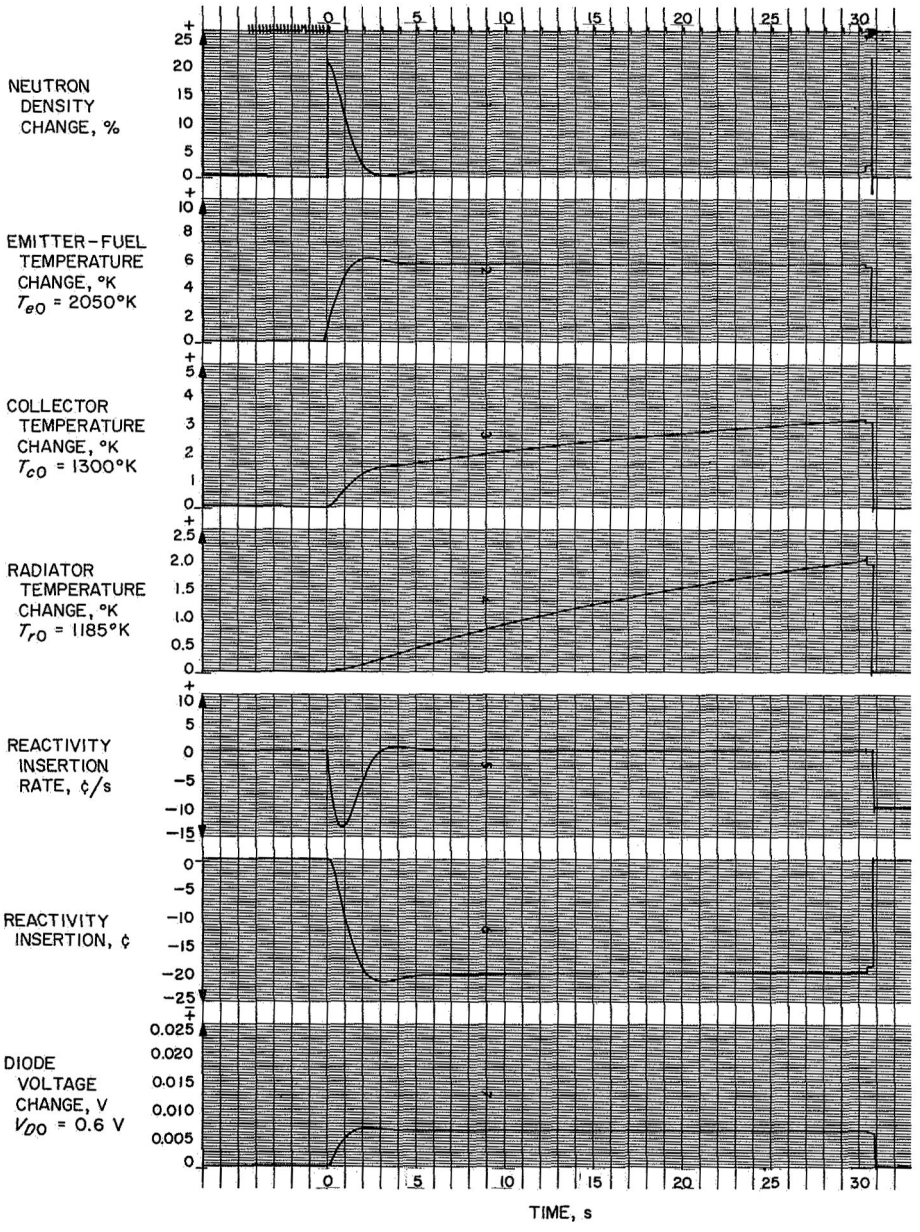

Fig. 30. Response of controlled linear system to a step disturbance in core reactivity of 20¢

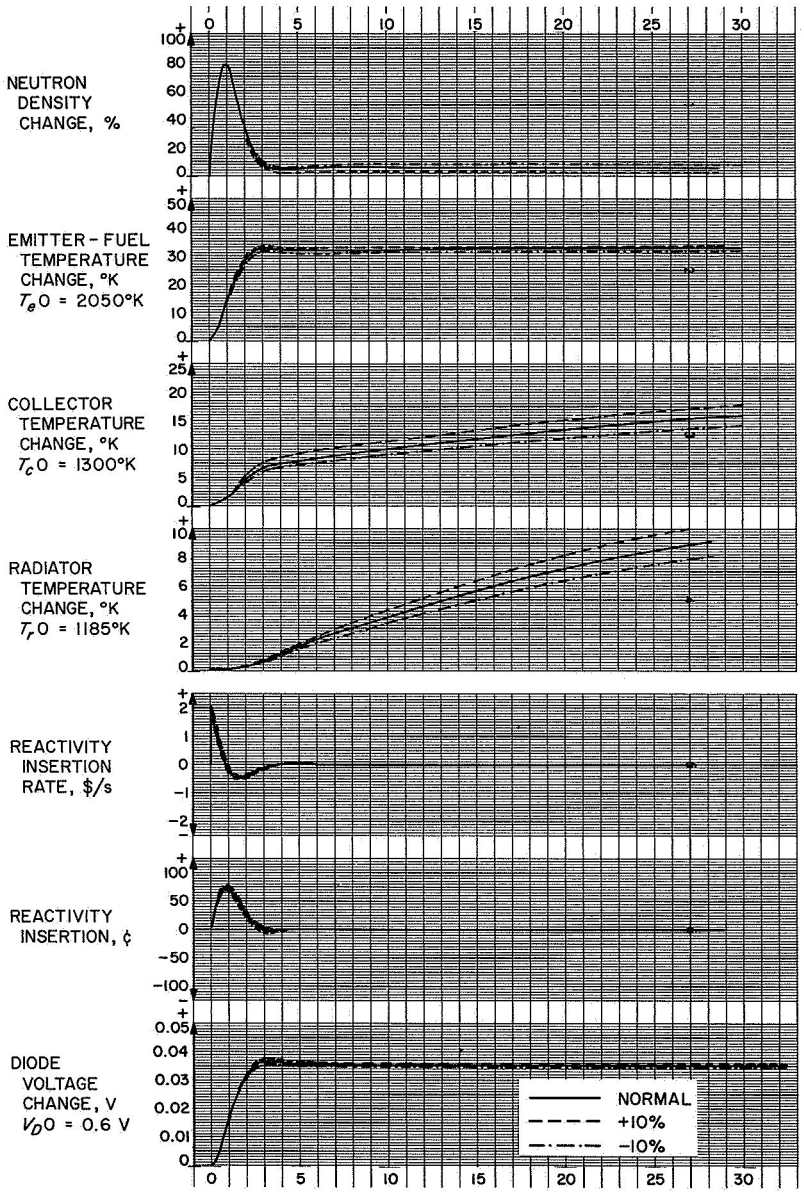

Fig. 31. Response of controlled linear system to a step command in voltage when coefficient of heat-transfer term in interelectrode gap is varied by ±10%

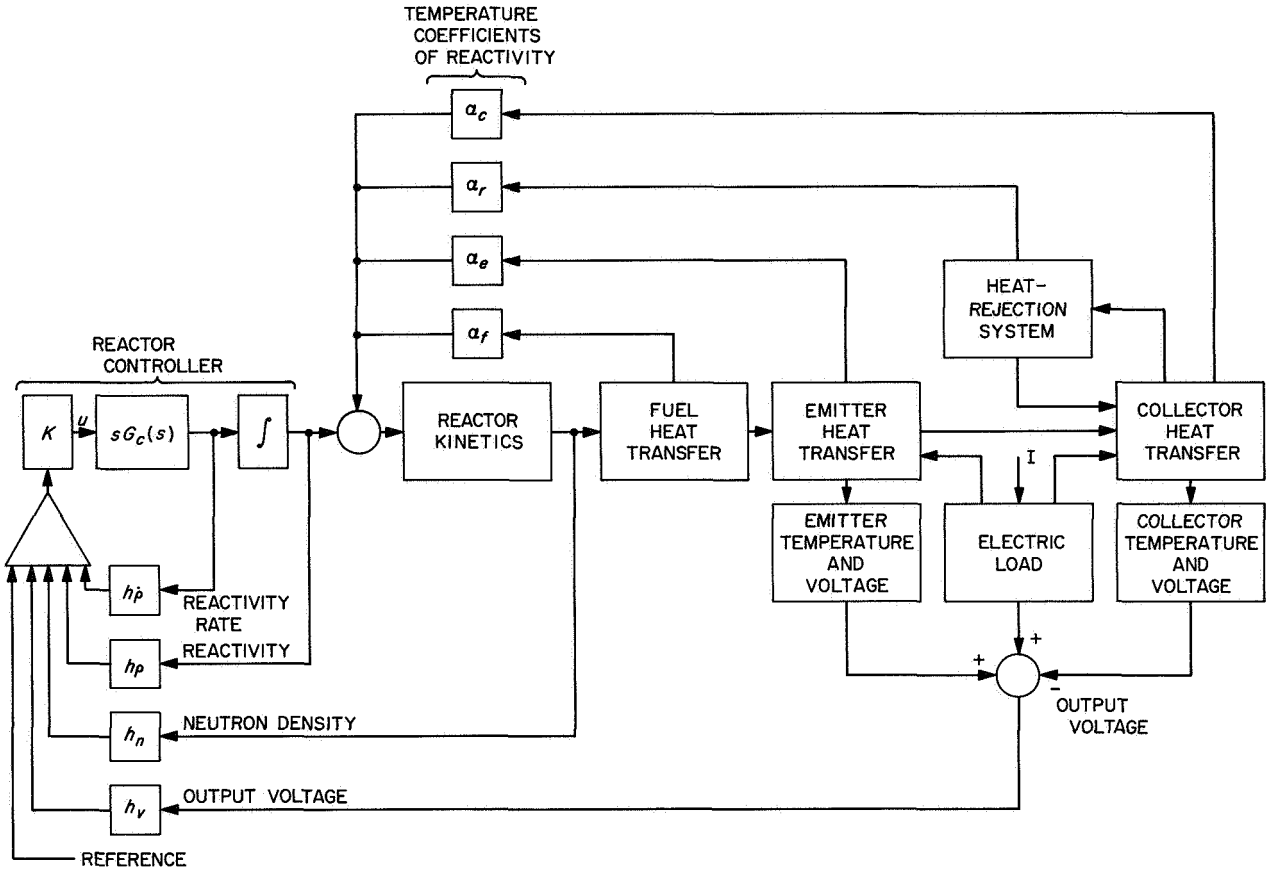

Fig. 32. State-variable feedback design of thermionic reactor controller

VI. Applications to the Nonlinear System

After completion of the investigations with the reduced controlled linear model, the controller design that evolved was applied to the original nonlinear model. The system described by Eqs. (1) through (24) was simulated on analog computers and the responses to perturbations were compared to those obtained with the linear model. Appendix B contains the analog-simulation diagrams.

A. Correlation With Results Obtained for the Linear Model

The differences between the response trajectories for the linear and nonlinear models were not expected to be large, and this was borne out by the simulation studies. In Fig. 33 the responses of the two models to a step command are directly compared. It can be seen that the desired system dynamics are closely obtained also for the nonlinear system; in this model, the time delays for the coolant loops were set equal to zero.

The main difference between the trajectories in Fig. 33 is that, because of a higher order description in the nonlinear model, this model shows a more oscillatory behavior. Also, the nonlinearities manifest themselves by not yielding exactly the same equilibrium temperatures as those shown by the linear model.

Figure 34 compares the responses of the linear and nonlinear system models to a large electric load change. The trajectories are again very similar, and the same general observations can be made as for Fig. 33. The output voltage returns to the original value with a small steady-state error.

Among other studies made with the nonlinear system simulation was an investigation of the effects of varying the magnitudes of the feedback coefficients, in which the responses were found to be similar to those obtained with the linear model. The response of the nonlinear system to Gaussian white noise was studied, with results as shown in Fig. 35. As expected, although the neutron density responds instantaneously (i.e., the prompt neutrons), the rest of the system is not appreciably affected.

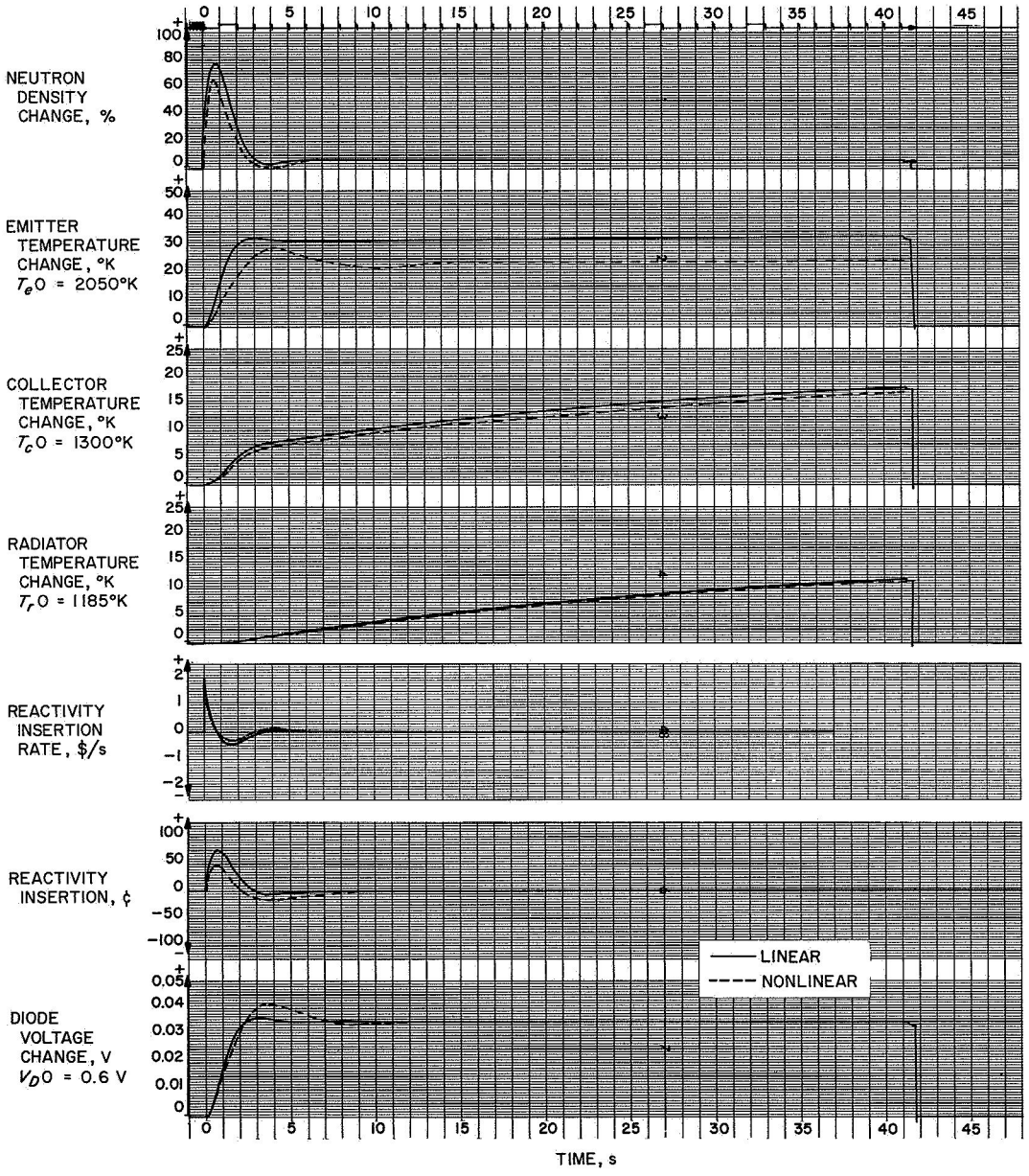

Fig. 33. Responses of linear and nonlinear controlled systems to a step command in voltage

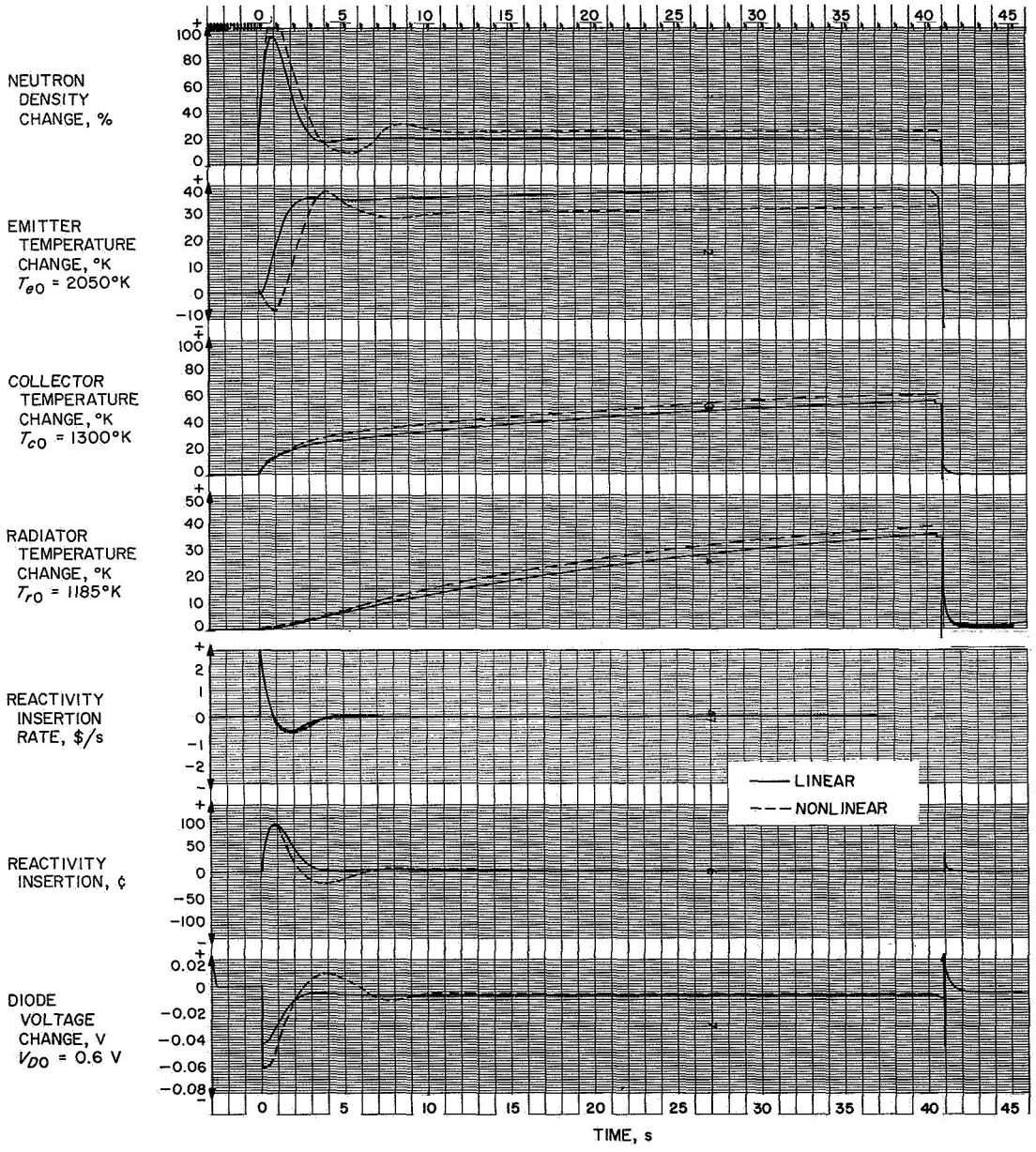

Fig. 34. Responses of linear and nonlinear controlled systems to a step disturbance of $-0.02\ \Omega\ cm^2$ in electric load

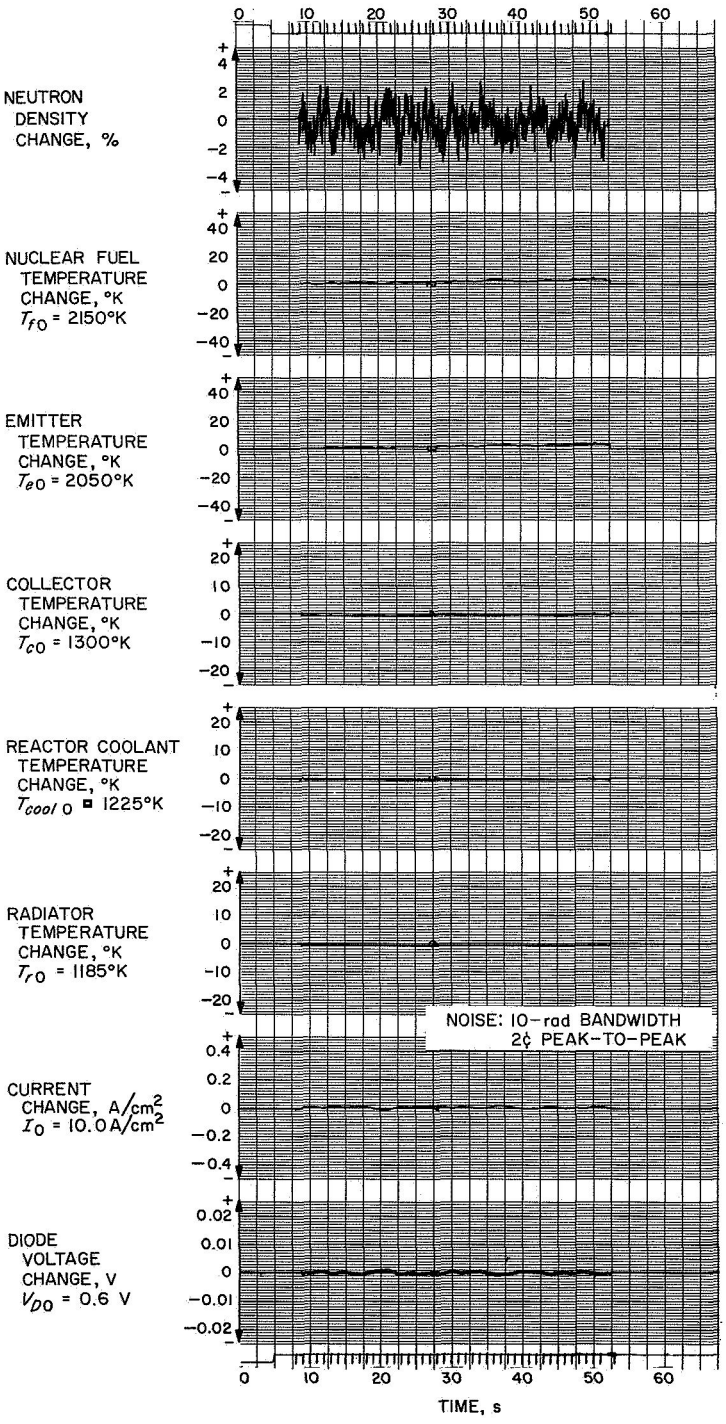

Fig. 35. Response of nonlinear controlled system to reactivity noise

B. Effect of Restricting the Control Signal to Limit Reactivity Rate

The reactivity rates shown in Figs. 33 and 34 are too large to be allowed in normal practice. As pointed out earlier, the rate can be lowered by limiting the control signal u, and this will not cause stability problems. The response of the nonlinear system model to restricting the control signal to limit the reactivity rate to 10¢/s is shown in Fig. 36. A comparison of the trajectories for the restricted control signal in Fig. 36 with the responses of the nonlinear controlled system (unrestricted) in Fig. 34 shows that the two trajectories are quite different in the beginning. As would be expected, the response has slowed down considerably. In Fig. 37 a comparison is made between the linear and nonlinear restricted models subjected to a step command in voltage. The overall behavior of the two models is similar, but the responses differ considerably from those for the unrestricted models shown in Fig. 33.

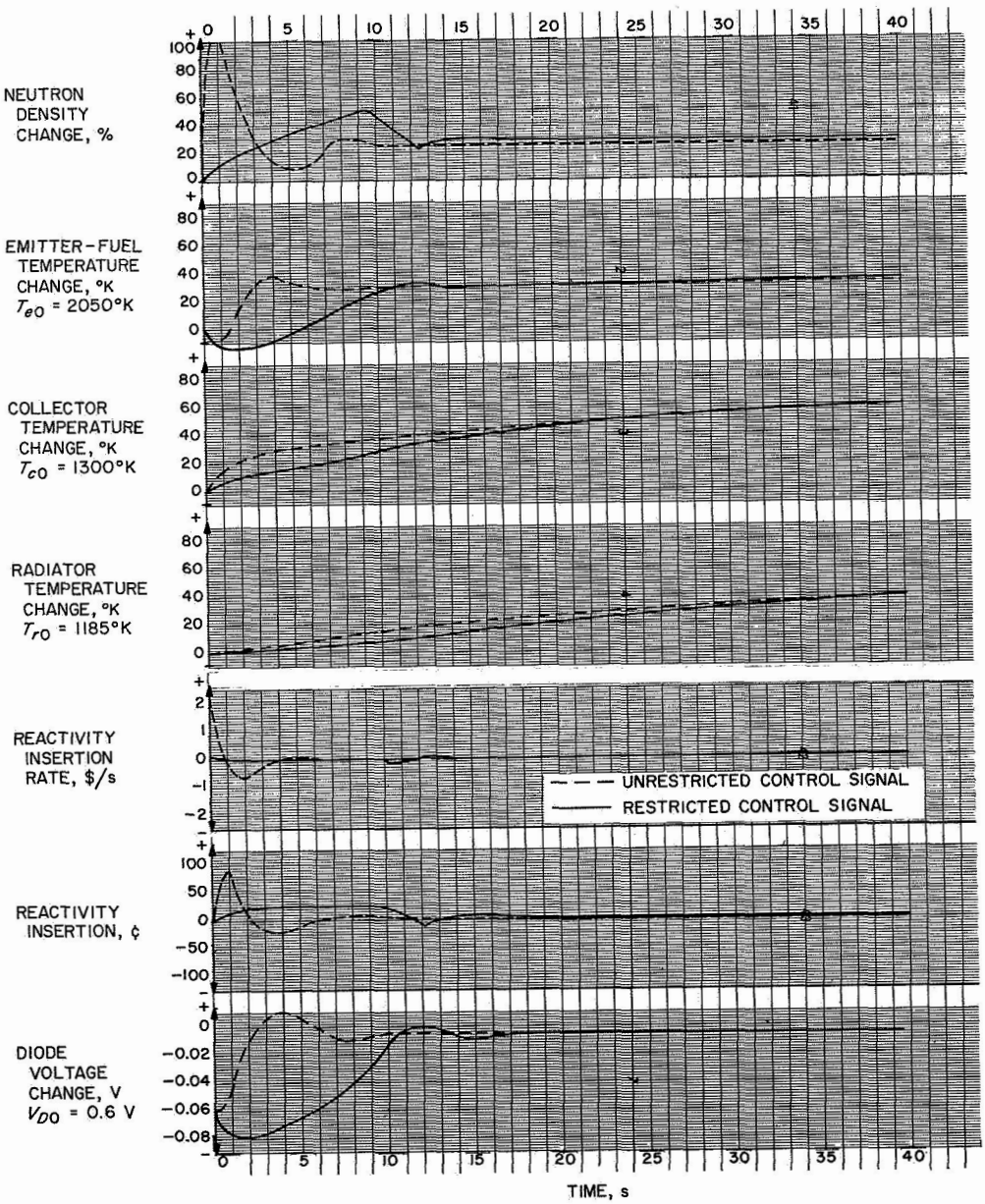

Fig. 36. Response of nonlinear controlled system to a step disturbance of −0.02 Ω cm² in electric load when the control signal is constrained to limit reactivity rate to 10¢/s

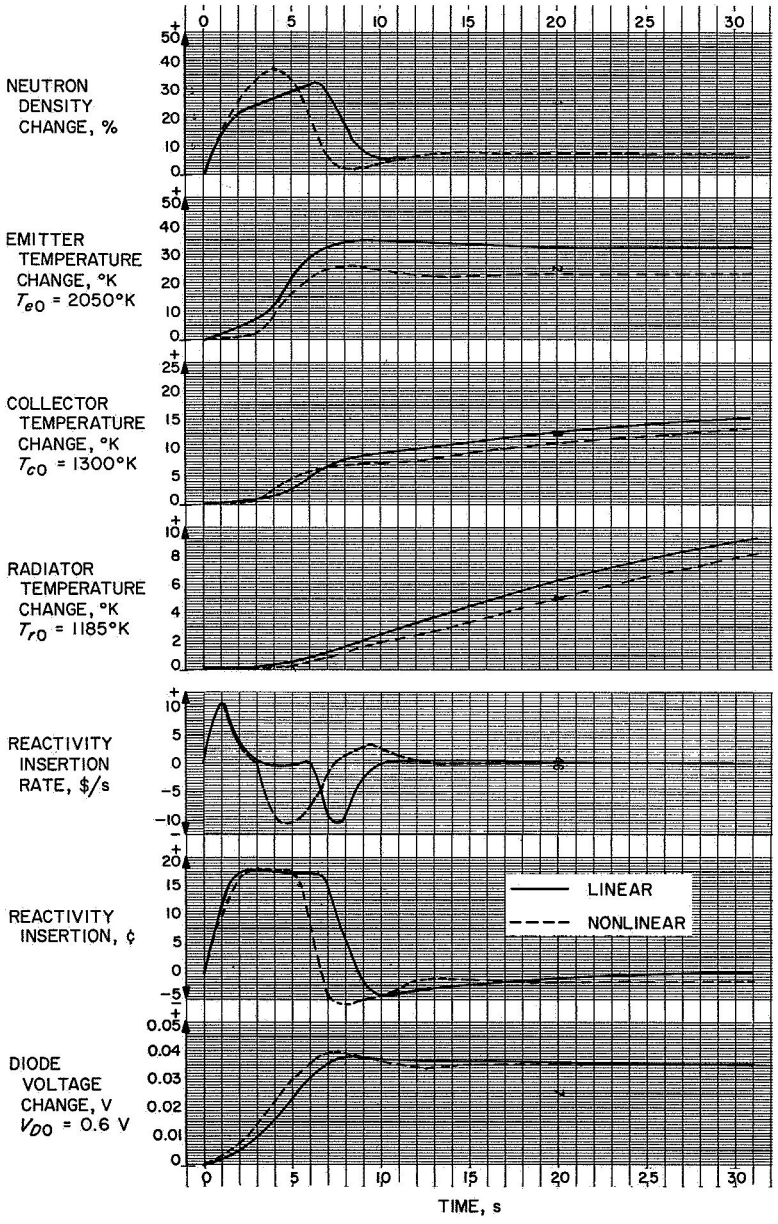

Fig. 37. Responses of linear and nonlinear controlled systems to a step command in voltage when the control signal is constrained to limit reactivity rate to 10¢/s

VII. Summary and Conclusions

This preliminary study was undertaken to develop a control system for an in-core thermionic reactor powerplant. A design characteristic of the thermionic reactor concept is the direct coupling between the reactor and the thermionic diodes, and as a consequence, electric load disturbances have a pronounced effect on the dynamics of the reactor system.

Investigations of the uncontrolled thermionic reactor powerplant showed that active control is required, and provided the necessary background for the control system studies. The inherent response to a change in electric power demand is not consistent with maintaining efficient operation over a range of electric loads. Through reactivity control, and thus thermal power control, the desired electrical power level must be programmed into the controller function. This function will depend on the application of the thermionic reactor. The investigations described in this report postulated a low-power nuclear–electric ion-propulsion space mission. In this application, it is desirable to maintain a nearly constant output voltage at the reactor terminals.

A companion study showed that only minor efficiency penalties are incurred by the use of constant voltage control instead of optimal voltage control, at least down to as low as 10% of rated full power.

The state-variable feedback design technique was used to develop the control law and to select the controller. System states are fed back through constant-gain elements so as to realize exactly a desired overall system response. If required, series compensation may be included and the effects of nonlinearities and disturbances may be systematically minimized. This linear design technique was applied to a reduced linearized version of a high-order nonlinear powerplant model. The controller design that evolved was then applied to the nonlinear model and found to give very nearly the same responses as those obtained with the reduced linear model.

Analog computer simulation techniques were used to determine the responses of the nonlinear model, and to verify analytical results obtained for the linear model.

In summary, the objectives of the study were to:

(1) Investigate the feasibility of constant-output voltage control.

(2) Investigate the applicability of the state-variable feedback design method.

(3) Investigate controller characteristics.

It was found that in general the response reactivity rate and reactivity were too large to be allowed in a practical system. However, by constraining the control signal, the reactivity rate can be lowered to acceptable levels without causing stability problems. This is not true if the rate itself is limited. The other beneficial effect obtained by constraining the control signal is that the system remains stable against the loss of any of the feedback elements. Again this is not true when the signal is unconstrained.

In determining the feedback coefficients used in this preliminary investigation, no attempt was made at the outset to incorporate the effects of nonlinearities caused by constraints. These effects were considered in a subsequent study of a controller design that gives improved response to external and internal system disturbances.[3]

From the results obtained in the work reported here the following general conclusions may be drawn:

(1) Constant-output voltage control is feasible.

(2) The state-variable feedback design method is applicable.

(3) Nonlinearity and stability problems do not arise if the design technique is properly applied.

(4) The sensitivity to disturbances and parameter variations can be made small.

(5) Sophisticated controller hardware is not necessary.

All results were obtained for thermionic diode current–voltage characteristics that do not cross each other in the range of interest. This is the case when cesium-reservoir temperature is somewhat higher than optimum. For certain perturbations, operating at optimum cesium pressure, and maintaining constant pressure, leads to oscillatory system behavior or emitter temperature runaway. Consequently, it is desirable to operate at higher-than-optimum cesium-reservoir temperatures to avoid such system behavior.

[3]Study entitled "A State-Variable Feedback Design for the Control System for an In-Core Thermionic Reactor," by L. E. Weaver, W. J. Summa, and H. Gronroos; in preparation for publication.

Appendix A

Equations and Diagram for Analog Computer Simulation of the Fourth-Order Linear Model of a Thermionic Reactor Space Powerplant

Equations (108) through (110) in Section V describe the fourth-order linear model of a thermionic reactor with controller. These equations were programmed on a 5800 DR Dystac analog computer to obtain response trajectories, and to study the effects of parameter variations. The simulation diagram is shown in Fig. A-1. The variables have been scaled to keep the computer gains as low as possible and to avoid low potentiometer settings. The computer equations are as follows:

$$(10\delta n) = (x_1) - 0.164\left(\frac{x_2}{10}\right) - 0.04\,(100x_3) - 0.313\left(\frac{x_4}{10}\right) + 10\,(10x_5) + 0.0014\,(1000\delta R_{LD})$$

$$(\dot{x}_1) = 0.1\,(10\delta n) - 0.1\,(x_1)$$

$$\left(\frac{\dot{x}_2}{10}\right) = -1.71\left(\frac{x_2}{10}\right) + 0.319\,(100x_3) + 1.66\left(\frac{x_4}{10}\right) + 1.87\,(1000\delta R_{LD})$$

$$(100\dot{x}_3 - 211\delta\dot{R}_{LD}) = 0.031\,(x_1) + 0.353\left(\frac{x_2}{10}\right) - 0.123\,(100x_3) - 0.344\left(\frac{x_4}{10}\right) + 0.625\,(1000\delta R_{LD})$$

$$\left(\frac{\dot{x}_4}{10}\right) = 0.082\left(\frac{x_2}{10}\right) - 0.114\left(\frac{x_4}{10}\right)$$

$$(10\dot{x}_5) = 10\,(x_6)$$

$$\dot{x}_6 = -0.2\,(10x_5) - 2\,(x_6) + 6.5\,(1000u)$$

$$1000u = -0.292\,(x_1) - 0.153\left(\frac{x_2}{10}\right) - 9.39\,(100x_3) + 0.080\left(\frac{x_4}{10}\right) - 3.04\,(10x_5) - 15.4(x_1) + (1000r)$$

$$\theta_2 = 1.72\left(\frac{x_2}{10}\right) + 8.52\,(100x_3) - 1.80\,(1000\delta R_{LD})$$

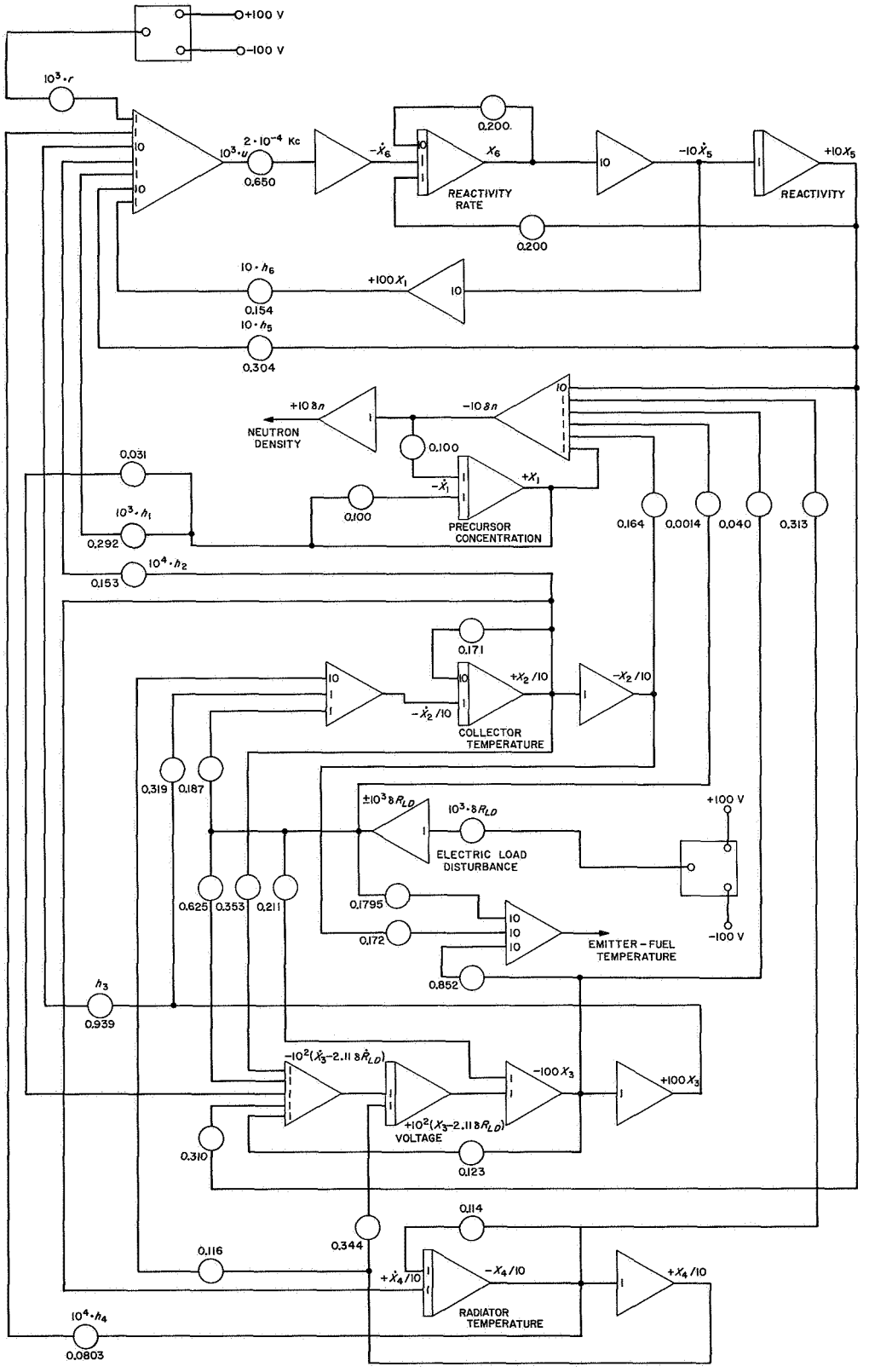

Fig. A-1. Analog-simulation diagram for fourth-order linear model of thermionic reactor space powerplant with controller

Appendix B

Equations and Diagrams for Analog Computer Simulation of the Complete Nonlinear Model of a Thermionic Reactor Space Powerplant

The high-order nonlinear model of a thermionic reactor space powerplant described by Eqs. (1) through (24) in Section III was simulated on several analog computers coupled together. Figure B-1 illustrates the equipment setup for the controller investigations, and Figs. B-2 through B-9 show the simulation diagrams. A diagram requiring fewer amplifiers could have been drawn up, but this representation was selected to minimize patching when changing time scale. The PACE computers used in the simulations did not have a switch for time-scale changes. The computer equations are as follows:

I. Neutron Kinetics in Prompt-Jump Approximation

$$
\begin{aligned}
(100\dot{c}_1) &= 0.522\,(5n) - 3.88\,(100c_1), & 100c_{10} &= 6.23\\
(10\dot{c}_2) &= 0.256\,(5n) - 1.40\,(10c_2), & 10c_{20} &= 9.13\\
(\dot{c}_3) &= 0.0816\,(5n) - 0.311\,(c_3), & c_{30} &= 13.12\\
(\dot{c}_4) &= 0.0375\,(5n) - 0.116\,(c_4), & c_{40} &= 16.18\\
\left(\frac{\dot{c}_5}{2}\right) &= 0.0105\,(5n) - 0.0317\left(\frac{c_5}{2}\right), & \frac{c_{50}}{5} &= 33.52\\
(\dot{c}_6) &= 0.0076\,(5n) - 0.0127\,(c_6), & c_6 &= 29.92
\end{aligned}
\tag{B-1}
$$

$$
5n = \frac{100\sum_{i=1}^{6}\lambda_i c_i}{20 - 20\rho}, \qquad n_0 = 10.0 \tag{B-2}
$$

$$
20\rho = 20\left[\rho_{control} + \sum_k \alpha_k (T_k - T_{k0})\right] \tag{B-3}
$$

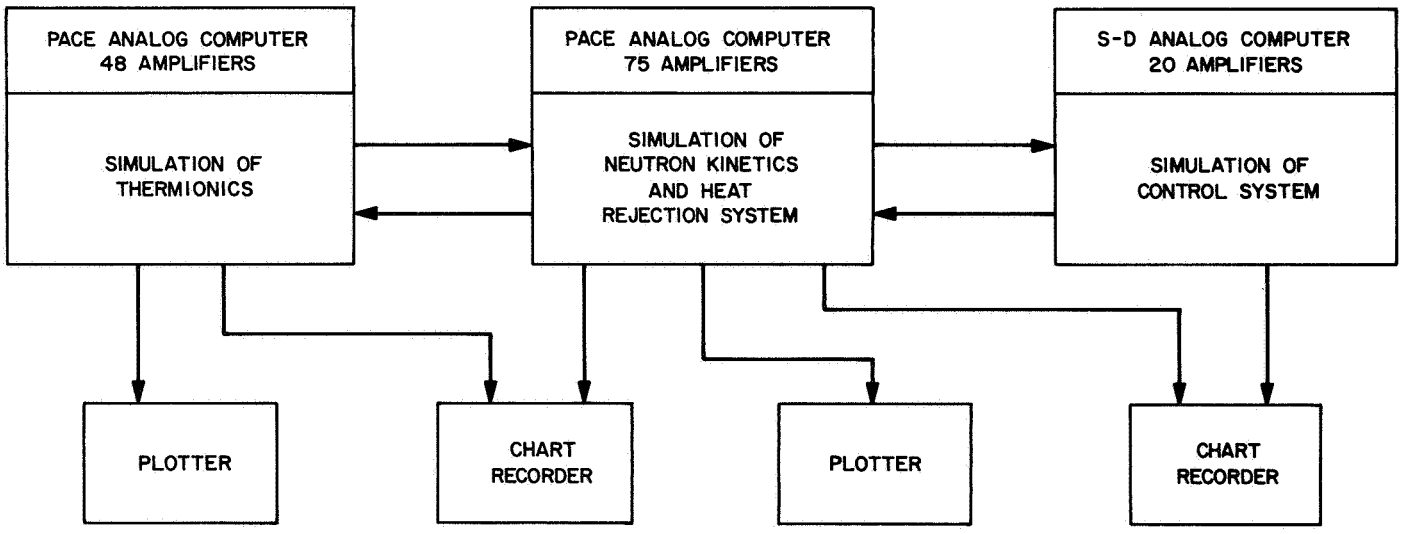

Fig. B-1. Equipment setup for computer simulation of thermionic reactor space powerplant—nonlinear model

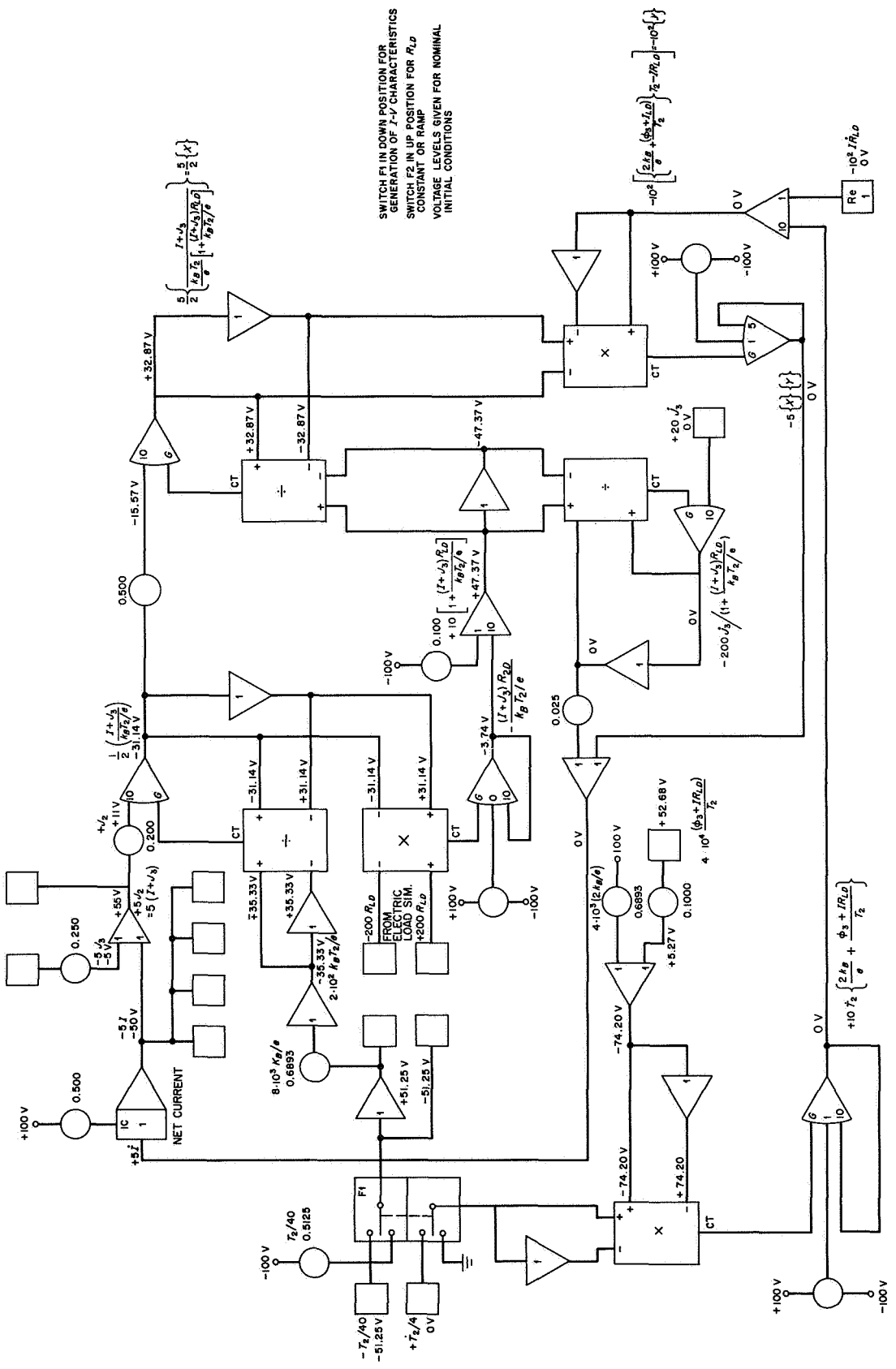

Fig. B-2. Analog-simulation diagram for nonlinear model of thermionic reactor space powerplant: thermionics; net current

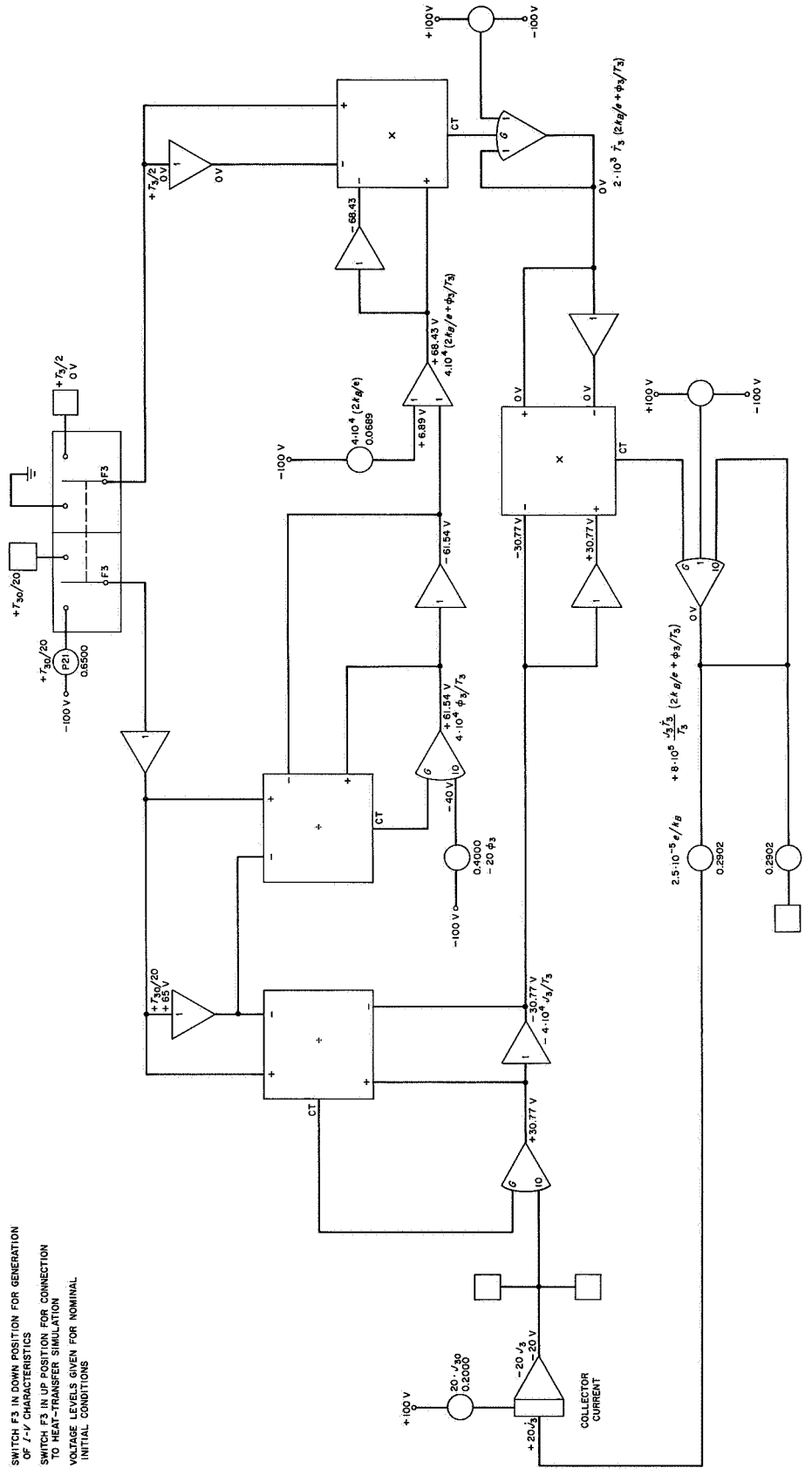

Fig. B-3. Analog-simulation diagram for nonlinear model of thermionic reactor space powerplant: thermionics; collector current

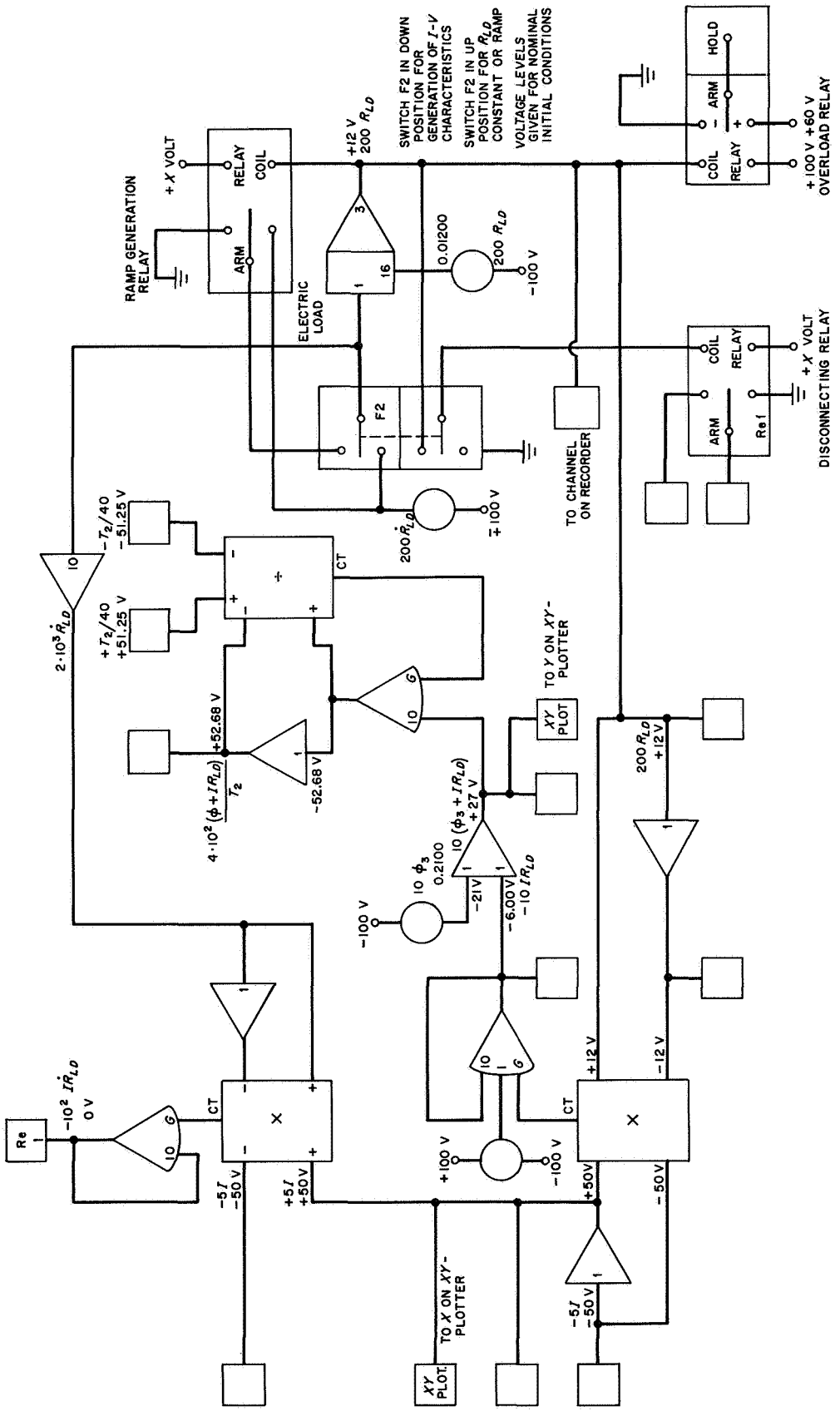

Fig. B-4. Analog-simulation diagram for nonlinear model of thermionic reactor space powerplant model: thermionics; electric load

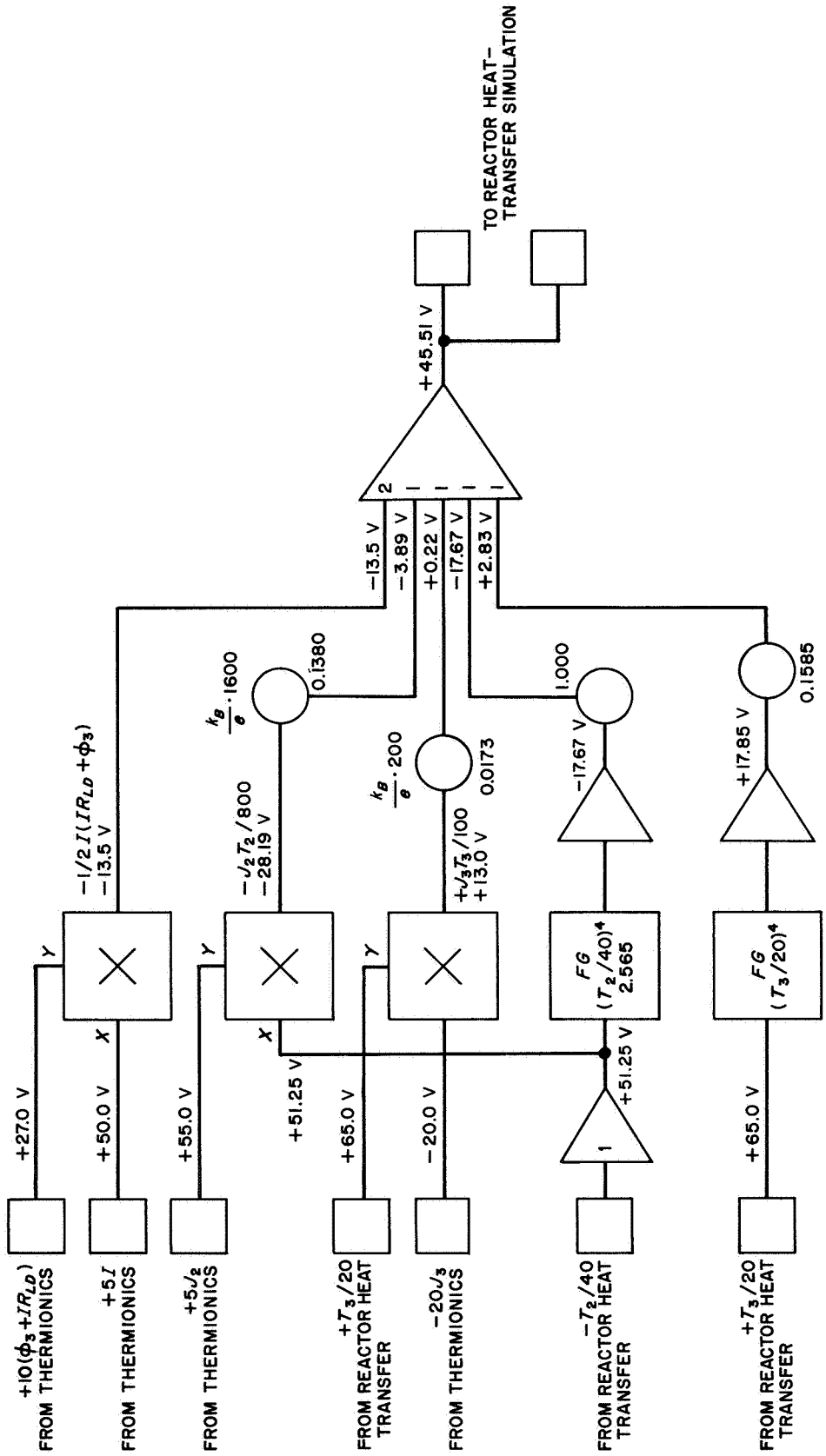

Fig. B-5. Analog-simulation diagram for nonlinear model of thermionic reactor space powerplant: energy transport in interelectrode gap

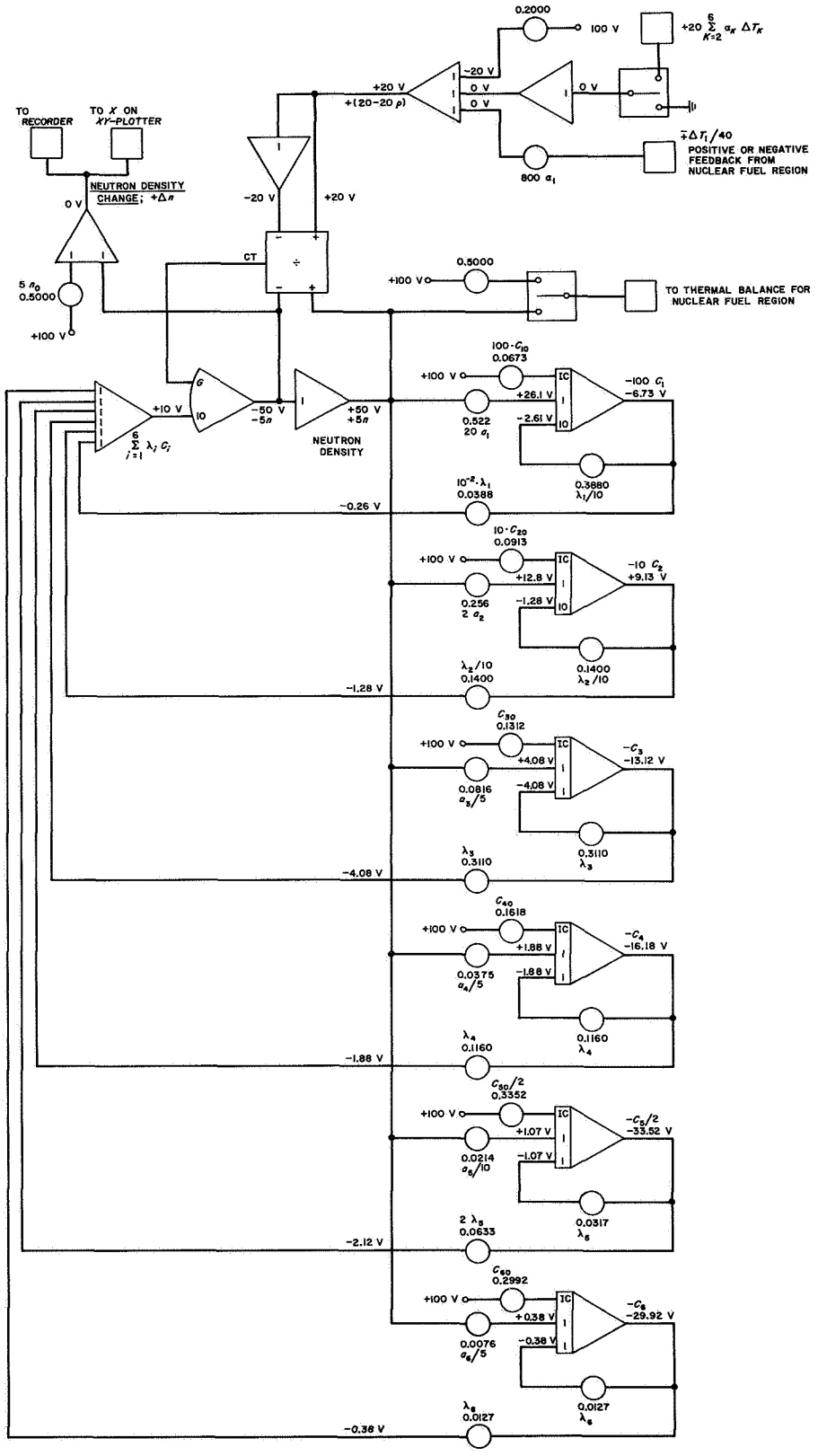

Fig. B-6. Analog-simulation diagram for nonlinear model of thermionic space powerplant: neutron kinetics

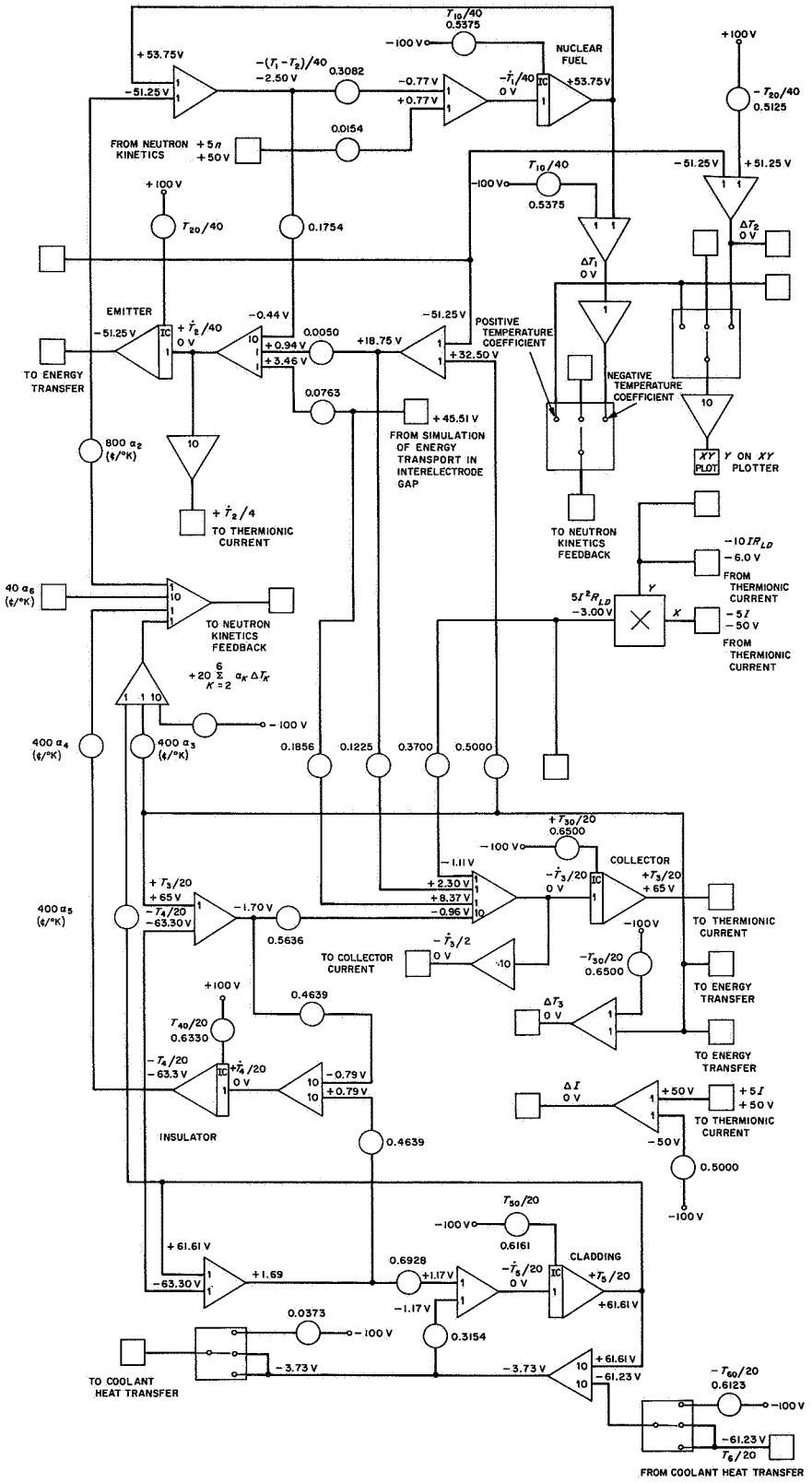

Fig. B-7. Analog-simulation diagram for nonlinear model of thermionic reactor space powerplant: reactor heat transfer

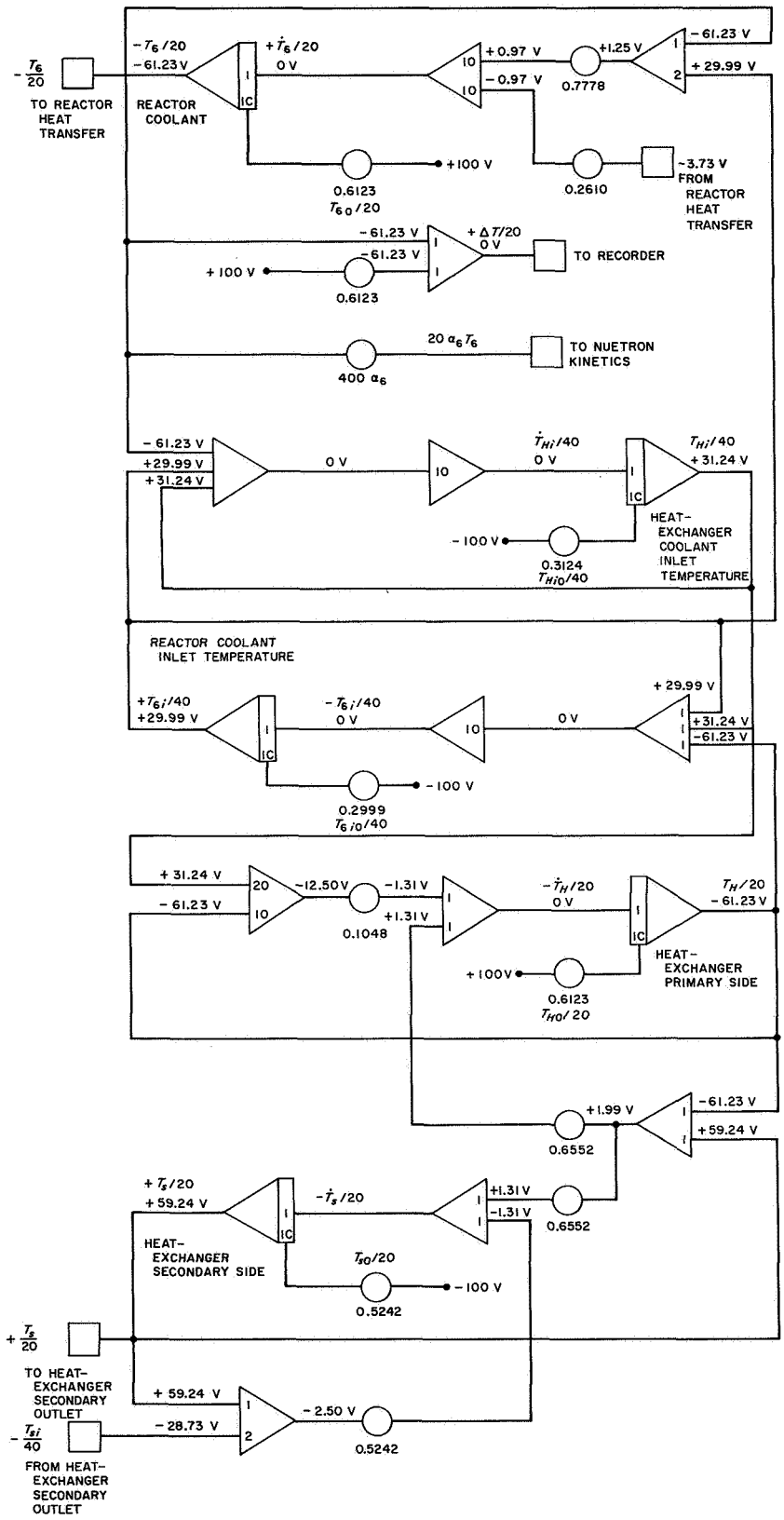

Fig. B-8. Analog-simulation diagram for nonlinear model of thermionic reactor space powerplant: coolant heat transfer

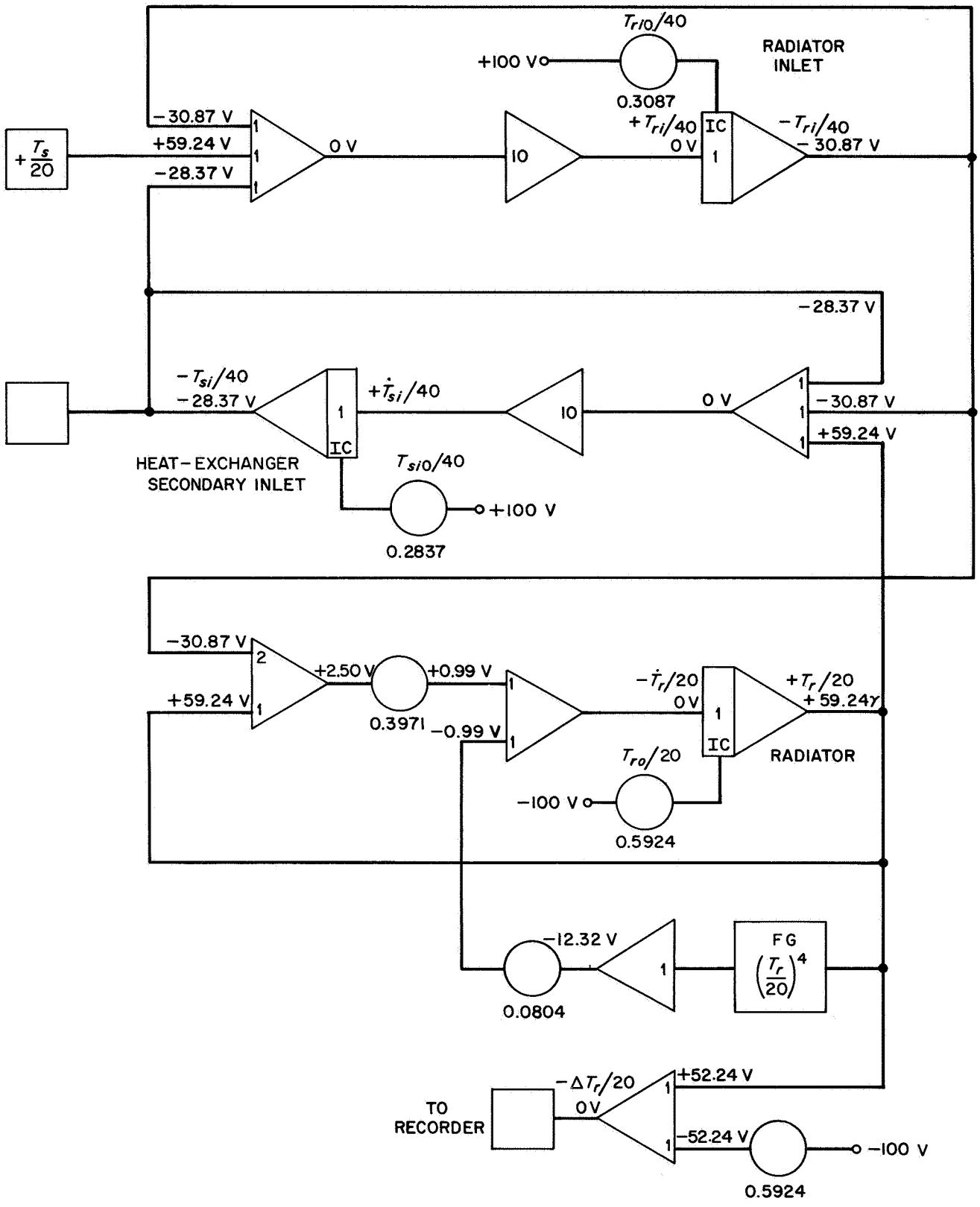

Fig. B-9. Analog-simulation diagram for nonlinear model of thermionic reactor space powerplant: coolant-loop heat transfer

II. Thermionics

The analog-simulation equations for the current–voltage characteristics are obtained by differentiation with respect to time and solving explicitly for the net current and the collector current. This method avoids the use of function generators for development of the exponentials, but the simulation produced by the equations is subject to drift because there are time-differentiated factors in all terms. However, when the thermionics simulation is coupled with the rest of the simulated system the whole system is stable. The computer equations are as follows:

$$\dot{I} = \frac{I + J_3}{\frac{k_B T_2}{e}\left[1 + \frac{(I + J_3) R_{LD}}{k_B \frac{T_2}{e}}\right]} \left\{\left[\frac{2k_B}{e} + \frac{(\phi_3 + IR_{LD})}{T_2}\right]\dot{T}_2 - I\dot{R}_{LD}\right\} - \frac{\dot{J}_3}{1 + \frac{(I + J_3) R_{LD}}{k_B \frac{T_2}{e}}}, \qquad J_2 = I - J_3 \tag{B-4}$$

$$\dot{J}_3 = \frac{J_3 \dot{T}_3}{k_B \frac{T_3}{e}}\left[\frac{2k_B}{e} + \frac{\phi_3}{T_3}\right] \tag{B-5}$$

$$q''_{2t} = I(IR_{LD} + \phi_3) + 0.1732 \cdot 10^{-3}(J_2 T_2 - J_3 T_3) + 10^{-12}(T_2^4 - T_3^4) \tag{B-6}$$

$$q''_{2e} = 0.0165\,(T_2 - T_3) \tag{B-7}$$

III. Reactor Core Heat Transfer

$$\left(\frac{\dot{T}_1}{40}\right) = 0.0771n - 0.3082\left(\frac{T_1}{40} - \frac{T_2}{40}\right) \tag{B-8}$$

$$\left(\frac{\dot{T}_2}{40}\right) = 1.754\left(\frac{T_1}{40} - \frac{T_2}{40}\right) - 0.0763q''_{2t} - 0.0049\left(\frac{T_2}{40} - 0.5\,\frac{T_3}{20}\right) \tag{B-9}$$

$$\left(\frac{\dot{T}_3}{20}\right) = 0.1856q''_{2t} + 0.0613\left(\frac{2T_2}{40} - \frac{T_3}{20}\right) - 0.1856I^2R_{LD} - 5.636\left(\frac{T_3}{20} - \frac{T_4}{20}\right) \tag{B-10}$$

$$\left(\frac{\dot{T}_4}{20}\right) = 4.639\left(\frac{T_3}{20} - \frac{T_4}{20}\right) - 4.639\left(\frac{T_4}{20} - \frac{T_5}{20}\right) \tag{B-11}$$

$$\left(\frac{\dot{T}_5}{20}\right) = 6.928\left(\frac{T_4}{20} - \frac{T_5}{20}\right) - 31.54\left(\frac{T_5}{20} - \frac{T_6}{20}\right) \tag{B-12}$$

$$\left(\frac{\dot{T}_6}{20}\right) = 26.10\left(\frac{T_5}{20} - \frac{T_6}{20}\right) - 7.778\left(\frac{T_6}{20} - \frac{T_{6i}}{20}\right) \tag{B-13}$$

IV. Coolant Loops

$$0.1\left(\frac{\dot{T}_{6i}}{20}\right) = \frac{2T_H}{20} - \frac{T_{6i}}{20} - \frac{T_{Hi}}{20} \tag{B-14}$$

$$0.1\left(\frac{\dot{T}_{Hi}}{20}\right) = \frac{2T_6}{20} - \frac{T_{6i}}{20} - \frac{T_{Hi}}{20} \tag{B-15}$$

$$\left(\frac{\dot{T}_H}{20}\right) = 1.048\left(\frac{T_{Hi}}{20} - \frac{T_H}{20}\right) - 0.6552\left(\frac{T_H}{20} - \frac{T_s}{20}\right) \tag{B-16}$$

$$\left(\frac{\dot{T}_s}{20}\right) = 0.6552\left(\frac{T_H}{20} - \frac{T_s}{20}\right) - 0.5242\left(\frac{T_s}{20} - \frac{T_{si}}{20}\right) \tag{B-17}$$

$$0.1\left(\frac{\dot{T}_{si}}{20}\right) = \frac{2T_r}{20} - \frac{T_{si}}{20} - \frac{T_{ri}}{20} \tag{B-18}$$

$$0.1\left(\frac{\dot{T}_{ri}}{20}\right) = \frac{2T_s}{20} - \frac{T_{si}}{20} - \frac{T_{ri}}{20} \tag{B-19}$$

$$\left(\frac{\dot{T}_r}{20}\right) = 0.3971\left(\frac{T_{ri}}{20} - \frac{T_r}{20}\right) - 0.0804\left[10^{-4}\left(\frac{T_r}{20}\right)^4\right] \tag{B-20}$$

Nomenclature

A	area
A	Richardson-Dushman constant
A	system matrix
a_i	relative delayed-neutron fraction (β_i/β)
a	system parameter
$\mathbf{b}$	control vector
b	system parameter
C_i	Λc_i
c_i	precursor density
c	heat capacity
$\mathbf{c}$	output vector
D	transfer-function denominator polynomial
e	electron charge
F	function
f	adjustment factor
f	function
G	transfer function for forward loop
H	transfer function for feedback loop
h	heat-transfer coefficient
h	feedback element
I	net current density
I	identity matrix
J	thermionic diode electrode current density
K	gain constant
k	thermal conductivity
k	slope
k_B	Boltzmann constant
L	length
M	mass
N	number of thermionic diodes
N	transfer-function numerator polynomial
n	neutron density
q	heat flow
R	ohmic electric load
r	radial dimension
r	reference signal
S	integral sensitivity
s	Laplace transform variable
T	temperature
t	thickness
t	time variable
U	overall heat-transfer coefficient
$\mathbf{u}$	control variable
u	sensitivity function
V	volume
v	velocity

Nomenclature (contd)

W	stability function	Λ	prompt-neutron generation time
w	flow rate	λ	system parameter
$\mathbf{x}$	state variable	λ_i	precursor decay constant
y	output variable	ρ	density
α	temperature coefficient of reactivity	ρ	reactivity
α	transfer-function pole	σ	nonlinear state variable
α	real number	σ_{SB}	Stephan-Boltzmann constant
α	conversion coefficient	τ	transport delay
ϵ	emissivity	Φ	resolvent matrix
η	efficiency	ϕ	work function
θ	temperature differential	ω	angular velocity

References

1. Weaver, L. E., and Vanesse, R. E., "State Variable Feedback Control of Multiregion Reactors," *Nucl. Sci. Eng.*, Vol. 29, pp. 264–271, 1967.
2. Weaver, L. E., *Reactor Dynamics and Control-State Space Techniques.* American Elsevier Publishing Co., Inc., New York, 1968.
3. Gronroos, H., "Analog Studies of Thermionic Reactor Dynamics," in *Supporting Research and Advanced Development,* Space Programs Summary 37-45, Vol. IV, pp. 136–141, Jet Propulsion Laboratory, Pasadena, Calif., June 30, 1967.
4. Davis, J. P., Gronroos, H. G., Phillips, W. M., *Review of Industry-Proposed In-Pile Thermionic Space Reactors: Volume 1. General,* Technical Memorandum 33-262. Jet Propulsion Laboratory, Pasadena, Calif., Oct. 15, 1965.
5. *Parametric Study of High Power In-Pile Nuclear Thermionic Space Powerplants,* Report PWA-2319. Pratt & Whitney Aircraft Div., United Aircraft Corp., East Hartford, Conn., Mar. 1, 1964.
6. Elder, F. A., and Staley, L. E., *An Experimental Model of a 2 KW, 2500 Volt Power Converter for Ion Thrustors Using Gate Controlled Switches in Two-Phase-Shifted Parallel Inverters,* NASA Report CR-54216. Westinghouse Electric Corp., Pittsburgh, Pa., May 1965.
7. *Development and Test of an Ion Engine System Employing Modular Power Conditioning,* Project Final Report SSD 60374R. Hughes Aircraft Company, El Segundo, Calif., Sept. 1966.
8. Masek, T. D., and Pawlik, E. V., "Thrust System Technology for Solar Electric Propulsion," AIAA Paper 68-541, presented at the AIAA Fourth Propulsion Joint Specialist Conference, Cleveland, Ohio, June 1968.
9. Kerrisk, D. J., and Kaufman, H. R., "Electric Propulsion Systems for Primary Spacecraft Propulsion," AIAA Paper 67-424, presented at the AIAA Third Propulsion Joint Specialist Conference, Washington, D.C., July 1967.

References (contd)

10. Schultz, M. A., *Control of Nuclear Reactors and Powerplants.* McGraw-Hill Book Co., Inc., New York, 1961.

11. Weaver, L. E., *System Analysis of Nuclear Reactor Dynamics.* Rowman & Littlefield, Inc., New York, 1963.

12. Ash, M., *Nuclear Reactor Kinetics.* McGraw-Hill Book Co., Inc., New York, 1965.

13. *The Technology of Nuclear Reactor Safety: Volume 1. Reactor Physics and Control.* Edited by T. J. Thompson and J. G. Beckerley. The M.I.T. Press, Cambridge, Mass., 1964.

14. Keepin, G. R., *Physics of Nuclear Kinetics.* Addison-Wesley Publishing Co., Reading, Mass., 1965.

15. Schock, A., "Effect of Cesium Pressure on Thermionic Stability," paper presented at the Second International Conference on Thermionic Electrical Power Generation, Stresa, Italy, May 27–31, 1968, sponsored by the European Nuclear Energy Agency.

16. Wilkins, D. R., *SIMCON—A Digital Computer Program for Computing Thermionic Converter Performance Characteristics,* Report GESR-2109. General Electric Co., Pleasanton, Calif., Feb. 1, 1968.

17. Brehm, R. L., *Estimates of Doppler Coefficients for In-Pile Thermionic Reactor Materials,* Technical Report 32-1077. Jet Propulsion Laboratory, Pasadena, Calif., Oct. 1, 1967.

18. Melsa, J. L., *A Digital Computer Program for the Analysis and Design of State Variable Feedback Systems.* Engineering Experiment Station, The University of Arizona, College of Engineering, Tucson, Ariz., Mar. 1967.

19. McCornock, M. D., *Peak and Integral Sensitivity Program.* Programmatics Inc., Los Angeles, Calif., prepared for Jet Propulsion Laboratory, Contract No. 951828, Aug. 1967.